Nature Communications

https://doi.org/10.1038/s41467-026-72639-7

Article in Press

Neuregulin-1 facilitates myelin regeneration through microglia-mediated mechanisms in a mouse model of chronic demyelination

Received: 18 November 2024

Accepted: 1 April 2026

Cite this article as: Ziaee, S.M., Nemati, S., Kataria, H. *et al.* Neuregulin-1 facilitates myelin regeneration through microglia-mediated mechanisms in a mouse model of chronic demyelination. *Nat Commun* (2026). https://doi.org/10.1038/s41467-026-72639-7

Seyyed Mohyeddin Ziaee, Shiva Nemati, Hardeep Kataria, Elisabet Jakova, Seyed Mojtaba Hosseini, Pejman Ghelich, Graham McLeod, Ali Tamayol, V. Wee Yong & Soheila Karimi-Abdolrezaee

Neuregulin-1 facilitates myelin regeneration through microglia-mediated mechanisms in a mouse model of chronic demyelination

[#]Seyyed Mohyeddin Ziaee[1], [#]Shiva Nemati[1], Hardeep Kataria[1], Elisabet Jakova[1], Seyed Mojtaba Hosseini[1], Pejman Ghelich[2], Graham McLeod[1], Ali Tamayol[2], V. Wee Yong[3] and *Soheila Karimi-Abdolrezaee[1,4]

[1] Department of Physiology and Pathophysiology, Manitoba Multiple Sclerosis Research Centre, Rady Faculty of Health Sciences, University of Manitoba, Winnipeg, Manitoba, Canada

[2] Department of Biomedical Engineering, University of Connecticut, Farmington, USA.

[3] Hotchkiss Brain Institute and the Department of Clinical Neurosciences, University of Calgary, Calgary, Alberta, Canada.

[4] Children Hospital Research Institute of Manitoba, Winnipeg, Manitoba, Canada

[#] Equal contributions of these two authors

***** Corresponding Author:
Soheila Karimi-Abdolrezaee, PhD
Rady Faculty of Health Sciences, University of Manitoba
629-Basic Medical Sciences Building
745 Bannatyne Avenue
Winnipeg, MB R3E 0J9 Canada
Soheila.Karimi@umanitoba.ca

Abstract

Impaired myelin repair, or remyelination, is a hallmark of progressive multiple sclerosis (MS) that drives brain degeneration and enduring neurological disabilities. Microglia crucially support remyelination through myelin phagocytosis and lipid metabolism. However, in chronic demyelinated MS lesions, microglia lose their reparative function by acquiring a foamy dysfunctional phenotype characterized by accumulation of lipid droplets due to impaired cholesterol processing of myelin debris. Here, we show a positive correlation between dysregulation of neuregulin-1 and impaired oligodendrocyte remyelination in mice with chronic demyelination. Therapeutic restoration of neuregulin-1 fosters myelin regeneration through microglia-dependent mechanisms. We demonstrate that Nrg-1 signaling supports microglia integrity and function in chronic demyelinated lesions by exploiting their capacity for the clearance of myelin debris and cholesterol recycling, biosynthesis and efflux. These findings signify the promise of neuregulin-1 as an endogenous target to facilitate microglia mediated-repair in progressive MS in which there is an unmet need for new treatments.

Introduction

Remyelination is an essential repair process for restoring neural function, maintaining axonal integrity, and reversing the symptoms of demyelination in multiple sclerosis (MS) [1-4]. Unlike the relapsing-remitting MS that some degree of spontaneous remyelination facilitates recovery, myelin repair is severely impaired in progressive forms of MS causing irreversible damage to the neural network and permanent neurological disabilities [2,5]. Although the underlying molecular mechanisms are yet to be elucidated, lack of support for the maturation of oligodendrocyte progenitor cells (OPCs) to myelinating oligodendrocytes is thought to contribute to the remyelination failure in chronic demyelinated lesions [6-13].

Microglia play diverse roles in CNS homeostasis and pathologies. In MS, microglia are involved in both neurodegenerative events and repair processes, depending on the phenotype they acquire through their interactions with the lesion environment [14-17]. Growing evidence has shown a pivotal role for microglia in remyelination, partially through their ability for myelin debris phagocytosis and cholesterol recycling [18-22]. Despite this potential, microglia often exhibit a dysfunctional phenotype in chronic active lesions of progressive MS and with aging that is characterized by impaired cholesterol metabolism and transport following myelin phagocytosis and thereby formation of foamy phagocytes [18,19,23-26]. Inefficiency of foamy microglia in cholesterol processing is attributed to dysregulation of cholesterol biosynthesis and export signaling pathways such as liver X receptors (LXRs) and peroxisome proliferator-activated receptors (PPARs) [18,19,23,27,28]. Hence, microglia dysfunction has been implicated in impaired remyelination and consequently sustained demyelination and neurodegeneration [18,19,23-25,29]. Abundance of foamy microglia in chronic active MS lesions [26,30-32], however, provides an opportunity for therapeutic interventions to restore their intrinsic capacity for remyelination. Thus, it is imperative to unravel how the innate capacity of microglia for remyelination is regulated in chronic demyelinated lesions.

In this study, we provide evidence that downregulation of neuregulin-1 (Nrg-1) in chronic demyelinated lesions is associated with microglia dysfunction and underlies impaired oligodendrocyte maturation and sustained demyelination in the brain. Nrg-1 is an important protein in the developing and adult CNS with an established role in myelination [33-35]. We recently implicated Nrg-1 dysregulation in pathogenesis of MS [36]. Importantly, we identified a positive immunomodulatory role for Nrg-1 in acute lesions of the experimental autoimmune encephalomyelitis (EAE) mouse model of MS characterized by a shift from a pro-inflammatory to

an anti-inflammatory immune response [36,37]. Here, we investigated the role of Nrg-1 in chronic demyelination using a mouse model of long-term cuprizone demyelination that recapitulates some of the key features of progressive MS including impaired remyelination and degeneration.[38] We report, for the first time, that pharmacological restoration of Nrg-1 levels allows remyelination in chronically demyelinated white matter. The beneficial effects of Nrg-1 are found to be microglia-dependent as microglia ablation from chronic demyelinated lesions abolishes Nrg-1 effects. Mechanistically, Nrg-1 signaling promotes microglia integrity and function by exploiting their capacity for myelin clearance and concomitant augmentation of microglial cholesterol biosynthesis and efflux machinery through activation of LXR and PPARγ pathways. Taken together, this study unravels an endogenous mechanism that underlies impaired remyelination in progressive MS, and introduces a therapeutic candidate as a regenerative therapy for the chronic phase of MS.

Results

Remyelination is impaired in chronic demyelinating lesions despite the presence of OPCs and is associated with dysregulation of Nrg-1β1.

We employed a cuprizone (CPZ) mouse model of demyelination that is well suited for investigating the status of spontaneous remyelination in a progressive manner. We induced demyelination in PDGFR-CreERT;Rosa26-mGFP(mT/mG) reporter mice that allows tracking new OPCs progenies by GFP expression to study proliferation, maturation and remyelination by newly generated oligodendrocytes in demyelinating lesions (Fig. 1 a). Mice were subjected to 5 and 10 weeks of CPZ diet to induce short-term verses long-term chronic demyelinated lesions, respectively. To allow remyelination, CPZ mice underwent a recovery period for 2- and 4 weeks

with re-introduction of normal diet in short-term and chronic paradigms, respectively. We assessed remyelination within the corpus callosum by Black Gold II (BGII) staining that provides a high resolution and myelin-specific histochemical detection method [39]. Our analyses confirmed robust demyelination in the corpus callosum of CPZ mice after both short-term (86%) and chronic demyelination (94%) compared to their age-matched healthy controls. Mice with short-term demyelination showed significant spontaneous remyelination after 2 weeks of recovery achieving 68% of the baseline control myelination, while extent of remyelination in chronic demyelinated lesions was inadequate (32% of baseline) even 4 weeks after CPZ withdrawal (Fig. 1 b-c). Importantly, we found that impaired remyelination after prolonged demyelination occurs despite the presence of GFP+ oligodendrocyte progenies in the corpus callosum. This suggests that oligodendrocyte population is replenished; however, their maturation to myelin forming cells is inhibited in the milieu of chronic demyelinated lesions.

We previously showed dysregulation of Nrg-1β1 in human MS lesions, as well as in lesions of experimental autoimmune encephalomyelitis (EAE) mouse model of MS with a positive association with disease pathogenesis and progression [36]. Given Nrg-1β1 is well-known for its developmental role in myelination [35], we sought to investigate the expression levels of Nrg-1β1 in short-term and chronic CPZ lesions and determine its potential impact on the success of remyelination. Immunohistochemical analysis revealed a significant decline of Nrg-1β1 levels in the cortex (89% and 85% reduction) and corpus callosum (90% and 91% reduction) of CPZ mice after both short-term and chronic demyelination, respectively, compared to the age-matched control mice (Fig. 1 d-k). Downregulation of Nrg-1β1 was restored significantly during the recovery phased after short-term demyelination in the cortex and corpus callosum to 74% and 78% of the baseline control levels, respectively. However, Nrg-1 decline persisted in chronic

demyelinated lesions with no restoration even after 4 weeks of recovery as there was still 84% and 89% reduction in the Nrg-1 expression levels in the cortex and corpus callosum, respectively, compared to the baseline levels in the age-matched control mice (Fig. 1 d-k). These findings indicated a positive correlation between persistent dysregulation of Nrg-1β1 in chronic demyelinating lesions and impaired remyelination. To determine which cell types express Nrg-1 in the brain of healthy and cuprizone mice, we conducted co-immunolabeling for Nrg-1 and various neural markers. Our immunohistochemical staining of the cortex and corpus callosum showed that neurons and oligodendrocytes are the primary sources of Nrg-1 in the normal brain. Nrg-1 is also localized in axons and is detected in the white matter (Supplementary Fig. 1a). Microglia also express Nrg-1 in the healthy brain both in the cortex and corpus callosum, but to a lesser degree. However, we did not detect immunohistochemical localization of Nrg-1 within astrocytes, which was confirmed by z-stack optical slicing using a confocal microscope (Supplementary Fig. 1a). These data confirmed our previous findings in the CNS of rodents [40]. Nrg-1 immunostaining in CPZ demyelinated lesions, at both short-term (5 weeks) and long-term (10 weeks) timepoints showed that Nrg-1 is dramatically depleted in all expressing cell types. These data suggest that downregulation of Nrg-1 within the white matter lesions likely reflects oligodendrocyte loss as well as injury and loss of axons and/or reduction of neuronal Nrg-1.

We next asked whether the reduced levels of Nrg1 are restored in both axons and oligodendrocytes after short-term CPZ. Immunohistochemical co-localization analysis of Nrg-1 in axons (marked by β-Tubulin III, TUBIII) in the corpus callosum of mice with 5 weeks CPZ showed 89% reduction in Nrg-1 expression compared to the baseline control levels (Supplementary Fig. 1b). After 2 weeks of recovery, Nrg-1 levels were significantly increased in axons (6.5-fold) compared to the 5 weeks CPZ mice. Axonal Nrg-1 was restored during the

recovery from short-term CPZ to 69% of the baseline levels but it remained significantly lower than the control level. Nrg-1 expression was also markedly reduced (68%) in oligodendrocytes (marked by APC) after 5 weeks CPZ compared to the control group (Supplementary Fig. 1c). After 2 weeks recovery, Nrg-1 levels were significantly improved in oligodendrocytes compared to the 5 weeks CPZ mice (2.6-fold increase) and were recovered to 83% of the baseline level that was no longer statistically significant than the expression levels of Nrg-1 in the control mice. These data suggest that CPZ demyelination results in significant reduction in Nrg-1 levels in both axons and oligodendrocytes, although its reduction is more pronounced in axons. During the recovery period after short-term demyelination, Nrg-1 levels were also significantly recovered in both axons and oligodendrocytes; however, the degree of Nrg-1 restoration was higher in axons compared to oligodendrocytes during the post-CPZ recovery period. Following short-term CPZ, both populations also contributed to Nrg-1 recovery; however, the recovery in Nrg-1 levels was proportional to the degree of Nrg-1 depletion in each cell type during CPZ demyelination.

Abundance of Lipid laden microglia is a hallmark of chronic CPZ lesions and in human secondary progressive MS lesions.

Microglia play critical roles in remyelination [20-22,41-43]. While microglia are abundant in chronic demyelinating lesions, it has been shown that their reparative capacity diminishes with MS progression as they acquire a disease-associated phenotype [18,19,23,25,30,44]. One hallmark of chronic demyelinated lesions is an accumulation of myelin-derived lipids within microglia [19,23,25,44]. Here, we also confirm the presence of microglia in chronic lesions post-mortem secondary progressive MS (SPMS) using co-immunolabeling for CD11b that marks myeloid cells with TMEM119 (a specific microglia marker). Our assessment also confirms the abundance of lipid-laden foamy

phagocytes within SPMS lesions, as indicated by Oil Red-O (ORO) staining for esterified lipid droplets [19,26] (Fig. 2 a). Information on human SPMS samples is provided in Supplementary Table 1. We found that most lipid-laden phagocytes in SPMS lesions were microglia (CD11b+/TMEM119+). We previously reported a significant decline in the levels of Nrg-1 in the chronic active lesions of SPMS [36] that correlates Nrg-1 dysregulation with the accumulation of foamy microglia in these lesions. Likewise, in CPZ-induced chronic demyelinated lesions, our findings correlate Nrg-1 downregulation with the abundance of ORO positive lipid-laden phagocytes (Fig. 2 b). Of note, our assessment showed significant predominance of CD11b+/TMEM119+ microglia in comparison to CD11b+/TMEM119- macrophages within chronic demyelinated lesions after 2 weeks (87.12% vs. 12.75%, respectively) and 4 weeks (90.2% vs. 9.76%, respectively) following CPZ withdrawal (Fig. 2 c-d). Altogether, our findings show that remyelination is impaired in chronic CPZ demyelinated lesions despite the repopulation of new oligodendroglial cells during the recovery period. This suggests that maturation of newly formed oligodendrocytes into a myelinating phenotype is hindered. Thus, impaired remyelination in the chronically demyelinated lesions may be attributed to the accumulation of foamy microglia that are shown to have a diminished reparative capacity for remyelination[18,19,23,25,30,44].

Nrg-1β1 availability promotes remyelination in chronic demyelinated lesions in a microglia dependent manner.

To determine whether Nrg-1 downregulation in chronic demyelinated lesions affects the process of oligodendrogenesis and remyelination, we therapeutically restored the diminished levels of Nrg-1β1 in PDGFRα-Cre mice after 10 weeks of CPZ demyelination by peptide therapy. During the post-CPZ withdrawal recovery period, mice received 600ng (30µg/kg) of human recombinant Nrg-

1β1 peptide or vehicle (0.1% BSA in saline) per day by subcutaneous injections (Fig. 3 a-b) as we had previously employed in EAE mice [36]. This human recombinant Nrg-1β1 peptide is ~8 kDa and contains the EGF-Like domain that is shared by all active Nrg-1 isoforms. Of note, the EGF-like domain is necessary and sufficient for bioactivity of Nrg-1 ligand as it specifically and with high affinity binds to ErbB3 or ErbB4 receptors that heterodimerizes with ErbB2 to activate Nrg-1 downstream pathways[35]. It is also well-established that Nrg-1 ligand does not bind to EGF receptor or ErbB1, and EGF also does not bind to ErbB3 or ErbB4. This peptide has been used extensively for activation of Nrg-1 signaling [36,37,45,46] . Importantly, Nrg-1β1 peptide is shown to readily pass the blood-brain-barrier [44]. Our quantitative analysis of myelin by BGII signal intensity confirmed a robust and significant degree of demyelination (~92% decrease) in the corpus callosum of PDGFR-α Cre mice after 10 weeks of CPZ diet compared to the age-matched control mice (Fig. 3 c-d). After 2 and 4 weeks of recovery period, the vehicle treated lesions showed low degree of spontaneous remyelination (25% and 32%, respectively) compared to the normal baseline of myelination. Nrg-1β1-treated mice at both time-points showed a significantly higher level of remyelination compared to vehicle treated mice, with a more pronounced remyelination after 4 weeks of recovery that restored myelination to 85% of the baseline levels in the age-matched healthy controls (Fig. 3 c-d).

Since removal of myelin debris is critical for remyelination, we further asked whether Nrg-1β1 treatment promotes clearance of damaged myelin in demyelinating lesions of CPZ mice. Our quantitative immunohistochemical analysis for degraded myelin basic protein (dMBP) in the corpus callosum showed a robust 50.71-fold increase after 10 weeks of CPZ diet compared to the healthy controls with negligible baseline expression of dMBP, as expected (Fig. 3 c, e). During 2 weeks of spontaneous recovery post-CPZ diet, high levels of dMBP continued (59.18-fold) in

vehicle-treated CPZ mice compared to the basal levels of dMBP in the control healthy mice. Nrg-1 treatment, however, significantly (24.29%) reduced dMBP in CPZ lesions during the 2-week recovery period compared to the vehicle treated CPZ mice. After 4 weeks recovery, dMBP levels showed an overall reduction in vehicle-treated mice (32.31%) compared to the 10 weeks CPZ group. Nrg-1 treatment significantly reduced dMBP expression levels during the 4-week recovery period compared to both vehicle-treated mice (35.5%) and mice with 10 weeks of CPZ demyelination (56.34%) (Fig. 3 c, e). These findings suggest that Nrg-1 treatment promotes the clearance of myelin debris in chronic demyelinating lesions.

We previously identified an immunomodulatory role for Nrg-1 in EAE mice in promoting a pro-regenerative and disease-modifying phenotype in microglia [36]. Here, we investigated whether the beneficial effects of Nrg-1β1 treatment on chronic remyelination is through microglia regulation. Of note, we previously confirmed the expression of ErbB receptors in primary mouse microglia and bone marrow derived macrophages in vitro under both control and activated states[36]. Here, we further confirmed that CD11b+ cells (representing microglia and macrophages) express all three Nrg-1 receptors (ErbB-2, ErbB-3, and ErbB-4) in the brains of healthy control and CPZ-treated mice (Supplementary Fig. 2 a-c). We also assessed the expression pattern of ErbB-2, ErbB-3 and ErbB-4 receptors in the corpus callosum after chronic demyelination and under Nrg-1 treatment. Our immunohistochemical analysis showed a robust reduction in the overall expression levels of ErbB-2 (97%), ErbB-3 (95%), ErbB-4 (86%) receptors in chronic CPZ lesions compared to the control mice that were not spontaneously recovered after 4 weeks of recovery post-CPZ (Supplementary Fig. 2 a-c). Nrg-1 treatment, however, significantly increased the expression levels of all ErbB receptors compared to the vehicle treated group that resulted in full restoration of the ErbB3 and ErbB4 expression to the control basal level. Moreover, we specifically assessed

the expression levels of ErbB receptors in microglia that showed a similar pattern (Supplementary Fig. 2a-c).

To determine the role of microglia in Nrg-1 mediated effects on remyelination, we ablated microglia from the CNS by adding PLX5622, an inhibitor of CSF-1R (colony stimulating factor-1 receptor) [47], to the diet of the mice starting from 1 week before CPZ-withdrawal and continued throughout the treatment and recovery period. We first confirmed the efficacy of one-week PLX5622 treatment in microglia ablation prior to the start of Nrg-1 treatment. Our immunohistochemical assessment of Iba-1+ cells in the chronically demyelinated lesions of CPZ showed pronounced depletion of microglia (88.92% decrease) in PLX5622 treated CPZ mice compared to the non-PLX5622 treated counterparts at the start of Nrg-1β1 treatment that continued with the same efficacy during the 4 weeks of Nrg-1 treatment (Fig. 3 b). These experiments showed that the beneficial effects of Nrg-1β1 treatment on both removal of myelin debris and remyelination were abolished in those chronic CPZ mice that received PLX5622 during the 2- and 4 weeks post-CPZ recovery to a level that was no longer statistically different than vehicle-treated CPZ mice (Fig. 2 c-e).

We further assessed the degree of remyelination and ultrastructural properties of new myelin in the corpus callosum of chronic CPZ using transmission electron microscopy (TEM) (Fig. 3 f-j). Electron-micrographs showed extensive demyelination in the corpus callosum after 10 weeks of CPZ diet as expected (Fig. 3 g). Assessment of myelin g-ratio in the corpus callosum of the 10-week CPZ group showed a significantly higher g-ratio value (0.863) indicative of lower myelin thickness compared to the age-matched control group (0.685) (Fig. 3 h-i). After 4 weeks of recovery post-CPZ, g-ratio of the vehicle treated group (0.806) was modestly yet significantly improved compared to the 10-week CPZ value (0.863); however, it remained robustly and

significantly higher than the control mice (0.685) confirming our BGII myelin assessment that showed poor spontaneous remyelination in chronic demyelinated lesions. Importantly, 4 weeks of Nrg-1β1 treatment significantly increased the overall thickness of myelin in chronic CPZ mice compared to both 10-week CPZ and 4-week vehicle-treated groups, evidenced by a reduced g-ratio (0.725) that was no longer significantly different from the baseline g-ratio that was observed in the age-matched control mice. In the PLX5622 treated animals, Nrg-1β1 treatment did not show any beneficial effects on myelin g-ratio compared to vehicle treatment (0.810 in PLX+Nrg-1β1 vs. 0.811 in PLX+vehicle). The pooled g-ratio of quantified axons from every animal in each treatment group also confirmed a significantly thinner myelin sheath in vehicle treated animals compared to control, which was restored by administration of Nrg-1β1. This beneficial effect of Nrg-1β1 on myelin thickness could no longer be observed in PLX5622 microglia-depleted mice (Fig. 3 i). When we binned axons into different diameters, the same pattern in the g-ratio could still be observed in all axon diameters across treatment groups (Fig. 3 i). Notably, in the lower axon diameter bins, the difference between the treatment groups was more pronounced. By investigating the frequency distribution of myelin g-ratio, we found that the percentage of thinly myelinated axons (g-ratio > 0.8) was lower in Nrg-1β1-treated mice in comparison to vehicle-treated mice (18.06% vs. 56.22%, respectively), while in PLX5622 treated groups, the percentage was comparable between Nrg-1β1- and vehicle-treated groups (56.50% vs. 61.93%, respectively) (Fig. 3 h-j). Moreover, the percentage of heavily myelinated axons (g-ratio < 0.6) was higher in Nrg-1β1 treated mice compared to the vehicle treated group (7.98% vs. 1.64%, respectively) and closer to the normal control mice (18.80%). In the PLX5622 treated groups, the percentage was comparable between Nrg-1β1 and vehicle-treated mice (1.75% vs. 2.02%, respectively) (Fig. 3j).

We next asked whether Nrg-1β1 treatment after prolonged demyelination has any effects on the number of myelinated axons. Analysis of the density of myelinated axons on electron-micrographs of the corpus callosum showed a robust and significant decrease in the number of myelinated axons after 10 weeks of CPZ-induced demyelination (14.5-fold) compared to age-matched control mice, as expected (Fig. 3 k-l). After 4 weeks of recovery post-CPZ, there was no significant improvement in the number of myelinated axons in vehicle-treated mice compared to mice with 10 weeks CPZ, while mice with Nrg-1β1 treatment showed a significantly higher (5.3-fold) number of myelinated axons compared to 10 weeks CPZ group. However, there was no significant difference between Nrg-1β1-treated mice and their vehicle-treated counterparts. The beneficial effect of Nrg-1β1 treatment was not observed in PLX5622 treated mice. Collectively, these findings provided compelling evidence that Nrg-1 promotes chronic remyelination through microglia-dependent mechanisms.

Nrg-1β1 treatment enhances OPC proliferation, oligodendrogenesis and oligodendrocyte maturation partially through microglia

Impaired remyelination in chronic MS lesions has been attributed to a decline in the proliferation of OPCs or their ability to differentiate into mature myelinating oligodendrocytes [1]. To determine the impact of Nrg-1β1 treatment on various steps of the remyelination process, we took advantage of PDGFRα-Cre mice to track OPCs progenies. First, we tracked newly generated OPCs during the early recovery period after CPZ withdrawal by daily injections of EdU (Fig. 4 a). Our immunohistochemical assessment of the demyelinated lesions of corpus callosum for Olig2, a lineage marker of oligodendrocytes, confirmed a significant decrease in the number of Olig2+/GFP+ oligodendroglia after 10 weeks of CPZ diet (78% decrease) compared to the age-

matched healthy control (Fig. 4 b-c). The population of Olig2+/GFP+ cells within the corpus callosum increasingly recovered and reached the baseline control levels after 4 weeks recovery period post-CPZ withdrawal, suggesting the spontaneous repopulation of the lesion site with OPCs. Nrg-1β1 treatment significantly accelerated repopulation of Olig2+/GFP+ cells during the early phase of recovery at 2 weeks post-CPZ compared to the vehicle treated counterparts (1.8-fold) that restored oligodendrogenesis to a level comparable to the basal levels of the healthy control mice. The same trend was observed at 4 weeks recovery period although the difference between Nrg-1β1 and vehicle treated groups did not reach statistical significance (Fig. 4 c). The effect of Nrg-1β1 persisted in mice that received PLX5622 suggesting that Nrg-1 effects on the overall number of oligodendrocyte population was not microglia dependent (Fig. 4 b-c). Furthermore, we assessed the proliferative activity of OPCs during the early phase of remyelination by co-labeling of oligodendrocyte progenies marked as Olig2+/GFP+ cells with EdU. We found a 1.7-fold increase in proliferating Olig2+/GFP+/EdU+ cells under Nrg-1β1 treatment after 2 weeks of recovery period compared to vehicle treatment (Fig. 4 d). This trend persisted at the 4-week timepoint, where the population of Olig2+/GFP+/EdU+ cells increased by 1.8-fold in the vehicle-treated group compared to the 2-week recovery period. Nrg-1β1 treatment further augmented the abundance of these newly generated cells (1.5-fold increase) during the 4-week recovery period compared to the vehicle group. However, this increase was found to be independent of microglia, as PLX5622 did not alter the outcomes of Nrg-1β1 and vehicle treatment on the number of Olig2+/GFP+/EdU+ cells (Fig. 4 d). These results differ from Nrg-1-enhanced remyelination that is microglia-dependent as shown above, suggesting Nrg1 may regulate OPC proliferation and oligodendrogenesis differently than remyelination in chronic demyelinated lesions.

We next studied maturation of the newly generated oligodendroglia. Following a 10-week CPZ diet, there was a significant depletion of APC+/GFP+ mature oligodendrocytes within the corpus callosum consistent with demyelination. Two weeks after CPZ withdrawal, there was approximately 51% spontaneous restoration of APC+/GFP+ mature oligodendrocytes in the vehicle treated mice compared to the control group (Fig. 4 e-f). Of note, Nrg-1β1-treated mice exhibited a significantly higher number of APC+/GFP+ oligodendrocytes compared to the vehicle-treated group, reaching 90% of the baseline levels in the control conditions. Depletion of microglia using PLX5622 resulted in significant attenuation (50%) in the beneficial effects of Nrg-1β1 treatment on maturation of the newly formed oligodendrocytes. Moreover, we found similar results at the 4-week recovery timepoint. These data identify that Nrg-1β1 treatment enhances the differentiation of OPCs to mature oligodendrocytes partially through microglia dependent mechanisms.

We further examined the extent of oligodendrocyte maturation among the newly generated oligodendrocytes during early remyelination. Our analysis revealed a 1.7-fold increase in APC+/GFP+/EdU+ population with Nrg-1β1 treatment after 2 weeks of recovery compared to vehicle (Fig. 4 e, g). This trend persisted at the 4-week recovery time point, where Nrg-1β1 treatment significantly enhanced oligodendrocyte maturation (1.55-fold increase). Importantly, this augmentation was found to be unaffected by microglial depletion in Nrg-1β1 treatment group at both 2- and 4 weeks recovery period. In summary, these findings demonstrate that Nrg-1β1 treatment fosters OPC proliferation, oligodendrogenesis and oligodendrocyte maturation. Nrg-1β1 promotes oligodendrocyte maturation and remyelination in a microglia-dependent manner, while its effects on OPC proliferation is microglia-independent.

Nrg-1β1 treatment promotes microglia number and integrity in chronic demyelinating.

Excessive lipid accumulation in microglia by myelin phagocytosis and their impaired ability to process and release cholesterol induce cell death in foamy microglia [18,25,48]. Given Nrg-1β1 treatment attenuated microglia foaminess, we next asked whether it promotes microglia integrity and survival in demyelinating lesions. We first conducted microglia count by co-immunostaining for CD11b and the microglia-specific marker P2Y12 in chronic CPZ lesions across all experimental groups (Fig. 5 a-b). Our data confirmed the predominance of CD11b+P2Y12+ cells (indicative of microglia) over CD11b+P2Y12- cells (indicative of macrophages) within CPZ demyelinated lesions at both 2- and 4 weeks post-CPZ withdrawal in vehicle and Nrg-1β1 treatments (Fig. 5 a-b). Nrg-1β1 treatment resulted in a significant increase in the abundance of CD11b+P2Y12+ microglia at both 2 weeks (1.58-fold) and 4 weeks (1.43-fold) recovery timepoints compared to vehicle treatment (Fig. 5 b). The number of CD11b+P2Y12- macrophages remained unaffected in demyelinated lesions across all treatment groups and time points.

We next asked whether the elevated number of microglia under Nrg-1 treatment may reflect an increase in their proliferative activity. We assessed the number of proliferating microglia by co-labeling of EdU and CD11b in the lesions of CPZ mice that received EdU at week 10 post-CPZ and during post-CPZ recovery period under vehicle and Nrg-1 treatments. Analysis of EdU+/CD11b+ microglia in CPZ lesions after 10 weeks of demyelination showed a significant 4.49-fold increase in the proliferative activity of microglia compared to the healthy controls, which was expected as demyelination elicits microgliosis (Fig. 5 c-d). Next, we analyzed microglia proliferation during the earlier stage of remyelination post CPZ-induced demyelination. Assessment of EdU+ CD11b+ cells during the 2 weeks of recovery post-CPZ showed a significant decrease in microglia proliferation in the corpus callosum of vehicle treated mice (3.09-fold)

compared to those mice after 10 weeks of CPZ diet. Decrease in microglia proliferation was less pronounced in the Nrg-1 treated mice (1.49-fold) compared to the mice with 10 weeks of CPZ diet. Importantly, Nrg-1 treatment significantly enhanced microglia proliferation (2.07-fold) compared to vehicle treatment during the 2-week recovery period (Fig. 5 c-d). Moreover, we found that the long-term proliferation activity of microglia remained unchanged in the 4-week vehicle treated mice compared to their proliferative status after 2 weeks of recovery. Nrg-1 treated mice showed a significant rise in the number of EdU+ CD11b+ cells after 4 weeks of recovery that was comparable to the number of proliferating microglia in mice with 10 weeks CPZ demyelination and significantly higher (2.39-fold) than the vehicle treated counterparts.

We further examined whether Nrg-1β1 treatment promoted microglial abundance within the chronically demyelinated lesions by mitigating their cell death that is a characteristic of dysfunctional lipid droplet-rich foamy phagocytes [23,25]. Microglia cell death in remyelinating lesions is reported to be mediated through necroptosis [20]. Our analyses revealed a significant increase (8.53-fold) in the percentage of necroptotic microglia (marked by the necroptosis marker RIP3) in the corpus callosum of mice after 10 weeks of CPZ demyelination compared to the age-matched control mice (Fig. 5 e-f). During the recovery period, we observed a significantly higher percentage of necroptotic microglia at 2 weeks (39.7%) and 4 weeks (36.3%) post-CPZ compared to 10 weeks of CPZ diet (28.8%). Nrg-1β1 treatment significantly reduced the occurrence of RIP3+/CD11b+ cells at both the 2-week (16.5%) and 4-week (15.6%) recovery periods. These data show that Nrg-1 treatment promotes microglia proliferation and survival during the recovery from CPZ-induced demyelination. Nrg-1 effects on microglia proliferation evolves over time, whereas its positive effects on attenuating microglia necroptosis remains unchanged during the 2- and 4-week recovery periods. Altogether, our findings indicate that the availability of Nrg-1β1

promotes microglial abundance and integrity within the chronic demyelinated lesions, which is critical for remyelination.

Nrg-1β1 treatment attenuates microglia lipid load in chronic demyelinated lesions and preserves myelin during active CPZ demyelination.

We next examined the effects of Nrg-1β1 treatment on microglia lipid load within the chronically demyelinated lesions of CPZ mice. We studied esterified lipids by ORO staining as an indicator of the accumulation of intracellular myelin-derived cholesterol, a characteristic phenotype of foamy microglia and macrophages [19,26]. ORO intensity measurement showed a notable and significant increase in the overall levels of esterified lipids within the corpus callosum following 10 weeks of CPZ diet (5.66-fold) compared to the age-matched healthy mice. During the post-CPZ recovery period, the levels of esterified lipids were generally decreased over time in both vehicle- and Nrg-1- treated mice (Fig. 6 a-b). We further assessed the degree of intracellular myelin-derived cholesterol accumulation per microglia by normalizing the ORO signal intensity to the number of Iba-1+ cells per area in each treatment group (Fig. 6 c-d). Our findings revealed a robust and significant reduction (72%) in the intracellular esterified lipids in microglia following Nrg-1β1 treatment after a 2-week recovery period indicating that Nrg-1β1 treatment attenuates the intracellular accumulation of lipids and foaminess in microglia within the chronic CPZ demyelinated lesions. We also assessed the degree of ORO accumulation in demyelinating lesions of corpus callosum in PLX5622 treated CPZ mice and found no significant difference in the lesional levels of ORO of mice under the vehicle and Nrg-1β1 treatments in comparison to their respective counterparts (Fig. 6 a-b). We also examined the ORO content in the remaining microglia that persisted after PLX5622 treatment in CPZ mice under both vehicle and Nrg-1 treatments. Our

quantitative analysis of Iba-1+ cells showed that the number of remaining microglia was comparable between the PLX5622-vehicle and PLX5622-Nrg-1β1 treated mice (Fig. 6 e-f). Moreover, there was no difference in the cellular ORO content of Iba-1+ microglia (indicative of foaminess) between the PLX5622-vehicle and PLX5622- Nrg-1β1 treated mice, suggesting no significant effect of Nrg-1β1 on the lipid load of the small population of microglia (~11%) that were not depleted by PLX5622 treatment. Given astrocytes are shown to phagocytose myelin debris and process lipids in demyelinating lesions[49], we next studied the involvement of astrocytes in lipid processing in the absence of microglia in PLX5622 treated CPZ mice, and whether Nrg-1β1 treatment can influence astrocytic lipid processing. Analysis of ORO in GFAP+ astrocytes demonstrated the presence of ORO inside astrocytes (Fig. 6 g-h). Nrg-1β1 treatment significantly reduced intracellular astrocytic ORO content (37.98%) in CPZ lesions of PLX5622 treated mice compared to the vehicle treated counterparts indicating the potential of Nrg-1 treatment in enhancing astrocyte lipid processing following microglia depletion.

We further investigated the potential impact of Nrg-1β1 treatment on the expression of cholesterol efflux transporter, ABCA-1, in the chronic CPZ-induced demyelinated lesions. Immunohistochemical analysis of ABCA-1 expression levels in CD11b+ myeloid cells revealed that Nrg-1β1 treatment results in a significant increase (2.06-fold) in ABCA-1 levels per myeloid cell at 2 weeks post-CPZ diet compared to the vehicle treated CPZ mice (Fig. 6 i-j). However, no significant differences were observed at the 4-week recovery endpoint. These findings indicate that Nrg-1β1 treatment plays a role in the clearance of myelin debris and modulation of the cholesterol efflux machinery by microglia in the chronically demyelinated lesions.

Next, we asked whether availability of Nrg-1β1 treatment during active CPZ demyelination could preserve myelin. One week after the start of CPZ diet, mice received daily vehicle or Nrg-

1β1 treatment for 9 weeks until the experimental endpoint at the week 10 post-CPZ diet (Fig. 6 k). Analysis of myelination with BGII staining revealed that vehicle treated mice showed 89% reduction in myelination in the corpus callosum after 10 weeks of CPZ diet compared to the healthy baseline myelination. Nrg-1β1 treatment resulted in significant preservation of myelin (58% of baseline myelin content in control mice) that was 5.25-fold higher than the myelin content of vehicle treated 10-week CPZ mice (Fig. 6 l). Moreover, we assessed the levels of degraded myelin in CPZ lesions to confirm these data. Immunohistochemical analysis showed a robust increase in dMBP levels in the corpus callosum of vehicle treated mice (49.29-fold) after 10 weeks of CPZ diet compared to the healthy control mice, which was attenuated significantly (3.03-fold) in mice that received Nrg-1β1 treatment confirming myelin preservation (Fig. 6 m-n). Furthermore, assessment of ORO levels for accumulation of cellular lipid load in phagocytic cells in the corpus callosum of vehicle treated CPZ mice after 10 weeks of demyelination showed a significant (9.89-fold) increase in ORO compared to the baseline observed in the control mice. Nrg-1β1 treatment resulted in a 4.45-fold decrease in ORO signal compared to the vehicle treated counterparts that was no longer significantly different from control mice (Fig. 6 o-p). Altogether, these data indicate that the availability of Nrg-1 during active CPZ demyelination period can preserve and/or regenerate myelin.

Nrg-1β1 treatment enhances remyelination in demyelinated lesions of EAE mice.

We evaluated the effects of Nrg-1β1 treatment on oligodendrogenesis and remyelination in another chronic mouse model of MS, EAE, which represents an immunologically relevant disease model. In our previous work, we showed that Nrg-1β1 is depleted in EAE lesions and its therapeutic restoration positively modulates adaptive and innate immune responses including promoting a pro-

regenerative phenotype in microglia, and attenuating the disease severity by significant reduction in clinical scoring [36]. Here, we first examined the effects of Nrg-1β1 on oligodendrocytes in EAE lesions after 14 days of treatment (600 ng/day or 30μg/kg) starting at the EAE peak (around day 17-19 post EAE induction), as we previously described[36]. Analysis of Olig2+ oligodendrocytes in the EAE spinal cord lesions showed that Nrg-1β1 treatment significantly increased (1.58-fold) the overall number of oligodendrocytes compared to vehicle treated EAE mice (Fig. 7 a-b). To specifically determine the effects of Nrg-1β1 treatment on generation of new oligodendrocytes, EAE mice received EdU during the treatment period. We found a significant increase (4.60-fold) in the number of newly generated oligodendrocytes (Olig2+/EdU+) in the remyelinating lesions of Nrg-1 treated EAE mice compared to the vehicle treated EAE mice (Fig. 7 a, c).

Ultrastructural assessment of myelin g-ratio in the spinal cord of EAE mice at 42 days post EAE induction (~25 days after the EAE peak) demonstrated a significantly higher g-ratio value (0.70) compared to the age-matched control group (0.67) indicative of lower myelin thickness in EAE lesions (Fig. 7 d-e). EAE mice that received Nrg-1β1 treatment showed a significant improvement in myelin g-ratio (0.66) compared to the vehicle-treated mice that was restored to the baseline g-ratio of the healthy control mice (Fig. 7 e). Pooling of the calculated g-ratio from each animal within experimental groups further demonstrated a significant decrease in g-ratio across all axon diameters (Fig. 7 f). Additionally, frequency distribution of myelin g-ratio revealed significant changes in the pattern of myelin thickness following Nrg-1β1 treatment (Fig. 7 g).

We further analyzed the number of microglia and macrophages in EAE lesions after 2 weeks of Nrg-1β1 treatment. Our assessments showed no changes in the abundance of microglia (CD11b+/TMEM119+ cells) in EAE lesions under Nrg-1 treatment (Fig. 7 h), which confirms our previous report[36]. Assessment of macrophages (CD11b+/TMEM119- cells) in EAE lesions also

showed no significant changes between Nrg-1 and vehicle treated EAE (Fig. 7 h). However, analysis of ORO showed a significant reduction (24.43%) in the cellular lipid load in the EAE lesions of Nrg-1β1 treated mice compared to the vehicle treated counterparts (Fig. 7 i). Moreover, we analyzed cumulative disease burden for each animal as area under the curve from daily clinical scoring of EAE mice for 42 days. These data showed that Nrg-1β1 treatment starting at the peak of the disease reduces EAE disability compared to the vehicle treated mice that was significantly different at several timepoints (Fig. 7 j). However, the overall area under the curve did not reach the statistical significance point (p=0.054). Of note, our previous study in a larger number of mice and at various therapeutic timepoints showed a significant decrease in the disease severity of the EAE mice that received Nrg-1β1 treatment at the EAE onset, peak, post-peak as well as prophylactically at the time of EAE induction [36]. Taken together, our results in two chronic demyelinating animal models of MS demonstrate the beneficial effects of Nrg-1 treatment on promoting oligodendrogenesis that results in enhanced remyelination.

Ablation of endogenous Nrg-1 results in spontaneous demyelination and suppresses remyelination in chronic demyelinated lesions

We sought to further elucidate the impact of endogenous Nrg-1 on remyelination of chronically demyelinated CPZ lesions using a loss of function approach. We ablated Nrg-1 in adult mice using a tamoxifen inducible Cre conditional Nrg-1 knockout ($Nrg1^{fl/fl}$: UBC-Cre ^{ERTM}) model (Nrg-1 cKO). Upon Cre expression, exons 7-9 of Nrg-1 are excised, which encode EGF-like active domain that is crucial for Nrg-1 signaling [50]. We confirmed 79% and 80% reduction in the expression of Nrg-1 EGF-like domain in the cortex and corpus callosum of Nrg-1 cKO mice, respectively, compared to the Cre negative wild type (WT) mice (Fig. 8 a-c). At 16 weeks after

the start of tamoxifen injection (i.e. 14 weeks after 2 weeks of washout period), BGII myelin analysis showed 48% decrease in BGII myelin staining in the corpus callosum of Nrg-1 cKO mice spontaneously compared to WT controls (Fig. 8 d-e). Nrg-1 cKO mice that underwent 10 weeks of CPZ diet and 4 weeks of recovery period (i.e. 10+4 weeks paradigm), they showed significantly less spontaneous remyelination (60% decrease) during the recovery period as compared to the vehicle treated WT CPZ mice. Further analysis of dMBP in Nrg-1 cKO mice on normal diet at 16 weeks post-tamoxifen showed a significant and robust increase in dMBP levels (35.33-fold increase) compared to the negligible basal level of dMBP in the age-matched WT counterparts, confirming spontaneous demyelination (Fig. 8 f-g). Nrg-1 cKO mice that received CPZ diet for 10 weeks also showed a significantly higher level of dMBP (1.44-fold) compared to the Nrg-1 cKO mice on normal diet, although the difference was not significantly different than WT mice after 10 weeks of CPZ diet. When treated with exogenous Nrg-1β1 peptide in a rescue strategy during post-CPZ recovery period, BGII staining showed a significant increase in remyelination (4.15-fold) in CPZ demyelinated lesions of Nrg-1 cKO mice; however, it did not reach the levels observed in Nrg-1β1 treated CPZ WT mice (Fig. 8 d-e). Analysis of dMBP also showed that exogenous Nrg-1β1 treatment significantly reduced degraded myelin in both WT (1.86-fold) and Nrg-1 cKO mice (1.79-fold) compared to their vehicle-treated counterparts. Assessment of ORO revealed a significant increase in the lipid load of both WT (8.59-fold) and Nrg-1 cKO mice (11.08-fold) after 10 weeks of CPZ diet compared to their counterparts on normal diet that was decreased to the basal levels during the 4-week recovery period post CPZ withdrawal irrespective of exogenous Nrg-1β1 treatment (Fig. 8 h-i). These data show that Nrg-1 KO mice show significant spontaneous demyelination as evidenced by a decrease in myelination in corpus callosum and a concomitant increase in dMBP. However, there was no changes in the basal level of tissue and cellular lipids

(ORO) in demyelinating lesions of Nrg-1 cKO mice at the timepoint that we studied (Fig. 8 h-i). Of note, we examined myelination status of the brain in Nrg-1 cKO mice at the start of CPZ diet (i.e. two weeks after tamoxifen injection). Our analysis of BGII staining showed comparable levels of myelination in Nrg-1 cKO mice at 2 weeks post-tamoxifen compared to the age-matched WT control mice (Supplementary Fig. 3 a-b). We complemented our analysis with immunostaining for dMBP and found no detectable degraded myelin in Nrg-1 cKO mice at 2 weeks post tamoxifen and the start of CPZ diet (Supplementary Fig. 3 c-d). We also examined the presence of Iba-1+/DAPI+ cells and there was no change in the abundance of microglia between the Nrg-1 cKO and wildtype mice. Of note, we confirmed that microglia express ErbB-2, ErbB-3 and ErbB-4 receptors in Nrg-1 cKO mice (Supplementary Fig. 3e). These data suggest the absence of demyelination and microgliosis in Nrg-1 cKO mice at the start of CPZ-diet at 2 weeks post-tamoxifen.

Ultrastructural analyses of myelin g-ratio also revealed that Nrg-1 ablation results in significant spontaneous thinning of the myelin sheath (Fig. 8 j-m). Under CPZ demyelination, the overall g-ratio value in the Nrg-1 cKO group was not significantly different than the WT counterparts. The pooled g-ratio of all quantified axons from each group revealed a pattern suggesting higher g-ratios (i.e. lower myelin thickness) across all the axons in Nrg-1 cKO mice compared to WT controls (Fig. 8 j-k). Exogenous Nrg-1β1 treatment led to a significant increase in the overall myelin thickness in Nrg-1 cKO mice as indicated by a decrease in g-ratio (0.775), demonstrating the efficacy of Nrg-1β1 treatment in promoting myelin thickness (Fig. 8 k-l). Binning the axons into different diameters revealed consistent pattern of changes in g-ratio across all axon diameters (Fig. 8 l), with more pronounced differences in axons with lower diameters. The frequency distribution of myelin g-ratio also showed an increased percentage of thinly

myelinated and a decreased percentage of heavily myelinated axons in Nrg-1 cKO mice on a normal diet (43.85% and 4.63%, respectively) compared to WT controls (17.62% and 19.81%, respectively) (Fig. 8 m). Under CPZ demyelination and after 4 weeks of recovery period, the percentage of thinly myelinated axons was higher, in Nrg-1 cKO group compared to WT mice (68.56% in WT vs. 83.85% in Nrg-1 cKO). The percentage of heavily myelinated axons was negligible in these two groups (1.29% in WT vs. 0.07% in Nrg-1 cKO). However, with exogenous Nrg-1β1 treatment, Nrg-1 cKO mice in the rescue group showed a reduced frequency distribution of thinly myelinated and a higher percentage of heavily myelinated axons 4 weeks after CPZ withdrawal (42.07% and 6.19%, respectively). These results confirm that endogenous Nrg-1 is important for proper brain myelination in adulthood and plays an important role in remyelination during chronic demyelinating episodes.

We next asked whether spontaneous disruption of myelin and reduced remyelination capacity in Nrg-1 cKO mice is a result of reduced oligodendrocyte numbers. Using immunohistochemical analysis for Olig2 and APC, we found a slight but not significant decrease (21%) in the abundance of Olig2+ cells in Nrg-1 cKO mice on a normal diet compared to WT controls (Supplementary Fig. 4 a, c). Following a 10-week CPZ diet, the number of Olig2+ cells dropped significantly in both WT and Nrg-1 cKO mice, as expected. After a 4-week recovery period post-CPZ withdrawal, both WT and Nrg-1 cKO mice showed comparable replenishment in the number of Olig2+ cells, although the levels failed to return to the control baseline (47% and 44% of baseline, respectively). Treatment with Nrg-1β1 during the recovery period restored the number of Olig2+ cells to the baseline levels in WT mice (92% of baseline). An increase was also observed in Nrg-1 cKO mice after Nrg-1β1 treatment (74% of baseline), although it was less pronounced than WT mice. Analysis of APC immunostaining also revealed a comparable number

of APC+ mature oligodendrocytes within the corpus callosum of Nrg-1 cKO mice on a normal diet compared to WT controls (Supplementary Fig. 4 b, d). After 10 weeks of CPZ diet, as expected, APC+ mature oligodendrocytes were scarcely present in the WT and Nrg-1 cKO mice. Following 4 weeks of recovery, the number of APC+ cells in the vehicle treated WT mice and Nrg-1 cKO mice was not statistically different. Moreover, Nrg-1β1 treatment led to a comparable increase in the number of APC+ cells in both WT mice and Nrg-1 cKO mice reaching the levels close to the baseline healthy aged-matched control mice. Altogether, we show that while ablation of endogenous Nrg-1 interrupts the process of myelination in the adult brain during homeostasis or in remyelination after a chronic demyelinating condition, it does not affect the number of oligodendrocytes per se within the 16-week conditional knockout timepoint in this study.

Nrg-1β1 promotes the capacity of microglia for myelin clearance and cholesterol recycling and release through PPARγ and LXR mediated machinery.

We next aimed to identify the cellular and molecular mechanisms by which Nrg-1β1 treatment regulate microglia function during the remyelination process using relevant in vitro platforms. In pure primary mouse cortical microglia cultures, we activated microglia, with lipopolysaccharide (LPS), a well-known pro-inflammatory stimulus, along with interferon-gamma (IFN-γ), an MS pathogenic cytokine. Nrg-1β1 treatment was added to the microglia cultures in both control non-activated and activated (LPS+IFN-γ) states. To assess the effects of Nrg-1β1 on the capacity of microglia for phagocytosis of myelin debris, primary microglia were exposed to myelin fragments extracted from yellow fluorescent protein (YFP) transgenic mouse (129 Tg (CAGEYFP) 7AC5Nagy/J) to allow tracking myelin phagocytosis. Of note, in this transgenic mouse, YFP is expressed under beta-actin promoter that is in the cytoskeleton associated with myelin sheath. We

verified specificity and co-localization of YFP signal in myelin fragments phagocytosed by microglia by fluoromyelin staining and confocal Z-stack images (Supplementary Fig. 5 a-b). Analysis of YFP signal intensity in microglia exposed to myelin fragments showed that LPS+IFN-γ activated microglia exhibited higher ability for myelin phagocytosis compared to non-activated control microglia after 6 and 24 hours of myelin exposure (1.73-fold at 6hr and 1.94-fold at 24 hr) (Fig. 9 a-c, Supplementary Fig. 5c). Nrg-1β1 treatment significantly promoted myelin phagocytosis of activated microglia (2.98-fold at 6hr and 3.11-fold at 24 hr), while it had no significant effect on non-activated control microglia suggesting that Nrg-1 primarily modulates inflammatory microglia. We further investigated the inflammatory status of microglia under Nrg-1 treatment. Our quantitative PCR of activated microglia confirmed robust upregulation of several key pro-inflammatory cytokines including *TNF-α* (223.58-fold), *IL-6* (300.36-fold), and *IL-1β* (87.87-fold) compared to non-activated microglia in culture. Nrg-1 treatment in activated microglia culture significantly reduced upregulated levels of *TNF-α* (4.42-fold), *IL-6* (5.41-fold), *IL-1β* (4.50-fold) compared to non-treated activated microglia (Fig. 9 d). Nrg-1 treatment in control non-activated microglia had no effects on the baseline of cytokine expression in microglia.

To determine whether the elevated extent of myelin phagocytosis would result in cholesterol accumulation within microglia, we stained microglia cultures under various conditions with Filipin III (FIII) and ORO, which detect free cholesterol and esterified lipids, respectively (Fig. 9 e). We observed a significant increase in both FIII (4.6-fold) and ORO (2.1-fold) signal intensity in LPS+IFN-γ-activated microglia with Nrg-1β1 treatment after 24 hours of myelin exposure compared to non-treated activated microglia (Fig. 9 e-f). When myelin exposure was prolonged to 72 hours, FIII and ORO levels in activated microglia were higher compared to non-activated microglia (FIII: 1.74-fold, ORO: 1.99-fold) (Supplementary Fig. 5 c-e). However, in

contrast to its promoting effects on cholesterol accumulation at 24 hours, Nrg-1β1-treated activated microglia had comparable FIII and ORO content at 72 hours similar to the levels detected in non-treated activated microglia (Supplementary Fig. 5 c-e).

We next examined whether the positive effects of Nrg-1β1 treatment on reduced intracellular cholesterol is a result of enhanced cholesterol efflux. To this end, we assessed the expression levels of two key cholesterol efflux transporters, *Abcg-1* and *Abca-1*, in microglia as well as their cholesterol release to the media. Our quantitative PCR on microglia revealed that exposure to myelin fragments triggered an upregulation in *Abcg-1* and *Abca-1* mRNA expression in non-activated control microglia (8.25-fold in *Abcg-1* and 1.98-fold in *Abca-1*) compared to the control microglia with no myelin exposure (Fig. 9 g). Activation with LPS+IFN-γ resulted in a significant downregulation of *Abcg-1* (89.59%) in microglia exposed to myelin compared to the non-activated microglia with myelin exposure. Although *Abca-1* expression also showed (36.85%) decrease in activated microglia with myelin exposure compared to non-activated microglia, it was not statistically significant. Nrg-1β1 treatment had no significant effects on the expression levels of *Abcg-1* and *Abca-1* mRNA in activated microglia compared to non-treated activated microglia (Fig. 9 g).

Next, we studied cholesterol release by microglia under various conditions. We found a significant elevation in the cholesterol concentration of microglia conditioned media (MCM) across all conditions after 72 hours following myelin exposure, indicating the ability of microglia in processing of cholesterol in phagocytosed myelin, and its release extracellularly to their microenvironment (Fig. 9 h). Notably, upon activation with LPS+IFN-γ, myelin-exposed microglia exhibited a significant (20%) decrease in their cholesterol release. Nrg-1β1 treatment resulted in a significant increase in cholesterol concentration (1.56-fold) of the MCM from

activated microglia, demonstrating a positive role for Nrg-1 in enhancing cholesterol recycling and release by microglia during the phagocytosis of myelin debris.

We further examined whether the effects of Nrg-1β1 treatment on microglia cholesterol recycling and release are mediated through ErbB receptors. We used two specific inhibitors of ErbB-2 and ErbB-3, two key receptors that collaboratively mediate Nrg-1 signaling through heterodimerization. ErbB-3 has the ligand domain that allows binding to Nrg-1, while ErbB-2 has the tyrosine kinase domain to activate downstream pathways [35,51]. Heterodimerization of these two receptors with each other and with ErbB4 is critical for activity of Nrg-1 signaling. We first performed a concentration gradient study for Mubritinib (TAK-165) that is a potent and selective inhibitor of ErbB-2, and TX1-85-1 that potently inhibits ErbB-3 receptors and can also bind to ErbB-2 with a lower affinity. Multiple concentrations of TAK-165 (100nM, 250nM, 500nM, 1μM), and TX1-85-1 (2μM, 5μM, 10μM), alone and in combination, were tested to determine non-toxic and effective concentrations. For this proof-of-concept study, we first used primary cultures of mouse neural progenitor cells (NPCs) that highly express ErbB receptors[40] and yield a high number of cells in culture for the initial proof-of-concept testing (Supplementary Fig. 6). For toxicity, Live/Dead Assay was performed in NPC culture after 24 hours of treatment with the ErbB inhibitors. While these ErbB inhibitors slightly decreased cell viability, the survival rate of NPCs was reduced more significantly at 1μM for TAK165 and at 10μM for TX1-85-1 and robustly with the combination of 1μM of TAK165 + 10μM of TX185-1. For evaluating the efficacy of these inhibitors in blocking Nrg-1 effects, we treated the cells with ErbB inhibitors for 4 hours followed by 1-hour Nrg-1 treatment. Then, immunostaining for phosphorylated Erk1/2, a known downstream effector of Nrg-1/ErbB signaling, was performed. We found Tx1-85-1 at 2μM and 5μM, and the combination of Tx1-85-1 (2μM) + TAK165 (250nM) and Tx1-85-1 (5μM) +

TAK165 (500nM) were effective in reversing the Nrg-1 induced activity of Erk1/2 in NPCs to its baseline control level while being relatively non-toxic (Supplementary Fig. 6). Next, we tested these concentrations in primary mouse microglia culture and confirmed similar results as NPCs (Supplementary Fig. 7). Our proof-of concept study in microglia showed the same efficacy for Tx1-85-1 at 2μM and 5μM and for Tx1 and TAK165 combination at [Tx1-85-1 (2μM) + TAK165 (250nM)] and [Tx1-85-1 (5μM) + TAK165 (500nM)] in blocking microglia Erk1/2 phosphorylation (Supplementary Fig. 7). Thus, we used Tx1-85-1 (2μM) and [Tx1-85-1 (2μM) + TAK165 (250nM)] for further studies in microglia. Using these concentrations in cultures of activated microglia that were treated with myelin particles, we found that co-inhibition of ErbB-2 and ErbB-3 receptors or solitary inhibition of ErbB-3 completely abolishes the positive effects of Nrg-1 on microglia cholesterol recycling and release (Fig. 9 i) confirming the involvement of Nrg-1/ErbB signaling in these processes.

To further unravel the molecular mechanisms underlying the effects of Nrg-1β1 on cholesterol transport and release in microglia, we studied two key pathways involved in these processes, the Liver X Receptor (LXR) and the Peroxisome Proliferator-Activated Receptor Gamma (PPARγ). LXR is known to regulate cholesterol processing and release[52]. PPARγ is implicated in lipid metabolism in myeloid cells and can modulate the expression of LXRα, along with other genes involved in fatty acid and cholesterol metabolism [27,28,53]. To verify whether Nrg-1 mediated effects on cholesterol excretion in LPS+IFN-γ activated microglia is mediated through the LXR and PPARγ pathways, we functionally blocked these pathways in microglia by GSK2033 and GW9662, respectively. To determine the optimal concentration of these inhibitors, we first conducted a gradient cell toxicity assay (Supplementary Fig. 8 a-c). Our analyses identified 10μM for GW9662 and 1μM for GSK2033 as effective concentrations in our experiments. Next, qPCR

analyses showed that blockade of LXR and PPARγ significantly suppresses ABCA-1 and ABCG-1 expression in activated microglia with or without Nrg-1β1 treatment, with the LXR antagonist GSK2033 exhibiting a more pronounced effect (Supplementary Fig. 8 d-e). Importantly, our functional assessment confirmed the involvement of LXR and PPARγ in Nrg-1 effects on cholesterol release by microglia because the beneficial effects of Nrg-1β1 were abrogated by blocking these pathways (Fig. 9 j). These findings identified that Nrg-1β1 promotes the capacity of microglia for cholesterol release through the LXR and PPAR-γ mediated cholesterol efflux machinery.

Nrg-1β1 treated microglia promote oligodendrocyte maturation and myelination via paracrine factors.

Since we found that Nrg-1β1 treatment promotes cholesterol release of activated microglia after myelin phagocytosis, we next investigated whether the increased cholesterol release by microglia promotes the capacity of OPCs for differentiation to mature myelinating oligodendrocytes. We designed a series of in vitro experiments in which we exposed mouse primary cortical OPCs to microglia conditioned media (MCM) from different conditions as described above with or without myelin exposure. We also included a control condition where OPCs were treated with Nrg-1β1 directly[37]. We first evaluated OPC transition into mature myelinating oligodendrocytes after 14 days in culture. Our analysis showed maturation of OPCs to oligodendrocytes in vitro as many cells expressed the oligodendrocyte marker O4 under various conditions (Fig. 10 a-b). Intensity measurement of O4 expression in these cultures revealed a significant increase in the maturation level of oligodendrocytes (2.15-fold) in cultures directly treated with Nrg-1β1 treatment compared to the control cultures. We also found the direct effects of Nrg-1β1 on promoting the number of

mature oligodendrocytes (1.49-fold) and expression level (3.00-fold) of myelin basic protein (MBP) compared to the control cultures. These data confirmed the known positive effects of Nrg-1β1 on oligodendrocytes in vitro (Fig. 10 a-c). Importantly, our analysis of OPC cultures treated with the MCM of Nrg-1β1 treated activated microglia (LPS+IFN-γ+Nrg-1β1) exposed to myelin exhibited significantly elevated levels of O4 expression (1.66-fold) compared to the MCM of LPS+IFN-γ+ activated microglia exposed to myelin and all other microglia conditions, albeit the number of O4+ cells was comparable (Fig. 10 b). Moreover, MCM of myelin+LPS+IFN-γ+Nrg-1β1 treated microglia significantly enhanced the expression levels of MBP in oligodendrocytes (1.68-fold) compared to the myelin+LPS+IFN-γ condition (Fig. 10 c). Our analysis showed no effects from the MCM of Nrg-1β1-treated microglia that were not exposed to myelin fragments on oligodendrocyte maturation, suggesting that Nrg-1β1 treatment promotes the capacity of activated microglia for supporting OPC maturation through myelin phagocytosis and lipid processing. These data also ruled out the potential direct effects of any residual Nrg-1 treatment in MCM on OPC maturation, as there were no beneficial effects from the MCM of Nrg-1β1 treated activated microglia without exposure to myelin fragments.

Next, we sought to determine whether activated microglia treated with Nrg-1β1 can promote the myelination capacity of oligodendrocytes in a paracrine manner. To this end, we cultured OPCs with MCM from myelin exposed activated microglia with and without Nrg-1β1 treatment on nanofibrous scaffolds designed to mimic axonal structures and provide a platform for oligodendrocytes to ensheath and myelinate (Fig. 10 d-e). We maintained oligodendrocytes for 4 weeks to ensure adequate time for maturation and myelination. Our myelination assessment using MBP immunostaining revealed that direct addition of Nrg-1β1 treatment to oligodendrocyte cultures significantly promoted the number (1.7-fold) and length (2.4-fold) of myelin sheaths per

wrapping oligodendrocyte (Fig. 10 d-e), which we had shown previously[37]. Oligodendrocytes that were exposed to MCM from Nrg-1β1 treated activated microglia exposed to myelin fragments also showed a significant increase in both the number (2.01-fold) and length (2.86-fold) of myelin sheaths per oligodendrocyte compared to the control MCM. Importantly, blocking ErbB receptors in microglia completely reversed the positive effects of MCM from the Nrg-1β1 treated microglia on oligodendrocyte myelination. These in vitro results support our in vivo data that availability of Nrg-1β1 fosters the potential of activated microglia to promote maturation of OPCs to myelinating oligodendrocytes through paracrine interactions that are mediated through ErbB receptors.

Transcriptomic analysis attests Nrg-1 treatment enhances microglial phagocytosis, cholesterol metabolism and cell survival in chronic cuprizone lesions

To further confirm our in vivo data regarding the effects of Nrg-1β1 treatment on microglia within the chronic CPZ lesions, we conducted bulk RNA sequencing on CD11b+ microglia isolated from the corpus callosum of control and CPZ mice 2 weeks after withdrawal of CPZ by magnetic activated cell sorting (MACS). Of note, our immunohistochemical analysis of chronic CPZ lesions determined that ~90% of CD11b+ cells constitute microglia (marked by TMEM119) (Fig. 4 c-d), confirming that microglia represent a large population of MACS isolated CD11b+ cells. RNAseq of isolated microglia from chronic CPZ lesions identified 382 differentially expressed genes (DEG) compared to the age-matched control group (Supplementary Fig. 9 a-c). The list of 382 DEG is provided in Source Data File. Among these transcripts, we detected an upregulation in select genes related to phagocytosis and cell death and downregulation of genes involved in lipid metabolism and cell survival in microglia within demyelinating lesions (Supplementary Fig. 9, b-c). Comparing Nrg-1 and vehicle treatment, 619 DEG were identified including select genes

associated with inflammation, phagocytosis, lipid metabolism and biosynthesis, cholesterol transport and efflux. The list of 619 DEG is provided in Source Data File. Moreover, there was an upregulation in some cell survival genes, while some genes implicated in cell death were downregulated in Nrg-1 treated mice compared to the vehicle treated counterparts. We also found significant upregulation of some genes associated with Akt, a key downstream pathway of Nrg-1 signaling, in Nrg-1 treated mice compared to vehicle counterparts. Overall, these complementary microglia transcriptomics data further confirm our in vivo and in vitro findings that Nrg-1 treatment increases microglia integrity and their capacity for phagocytosis and processing of myelin debris in chronic demyelinated lesions.

Discussion

In this study, we demonstrate that spontaneous remyelination is impaired after prolonged brain demyelination in mice. Remyelination failure is also a hallmark of chronic lesions in progressive MS, where it has been largely attributed to a maturation arrest of OPCs to myelinating oligodendrocytes [5-13]. Using a cuprizone (CPZ) model of chronic demyelination that results in impaired remyelination, and transgenic PDGFRα-Cre mice, we show that adequate remyelination fails despite the repopulation of oligodendrocyte lineage cells in these lesions. We provide evidence that correlates impaired oligodendrocyte maturation and remyelination with persistent dysregulation of Nrg-1 in chronically demyelinating lesions, a pathology that we had previously reported in human SPMS lesions [36]. Short-term CPZ demyelination also results in downregulation of Nrg-1 in the brain. However, following a recovery period, Nrg-1 expression is restored to its baseline levels in acute demyelinated lesions that is correlated with successful spontaneous remyelination. We show that Nrg-1 is primarily expressed by neurons and that it is also localized

in axons, and by oligodendrocytes in the adult brain as reported previously [35,40]. While the underlying mechanisms of Nrg-1 downregulation in demyelinated lesions needs in-depth investigations, it may reflect the loss of mature oligodendrocytes that are a major source of Nrg-1 and/or declined neuronal/axonal source of Nrg-1 due to degeneration and injury. In fact, the persistent depletion of Nrg-1 in chronic CPZ lesions and the lack of its restoration during the recovery period after prolonged demyelination supports this hypothesis that neurodegeneration and loss of mature oligodendroglia may attribute to Nrg-1 depletion in chronic demyelinated lesions. Furthermore, Nrg-1 restoration in acute CPZ lesions is attributed to the recovery of Nrg-1 levels in both axonal and oligodendroglial populations. Collectively, these findings identify Nrg-1 dysregulation as an endogenous mechanism that appears to be an underlying cause of poor remyelination in chronic demyelinated lesions. Therapeutically, we show that restoration of Nrg-1 is sufficient to support remyelination of chronically demyelinated axons by facilitating the transition of newly generated oligodendrocytes into a mature myelinating phenotype. Mechanistically, our parallel in vitro and in vivo findings reveal that Nrg-1β1 exerts its remyelination effects largely through modulation of microglia by shifting their phenotype from foamy dysfunctional to a reparative state characterized by enhanced myelin phagocytosis and cholesterol recycling and release. Adult mice with conditional ablation of Nrg-1 also show spontaneous demyelination and poorer remyelination following chronic CPZ-induced demyelination that further corroborates the impact of Nrg-1 dysregulation on impaired remyelination in chronic demyelinated lesions.

In the homeostatic adult brain, OPCs and oligodendrocytes maintain a low-rate level of cholesterol synthesis as they rely partially on other glia and neurons for the provision of cholesterol [54,55]. Evidence from MS and chronic CPZ demyelinated lesions also shows that cholesterol

biosynthesis by neurons contributes to remyelination by supporting OPC proliferation[56]. However, in chronic demyelinating lesions, astrocytes and myelin debris-clearing microglia become less efficient in supplying cholesterol to oligodendrocytes that contributes to sustained demyelination [18,19,23,25]. Microglia are highly plastic cells capable of adopting diverse phenotypes to perform various functions within the CNS [14,43,57,58]. In MS, microglia within active lesions are typically activated and engaged in either promoting or resolution of neuroinflammation and facilitating the repair processes [44,59-65]. Microglia promote remyelination through various mechanisms that include clearance of myelin debris by phagocytosis, intracellular recycling of myelin derived cholesterol, and supporting oligodendrocytes maturation and myelination by paracrine secretion of cholesterol as well as growth factors and cytokines such as activin-A, IGF1, IL1β, and TNFα [18,19,22,25,41-43,66-70]. In lesions of progressive MS, microglia are abundantly present [26,30-32]. However, with aging and chronicity of MS, microglia lose their capacity to support remyelination [18,19,23,25,44]. This inability is attributed to accumulation of intracellular myelin-derived lipids and acquiring a foamy phenotype [18,19,23-25]. The overloading of myelin debris and the burden of myelin processing eventually drive microglial dysfunction, with senescence as one proposed mechanism [18,19,23,25,29]. Recently, evidence from a genetic model of remyelination failure showed an upregulation in the lipid binding and lipid metabolism related genes, as well as an accumulation of neutral lipids within microglia that further support the crucial role of microglial lipid metabolism in successful remyelination [71]. Here, we demonstrate the abundance of lipid-laden dysfunctional foamy microglia within chronic lesions of human SPMS, as well as the brain of chronic CPZ mice. This is in agreement with previous studies that showed the existence of these cholesterol-laden foamy phagocytes within active MS lesions and in the rim of chronic mixed active/inactive lesions (chronic active lesions) of MS, both of which are present in the progressive phase of the disease

[26,30-32]. Altogether, it is increasingly recognized that the presence of foamy microglia is not only a marker of chronic demyelination but also contributes to sustained neuroinflammation [18,19,23,25,72].

We provide evidence that the downregulation of Nrg-1 appears to be an underlying mechanism that drives microglia dysfunction. Mechanistically, our collective data suggest that microglia within the corpus callosum of Nrg-1 treated CPZ mice demonstrate a pro-remyelination profile characterized by enhanced myelin phagocytosis, cholesterol metabolism and efflux that consequently promote microglia health by increasing their proliferation and reducing microglia cell death. This restoration of cholesterol recycling and excretion with Nrg-1 treatment likely underpins the reduction in lipid-laden microglia in chronic CPZ lesions and enhanced remyelination that we have observed in this study. Recent evidence shows that an increase in the intracellular levels of cholesterol precursors and derivatives following myelin internalization activates LXR pathway, a key regulator of lipid homeostasis [18,23]. Activation of LXR as well as PPAR-γ pathways is shown to facilitate the removal of excess cholesterol and preventing the formation of toxic lipid droplets [18,27,28,73-75]. However, as MS lesions progress to a chronic state, microglia accumulate cholesterol and are laden with lipid droplets that form cholesterol crystals [18,19,24,25]. Formation of these foamy phagocytes is shown to be the result of incomplete recycling of lipids from the internalized myelin debris, partly due to insufficient LXR activation [18,19,23,25,72]. Our in vitro findings also confirm an increase in phagocytosis of myelin debris along with a defective cholesterol efflux in pro-inflammatory primary microglia compared to homeostatic microglia.

Our data establish that Nrg-1 treatment elevates cholesterol excretion via modulation of LXR and PPAR-γ pathways. Recent studies have shown that promoting the activity of LXR pathway can enhance remyelination of demyelinated lesions [76,77]. Reports from the cardiovascular

system also suggest that Nrg-1 enhances cholesterol release in macrophages that attenuate formation of foamy macrophages and atherosclerosis [78]. The role of LXR and PPAR-γ in modulating microglial phenotype extends beyond cholesterol metabolism. These pathways also exert anti-inflammatory effects in microglia by attenuating the expression levels of pro-inflammatory cytokines via trans-repression of target genes of nuclear factor kappa B (NF-κB) [79-81]. We previously demonstrated that Nrg-1 treatment supports a phenotype shift in microglia and macrophages from pro-inflammatory to neuroprotective and pro-regenerative states in EAE, acute lysolecithin-induced demyelination, and spinal cord injury models [36,37,82]. Here, we also confirm that Nrg-1 treatment reduces the expression of pro-inflammatory cytokines in activated microglia. Thereby, we propose that by activating the LXR and PPAR-γ pathways, Nrg-1 may not only augment cholesterol efflux but also support a shift in microglia inflammatory profile towards a phenotype conducive to tissue repair and remyelination. This effect was indeed observed in our in vitro experiments, where the conditioned media collected from activated microglia treated with Nrg-1 promoted maturation of OPCs and supported myelination by the resulting oligodendrocytes. Our in vitro data also provide direct evidence that Nrg-1 mediates its positive effects on microglia myelin phagocytosis, lipid processing and oligodendrocyte myelination through ErbB-2 and ErbB-3, as blocking these receptors reversed Nrg-1 effects. However, further molecular studies are required to identify the intracellular cascades between Nrg-1/ErbB signaling and LXRs and PPARs pathways. In the PNS, Nrg-1 signaling, through heterodimerization of ErbB-2/ErbB-3 receptors, also supports cholesterol biosynthesis in Schwann cells by coordinating the activity of downstream $Ca2^{+}$/CAMK and MAPK pathways and regulating the expression of Maf transcription factor [83]. Thus, Nrg-1 may regulate cholesterol biosynthesis through various downstream pathways and in a context dependent manner. Overall, our findings underscore the potential of Nrg-1 treatment for

augmenting remyelination of chronically demyelinated white matter by promoting the reparative capacity of microglia for remyelination.

We demonstrate that the effect of Nrg1 on oligodendrocyte maturation and remyelination is microglia dependent while its effect on OPC proliferation is microglia independent. These differential outcomes may reflect the complexity and multi-step processes that are involved in oligodendrogenesis and oligodendrocyte maturation and remyelination. OPC proliferation and oligodendrocyte maturation represent different steps of these processes that are regulated by various cell types in the CNS including microglia [84,85]. While mechanistic studies are required to elucidate Nrg-1 regulation of OPC proliferation and oligodendrocyte maturation and myelination in demyelinating lesions, our current evidence suggests that Nrg-1 plays a more prominent role in regulating microglia lipid processing that is associated with remyelination. Given our data that Nrg-1 can regulate OPCs and oligodendrocytes directly, it is plausible that Nrg-1 promotes OPC proliferation through direct effects in vivo [37].

Although our in vivo and in vitro findings established the importance of microglia in mediating the beneficial effects of Nrg-1 treatment on remyelination, we cannot rule out its potential effects on astrocytes and their role in promoting lipid metabolism and remyelination in chronic demyelinating lesions. A recent study in acute lesions of LPC-induced demyelination has demonstrated that astrocytic downregulation of cholesterol biosynthesis pathways can lead to remyelination failure [86]. The presence of myelin debris and accumulation of lipid droplets have been shown in astrocytes within active demyelinating lesions of various diseases including MS [49] indicating the capacity of astrocytes for myelin phagocytosis and lipid processing. Our study also shows the ability of astrocytes in accumulating and processing lipids intracellularly in demyelinating lesions of CPZ mice in the absence of microglia that is enhanced by Nrg-1 treatment

providing evidence for the potential role of Nrg-1 in regulating astrocytic lipid processing. Our previous work also demonstrated that Nrg-1 treatment attenuate astrocyte reactivity to inflammatory stimuli including their expression of chondroitin sulfate proteoglycans (CSPGs) [87] that are known to inhibit remyelination [88,89]. Nonetheless, while astrocyte-mediated effects of Nrg-1 on remyelination is plausible, our current data from the chronic CPZ lesions affirms a prominent role for microglia as PLX5622 markedly reversed Nrg-1 beneficial effects on remyelination especially at the 2-week recovery period. Of note, PLX5622 also depletes border associated and monocyte derived macrophages [90,91]. However, our immunohistochemical characterization of CPZ-induced demyelinated lesions of corpus callosum showed that ~90% of CD11b myeloid cells are P2Y12 expressing microglia.

Nrg-1 treatment significantly increases microglia proliferation and reduces their necroptosis that collectively lead to an increase in the abundance of microglia within remyelinating lesions. We found that the effects of Nrg-1 on microglia proliferation evolves over time, whereas its positive effects on microglia survival remains unchanged during the recovery periods. Recent evidence suggests that necroptosis is a main pathway causing inflammatory microglial cell death in demyelinated lesions [20]. Necroptosis is mediated by receptor-interacting protein kinase 1 and 3 (RIPK1, RIPK3) and mixed lineage kinase domain-like protein (MLKL) and is associated with inflammation and cell lysis [92]. Blocking necroptosis by inhibiting RIPK1 is shown to modulate neuroinflammation and promote remyelination [93,94]. A study on skin flap transplantations has shown that Nrg-1 treatment successfully inhibits necroptosis and pyroptosis in ischemic flaps [95]. This effect was through the inhibition of STING (stimulator of interferon genes) activity. STING is a protein involved in secretion of several pro-inflammatory cytokines through AKT phosphorylation that is a well-known downstream pathway for Nrg-1 signaling [35,95,96]. Activation

of AKT downstream of the Nrg-1 signaling is also shown to prevent neurotoxicity [97,98]. Overall, our findings in chronic CPZ lesions point to the beneficial role of Nrg-1 in maintaining microglia integrity within chronic demyelinated lesions and thereby provides a supportive environment for remyelination.

Our Nrg-1 knockout studies provide further support that endogenous Nrg-1 plays an important role in myelination and maintaining myelin integrity. We found that conditional ablation of Nrg-1 in the adult CNS results in white matter hypomyelination and myelin thinning over time. Moreover, when Nrg-1 cKO mice were challenged with chronic CPZ demyelination, they showed an even lower degree of remyelination in the absence of Nrg-1 signaling, which could be rescued by exogenous Nrg-1 in chronic CPZ lesions of these mice. An early study also showed that a decrease in Nrg-1 type III expression in Nrg-$1^{+/-}$ heterozygote mice lead to hypomyelination in the PNS [99]. Deficiency of Bace1, an essential enzyme for Nrg-1 processing and ligand release, also leads to disruption of myelination in both the PNS and CNS of Bace1 null mice [100,101]. Moreover, Nrg-1/ErbB signaling plays important roles in maturation of Schwann cells and oligodendrocytes [35,37,40,102-104]. Although these developmental studies suggest the importance of endogenous Nrg-1 signaling in CNS myelination, the direct role of Nrg-1 in oligodendrocyte development and myelination is still controversial. For instance, removal of oligodendrocytic Nrg-1 signaling through knockout of Nrg-1 or its receptors is shown to result in their maturation arrest and hypomyelination of the CNS [104,105]. However, other studies revealed that knockout of Nrg-1/ErbB signaling from oligodendrocytes has no effects on overall CNS myelination, while overexpression of Nrg-1 resulted in hypermyelination of the CNS [106]. Of note, many of these studies are in developmental models. Here, in the adult mice, we show that Nrg-1 knockout does not affect the abundance of oligodendrocytes in the corpus callosum, while it eventually leads to myelin

disruption. The differential effects of Nrg-1 ablation on oligodendrocytes verses myelination suggest that Nrg-1 might be dispensable for oligodendrogenesis in the adult brain due to other compensatory mechanisms. Overall, further studies using oligodendrocyte and neuron specific Nrg-1 and/or ErbB receptor knockout are required to deconstruct the ramifications of Nrg-1 dysregulation in each cell type, and the underlying mechanisms of Nrg-1 signaling in regulating oligodendrogenesis and myelination in adulthood. Nonetheless, in demyelinating lesions, our current study in chronic CPZ lesions combined with our previous studies in EAE and MS white matter lesions[37] show that endogenous Nrg-1 is depleted from both axons and oligodendrocytes, which recapitulate the knockout model used in this study. Evidence from single nuclei RNA sequencing (snRNA-seq) of MS lesions and controls demonstrate that Nrg-1 is mainly expressed in mature oligodendrocytes [107,108], which is consistent with our data regarding Nrg-1 protein expression in the white matter of mice. Importantly, these studies collectively suggest that Nrg-1 expression is largely absent in oligodendrocyte clusters in the late-stage chronic lesions in progressive MS, while it is detected in early lesions and in lesions of relapsing remitting MS (RRMS) [107,108]. Nrg-1 transcripts are enriched in remyelinating oligodendrocytes in active MS lesions, whereas Nrg-1 expression is absent in inactive cores [109]. Taken together, existing single nuclei RNA-seq databases support our findings in chronic CPZ mice that Nrg-1 expression declines in chronic lesions, and its expression is associated with remyelinating lesions.

In conclusion, our study unravels dysregulation of Nrg-1 as an endogenous mechanism that underpins remyelination failure in chronic demyelinated lesions. Importantly, we show the potential of Nrg-1 as a treatment for promoting remyelination in chronic white matter lesions by shifting the phenotype of dysfunctional lipid-laden foamy microglia towards a pro-remyelinating state. From a clinical point of view, many people with MS eventually transition to a progressive

form of the disease in which disabilities accumulate due to impaired remyelination. There are currently minimal regenerative therapies available to successfully support remyelination in chronic lesions and alleviate neurodegeneration and the burden of progressive MS [110]. Nrg-1 is also known as a susceptibility gene in schizophrenia and bipolar disorder, where a group of affected individuals show abnormalities within the white matter [111-116]. Translationally, Nrg-1 peptide therapy is approved by the US Food and Drug Agency (NCT03388593) for Phase II/III trials in cardiac repair [104] indicating its safety for human application. Nrg-1β1 peptide also freely passes the blood-CNS-barrier through receptor mediated processes [117] in which is a major consideration for pharmacological based therapies for the CNS. Hence, Nrg-1 shows translational potential as a disease relevant therapeutic target for further investigations in progressive MS.

Methods

Mice and Animal studies

All procedures involving animals and experimental protocols received approval from the University of Manitoba's Animal Ethics Care Committee, following the Canadian Council of Animal Care's guidelines for the care and use of research animals [Protocol #: 20-065 (AC11646) and 24-054 (AC11942)]. Mice lines that were used in this study were on a C57BL/6J background unless otherwise is stated. Mice were kept in standard plastic cages in a room with a 12-hour light/dark cycle and access to drinking water and pelleted food ad libitum. Room temperature was between 19-21°C with humidity between 29-32 Relative Humidity (RH). PDGFRα-Cre^{ERTM} mice (Jackson Lab stock # 018280) [118] and the membrane-tethered Rosa26-mGFP(mT/mG) (Jackson Lab Stock # 007676) were purchased from the Jackson Laboratory, both on a C57/BL6J background, and cross-bred to obtain PDGFRα-Cre^{ERTM}: Rosa26mGFP (mT/mG) (in short

PDGFRα-Cre) mice. Following mouse primers were used for genotyping of PDGFRα-Cre line: PDGFR Cre F (TCA GCC TTA AGC TGG GAC AT), PDGFR Cre R (ATG TTT AGC TGG CCC AAA TG), PDFGR ITC F (CAA ATG TTG CTT GTC TGG TG), PDFGR ITC R (GTC AGT CGA GTG CAC AGT TT), Rosa (mT/mG) WT F (AGG GAG CTG CAG TGG AGT AG), Rosa (mT/mG) MU F (TAG AGC TTG CGG AAC CCT TC), Rosa (mT/mG) Co R (CTT TAA GCC TGC CCA GAA GA). All experiments included age-, sex-, and genotype-matched mice as controls. For Nrg-1 conditional knockout mice, the CRISPR/Cas9 system was utilized to generate mutant mice harboring floxed alleles of the Nrg1 gene ($Nrg1^{fl/fl}$), similar to the previously described global knockout Nrg-1 mice [50,119]. The $Nrg1^{fl/fl}$ mice were then bred with Cre driver mice to generate $Nrg1^{fl/fl}$: UBC-Cre ^{ERTM} mice (Nrg1 Cre). The loxP sites flanked exons 6–8, which encode the EGF-like domain of Nrg-1, the biologically active domain present in all Nrg-1 isoforms [35,50]. Upon tamoxifen administration, Cre recombination results in the ablation of the EGF-like domain. It should be noted that embryonic knockout of Nrg-1 is lethal due to its essential role in heart development [33,120]. This conditional knockout line was established and maintained in our laboratory. The following primers were used in genotyping of Nrg-1 knockout mice: UBC Cre F (GAC GTC ACC CGT TCT GTT G), UBC Cre R (AGG CAA ATT TTG GTG TAC GG), Nrg-1 3' Lox-P site WPG1249 (CTG CCT TCA ATC TAT GAC TAG TTT ATG), Nrg-1 3' Lox-P site WPG1311 (CCG GCC TCT CAT TTG AGT TCT), Nrg-1 5' Lox-P site WPG1253 (GTG CAT ACT CAG TGG TCC AT), Nrg-1 5' Lox-P site WPG1254 (GTC TGA CTG CCA ACA TTC T). Additionally, adult mice (12 weeks old) expressing enhanced yellow fluorescent protein (EYFP) [121] were used in this study to extract EYFP+ myelin particles from the central nervous system. These mice were from a transgenic colony [strain 129-Tg (ACTB-EYFP)2Nagy/J; in short: EYFP Tg] maintained at the University of Manitoba, Winnipeg, Canada. The initial colony founders were

generously supplied by Dr. Andras Nagy from the Lunenfeld-Tanenbaum Research Institute in Toronto, Ontario, Canada. All animals were provided by the Central Animal Facility, University of Manitoba, Canada.

Cuprizone induced demyelination, tamoxifen and EdU administration, and Nrg-1 treatment.

Male and female mice from the PDGFRα-Cre (123 mice), Nrg1-Cre (99 mice) and C57BL6 (61 mice) were enrolled in our in vivo cuprizone animal studies. At 4-6 weeks of age and two weeks before the start of cuprizone feeding, PDGFRα-Cre (100mg/kg) and Nrg1-Cre (18F0mg/kg) mice were intraperitoneally (I.P.) injected with tamoxifen to induce recombination. Tamoxifen (Biosynth, Cat. No. FT27994) was prepared in corn oil (Sigma Aldrich, Cat. No. C8267) at 30mg/ml concentration, and PDGFRα-Cre and Nrg1-Cre mice received 100mg/kg and 180mg/kg of tamoxifen daily for five days, respectively. At 6-8 weeks of age, male and female PDGFRα-Cre, Nrg1-Cre and C57BL6 mice were provided with either a standard milled rodent diet (North American Lab supplies) as a control or the same diet mixed with 0.2% w/w cuprizone (CPZ) [bis(cyclohexanone) oxaldihydrazone] (Thermo Scientific, Cat. No. A10628.22). This CPZ diet was continued for a total of 5 or 10 weeks to induce short-term or chronic demyelination, respectively. Following this period, the mice were switched back to a regular diet to allow for remyelination (Fig. 1 a). The animals were randomly assigned to either a vehicle or an Nrg-1 treatment group. Those in the Nrg-1 group received daily subcutaneous (S.C.) injections of Nrg-1β1 peptide (~8 kDa), containing the bioactive epidermal growth factor (EGF)-like domain (Shenandoah Biotechnology, USA, Cat. No. 100-46), at a dose of 600 ng/mouse/day (equivalent to 30 µg/kg). Mice in the vehicle group were given the same volume of a solution containing 0.1% bovine serum albumin (BSA) (Sigma-Aldrich, Cat. No. A9647) in saline, which was used as the

preparation medium for Nrg-1β1. To track proliferating cells, EdU (5-ethynyl 2´-deoxyuridine) (Biosynth Carbosynth Group, Cat. No. NE08701) was injected intraperitoneally (12.5 mg/kg body weight, in PBS) to mice according to the experimental timelines presented in the figures. EdU is a thymidine analogue incorporated into the DNA during cell cycle [122].

Microglia depletion

To achieve pharmacological depletion of microglia from the central nervous system (CNS), PLX5622 (Cayman Chemical, Cat. No. 28927), a colony stimulating factor 1 receptor (CSF-1R) inhibitor, was incorporated to the diet of the mice at a concentration of 1200 ppm [47,123]. The administration of PLX5622 was started at week 9 of CPZ diet (1 week prior to CPZ withdrawal) and was continued until the study endpoint, either 2- or 4 weeks post-CPZ withdrawal.

EAE induction, clinical scoring, and treatments

Eight-week-old C57BL/6J mice (N=15) were obtained from the University of Manitoba's Central Animal Facility. EAE was induced by immunization with myelin oligodendrocyte glycoprotein (MOG)35-55 [36]. After a 7-day acclimatization period, mice were immunized with 100µL (50µg) of MOG 35–55 peptide emulsified in complete Freund's adjuvant (CFA), which includes incomplete Freund's adjuvant with 5 mg/mL heat-inactivated Mycobacterium tuberculosis H37Ra (Fisher Scientific, Cat. No. DF0639-60-6). A 50 µL emulsion was injected subcutaneously (s.c.) on each side of the tail base. Additionally, 300 ng of pertussis toxin (List Biological Laboratories) was administered intraperitoneally (i.p.) on days 0 and 2 post-immunization. EAE mice were monitored daily, with clinical scores recorded as per previous methods [36]. EAE mice were then

randomly divided into vehicle and Nrg-1β1 treatment groups, receiving daily s.c. injections of either Nrg-1β1 peptide (600 ng/day) or vehicle as described above. Treatments were administered starting at the peak of the disease around day 17-19 (clinical score of 2.5-3) until day 42 post EAE induction.

Tissue processing

At designated endpoints, mice were deeply anesthetized with a mixture of isoflurane and propylene glycol (Fisher scientific, Cat. No. P3551) (40:60 v/v) and perfused with cold 0.1M phosphate-buffered saline (PBS) followed by 3.5% paraformaldehyde (PFA, Sigma, Cat. No. P6148) for immunohistochemical analysis. Brain tissue was then post-fixed overnight at 4°C in 10% sucrose (Sigma, Cat. No. S0389) within 3.5% PFA, then cryoprotected in 20% sucrose for an additional 24–48 hours and finally embedded in Tissue-Tek®-OCT (Electron Microscopy Sciences, Cat. No. 62550-01). Brain samples were sectioned at 16 µm thickness using a cryostat (Leica Biosystems) and stored at -80°C for subsequent analysis.

Immunofluorescence staining

Three coronal brain sections, spaced 100µm apart, were chosen from each animal for each immunohistochemical analysis. Frozen slides were first air-dried at room temperature (RT) and then rinsed with PBS for 5 minutes. Sections were blocked for 1 hour at RT with a solution containing 1% BSA , 5% non-fat milk, and 0.3% Triton X-100 (Sigma, Cat. No. T9284) in PBS. Next, the tissue sections were incubated overnight with the primary antibody in blocking solution at 4°C. After rinsing with PBS, the sections were incubated with the secondary antibodies (Alexa

405, Alexa 488, Alexa 568, or Alexa 647 conjugated; 1:500; Invitrogen) suitable for co-labeling with anti-mouse, anti-rabbit, anti-rat, anti-chicken, or anti-goat targets. Nuclear staining was performed with 4',6-diamidino-2-phenylindole (DAPI, Sigma, Cat. No. D9542), and the sections were cover-slipped with Mowiol mounting medium. Antibody specificity was confirmed with both a negative control, excluding the primary antibody in the immunostaining protocol or using IgG isotope control, as well as a positive control using tissues known to express the target antigen (Supplementary Fig. 10). All samples were processed in parallel under the same condition and imaged using a Zeiss LSM700 Spectral Confocal Microscope or a Zeiss AxioImager M2 fluorescence microscope (Zeiss) under consistent settings. The following primary antibodies were used in this study: Abca-1 (rabbit, 1:200, Sigma, Cat. No. SAB4300712), APC (mouse, 1:50, Millipore, Cat. No. OP80); CD11b (rat, 1:25, DSHB Cat. No. M1/70.15.11.5.2-s), EGF domain-specific Nrg-1β1 (goat, 1:200, R&D, Cat. No. AF396NA), ErbB-2 (rabbit, 1:50, Santa Cruz Biotechnology Inc, Cat. No. SC-284), ErbB-3, rabbit, 1:200, New England Biolabs Ltd, Cat. No. 12708S, ErbB-4 (mouse, 1:200, Santa Cruz Biotechnology Inc, Cat. No. sc-8050), p44/42 MAPK -(ERK) (rabbit, 1:250, Cell Signaling, Cat. No. 4695), GFAP (mouse, 1:800, Millipore, Cat. No. MAB360), ß-Tubulin III (mouse, 1:500, Millipore, Cat. No. T8660), GFP (mouse, 1:500, Millipore Cat. No. MAB3580), Iba-1(rabbit, 1:500, Wako Cat. No. 019-19741), MBP (mouse, 1:1000, Biolegend, Cat. No. 836504), MBP (rat, 1:200, Millipore, Cat. No. MAB386), dMBP (mouse, 1:250, Abnova, Cat. No. MAB8817), O4 (mouse, 1:200, R&D, Cat. No. MAB1326), Olig2 (rabbit, 1:1000, Millipore, Cat. No. AB9610), P2Y12 (rabbit, 1:200, Anaspec, Cat. No. 55043A), RIP3 (rabbit, 1:50, Pro Sci, Cat. No. 2283), Tmem-119 (mouse, 1:100, Abcam, Cat. No. ab209064). The following secondary antibodies were used in this study (all 1:600): Alexa Fluor® 405 (goat anti-mouse, Invitrogen Cat. No. A31553), Alexa Fluor® 405 (goat anti-rabbit, Invitrogen Cat. No.

A48254), Alexa Fluor® 488 (goat anti-mouse, Invitrogen Cat. No. A11029), Alexa Fluor® 488 (goat anti-Rabbit, Invitrogen Cat. No. A11034), Alexa Fluor® 488 (goat anti-Rat, Invitrogen Cat. No. A11006), Alexa Fluor® (568 goat anti-mouse, Invitrogen Cat. No. A11031), Alexa Fluor® 568 (goat anti-Rabbit, Invitrogen Cat. No. A11036), Alexa Fluor® 568 (goat anti-Rat, Invitrogen Cat. No. A11077), Alexa Fluor® 568 donkey anti-goat, Invitrogen Cat. No. A11055), Alexa Fluor® (647 goat anti-Mouse, Invitrogen Cat. No. A21236), Alexa Fluor® 647 (goat anti-Rat, Invitrogen Cat. No. A-21247), Alexa Fluor® 647 (goat anti-Rabbit, Invitrogen Cat. No. A21245), Alexa Fluor 647 Azide, Triethylammonium Salt, Invitrogen Cat. No. A10277).

Black Gold II myelin staining

Black Gold II staining (Black Gold II myelin stain [Histo-Chem Inc., 1BGII, Cat. No.1BGII]) was carried out following the manufacturer's protocol. Briefly, tissue sections were incubated in 0.3% Black Gold II at 60°C for 12–20 min until the finest myelin fibers were visibly stained. The slides were then fixed in 1% sodium thiosulfate (Sigma, Cat. No. 217263) for 3 min, rinsed in deionized water, dehydrated via a series of gradated ethyl alcohols, cleared in xylene for 30 minutes, and cover-slipped with Permount permanent mounting media (Fisher Chemical, Cat. No. SP15500). A total of 3 sections were examined per mouse, and 3-5 mice (both male and female) were analyzed per group.

ORO and Filipin III staining in vitro and in vivo

ORO staining was performed on PFA fixed cultured cells and tissue sections to visualise esterified lipids according to the manufacturer’s instructions. Briefly, cells and tissue sections were washed

in 60% isopropanol for 3 minutes, followed by staining with 0.3% ORO (Thermo Scientific Chemicals, Cat. No. AAA1298914) for 15 minutes. To determine the number of cultured cells per imaging field, hematoxylin incubation was used to counterstain for nuclei. Filipin III staining was utilized to detect free cholesterols in PFA fixed cells. The cells were incubated with 50 µg/ml of Filipin III (Sigma-Aldrich, Cat. No. F-9765) for 2 hours. To determine the number of cells per imaging field, Propidium Iodide (Polysciences, Cat. No. 03748-100) (1mg/mL) counterstaining for nuclei was used. Imaging was done using a Zeiss AxioImager M2 fluorescence microscope (Zeiss). Images were analyzed by measurement of the integrated density of the ORO and Filipin III signal using the ImageJ software.

Transmission electron microscopy

To process the tissues for electron microscopy, mice were deeply anesthetized with a mixture of isoflurane and propylene glycol (60:40 ratio) and perfused with ice-cold Sorensen's Phosphate buffer, followed by perfusion with a solution of 2% PFA and 2% glutaraldehyde in Sorensen's Phosphate buffer as we described before [37]. The corpus callosum within the region of interest was dissected and fixed again in 2% PFA/2% glutaraldehyde (Sigma, Cat. No. G5882) in Sorensen's Phosphate buffer for 2 hours and stored in Sucrose/Phosphate buffer at 4°C until used. Specimens were further fixed with 1% Osmium tetroxide (Electron Microscopy Sciences, Cat. No. 19100(EM)) at room temperature for 2 h and dehydrated through a series of graded ethanol, with a final methanol wash. Tissue was then transitioned through Propylene oxide (Electron Microscopy Sciences, Cat. No. 20401(EM)) and embedded in resin. Resin was allowed to cure in at 60°C for 30 hours. Samples were flat embedded to ensure the correct sectioning orientation for visualization of axons/myelin. Blocks were trimmed on a Leica EM Trim 2 (Vienna, Austria) with

a milling diamond. Sections 0.5-1µm thick were cut on a Leica ARTOS 3D (Vienna, Austria) ultramicrotome with a diamond knife and stained with toluidine blue to determine to region of interest. Thin sections were taken at 80-100nm and placed on 100 or 200 mesh Cu Grids from EMS (Cat. No. G200-Cu, Cat. No. G100-Cu) and stained with Uranyless (Cat. No. 22404) and Lead citrate (Cat. No. 22410 from EMS). Images were acquired using a Phillips CM10 Electron Microscope Model PW 6020/15 (Eindhoven, Netherlands) with a Tungsten filament (60 kV) at 800 – 64,000 x magnification with an Advantage HR-B Digital CCD camera and AMT software. Myelin g-ratio (the ratio of inner to outer diameter of myelinated axons) was used as a measure of myelination. Image J software was used for measurements on high-resolution digital images from non-overlapping, sequential microscope fields within the demyelinated area. For analysis, a grid was added to the images with evenly spaced tile dimensions. All axons present at the intersections of the grid lines were used for measurements. A minimum of 200 axons and 3 images were evaluated for each animal. The examiner was blinded to the experimental conditions and conducted all counts on the same computer with the same grid settings for consistency across all animals.

Magnetic-Activated Cell Sorting (MACS) and RNA sequencing

RNA sequencing was conducted on microglia/macrophages isolated from chronic CPZ mice (44 C57BL6 mice) using MACS sorting. Animals were euthanized under deep anesthesia induced by an isoflurane and propylene glycol (60:40 ratio) mixture, followed by cervical dislocation. Brains were quickly removed and placed in cold artificial cerebrospinal fluid (aCSF, 2 brains per each N and N=3-5 per group). The corpus callosum was dissected and enzymatically dissociated using a solution containing kynurenic acid 0.2 mg/ml (Sigma, Cat. No. K3375), trypsin 1.33 mg/ml

(Sigma, Cat. No. T1005), and hyaluronidase 0.2 mg/ml (Sigma, Cat. No. H6254) for 20 minutes at 37°C. The enzyme solution was then replaced with 1 mg/ml trypsin inhibitor (Sigma, Cat. No. 10109878001), and the cell suspension was filtered through a 40µm cell strainer. Cell labeling was performed using specific antibodies according to the MicroBead kit protocols (Miltenyi Biotec). Microglia/macrophages were labeled with an anti-CD11b antibody (1:10; Miltenyi Biotec, Cat. No. 130-093-636). Antibody incubation was carried out for 20 minutes at 4°C, followed by a 10-minute wash with PBS. Cells were isolated by passing the labeled cell suspension through magnetic columns (Miltenyi Biotec, Cat. No. 130-042-401) attached to a magnetic separator (Miltenyi Biotec, Cat. No. 130-091-051). RNA was extracted from the sorted cells by homogenization in TRI Reagent (Sigma, Cat. No. T9424), followed by purification using the PureLink RNA Mini Kit (Thermo Fisher Scientific, Cat. No. 12183018A). Library preparation and RNA sequencing were performed at Genome Quebec using the Illumina NovaSeq PE 100 platform. Transcriptomics analysis was conducted using Galaxy workflows [111–113] and the iDEP platform [124]. Alignment of transcripts to the mouse genome (mm10) was performed with the HISAT2 package, and gene counts were extracted using the featureCounts package. Differential gene expression was identified using the DESeq2 package, with criteria set at a False Discovery Rate (FDR) of less than 0.05 and fold changes greater than 2. Gene Ontology pathway analysis was performed with FDR values calculated using the Benjamini–Yekutieli method, applying a threshold of 0.05.

Total RNA isolation and quantitative PCR

Total RNA was extracted from isolated microglia using TRIzol reagent (Thermo Fisher Scientific, Cat. No. 15596026) according to the manufacturer's guidelines. DNase-treated RNA samples

were then used for quantitative PCR (qPCR) with a QuantiFast SYBR Green RT-PCR kit (Qiagen, Cat. No. 204154), following the manufacturer's instructions. Reactions were conducted using a LightCycler (RocheDiagnostics) as previously described [82]. Analysis of results was performed with LightCycler software version 3.5 (Roche diagnostics). Expression values were normalized to the mean of two housekeeping genes (Rplp0, Gapdh). Quantification was achieved via the ΔCt method, with values normalized to experimental control samples (set to 1). All primers were designed for optimal efficiency with criteria including primer length (18–22 bp), melting temperature (52–58 °C), GC content (40–60%), minimal repeats and amplicon length (<220 bp). All primers were intron spanning. Primers were designed using Primer-BLAST against mouse reference sequences (*Il1b*, NM_008361; *Il6*, NM_031168; *Tnf*, NM_001278601; *Abca1*, NM_013454; *Abcg1*, NM_009593; *Rplp0*, NM_007475; *Gapdh*, NM_001289726) and validated for specificity. The following mouse primers were used for qPCR: *Il1b* F (GCAACTGTTCCTGAACTCAACT), *Il1b* R (ATCTTTTGGGGTCCGTCAACT), *Il-6* F(TAGTCCTTCCTACCCCAATTTCC), *Il-6* R (TTGGTCCTTAGCCACTCCTTC), *Tnf F* (CCCTCACACTCAGATCATCTTCT), *Tnf* R (GCTACGACGTGGGCTACAG), *Abca1* F(CTG TTT CCC CCA ACT TCT G), *Abca1* R (TCT GCT CCA TCT CTG CTT TC), *Abcg1* F (TCT TTG ATG AGC CCA CCA GT), *Abcg1* R (GGG CCA GTC CTT TCA TCA), *Rplp0* F (AGA TTC GGG ATA TGC TGT TGG C), *Rplp0* R (TCG GGT CCT AGA CCA GTG TTC), *Gapdh* F *(*AGGTCGGTGTGAACGGATTTG), *Gapdh* R (TGTAGACCATGTAGTTGAGGTCA).

Myelin preparation

Animals were euthanized under deep anesthesia induced by an isoflurane and propylene glycol (60:40 ratio) mixture, followed by cervical dislocation. Myelin was extracted from the brains of 7

male and female EYFP-Tg mice (12 weeks old) [18]. The brains were first homogenized (5-10% (w/v) in a 0.32 M sucrose solution and centrifuged at low speed (200xg) for 5 minute to remove large cell debris. Then, the supernatant was carefully layered over a 0.85 M sucrose solution and centrifuged at 75,000xg for 30 min. The resulting interphase, which contained partially purified myelin, was carefully collected, rinsed with water, and centrifuged again at 75,000xg for 25 minutes. To induce osmotic shock, the myelin was incubated in water for 15 minutes, followed by another centrifugation step at 12,000xg for 25 minutes. The pellet was then resuspended in a 0.35 M sucrose solution, layered on top of a 0.85 M sucrose solution, and centrifuged for 1 hour at 15,000xg. After this step, the purified myelin was rinsed with water and subjected to a final centrifugation for 30 minutes at 15,000xg. The pellet was then resuspended in sterile PBS, homogenized thoroughly, and stored at –80 °C until further use.

Preparation of electrospun polycaprolactone (PCL) nanofibers

Transparent solution 12% w/v polycaprolactone (PCL) in fluorinated alcohol of 2,2,2-trifluoroethanol (TFE) was prepared by dissolving PCL polymers in TFE with sufficient stirring under room temperature. An adjustable high-voltage power supply was used to apply 10 kV DC voltage. The PCL solution was placed in a 5-mL syringe and loaded into a Harvard Apparatus PhD 2000 syringe pump (with a continuous flow rate of 0.2ml/min. Under a chemical fume hood, the positive electrode of the high-voltage power supply was clamped directly to a needle (23 G). The negative electrode was connected to a metallic rotatory collector wrapped with aluminum foil. Collecting circular 12mm diameter cover glasses were placed on the aluminum foil surface using double-sided carbon tape. The distance between the needle and collector was set to 12cm and the speed of the collector was set on 377 xg toward the needle to produce relatively aligned PCL fibers.

The quality of the fiber's alignment and density was assessed using a tabletop Hitachi scanning electron microscope (TM-1000, HITACHI). All electro-spun fibrous membranes on the cover glasses were detached from the collector and placed in 24 well plates under vacuum for 24 hours to ensure the evaporation of the solvent. The samples were then washed with 70% ethanol for 5 min and then three times with DPBS for 5 min each. The samples were then exposed to UV for 1 hour to be sterilized.

Isolation of mouse microglia, OPC and NPCs for in vitro studies

Microglia and OPCs cultures were isolated from male and female neonatal CD1 mouse pups (P0-P2) [36,37]. A total number of 160 CD1 mouse pups were used in our in vitro studies. Briefly, mice were euthanized under deep anesthesia induced by an isoflurane and propylene glycol (60:40 ratio) mixture and then decapitated. Cerebral cortices, followed by enzymatic digestion at 37°C for 45 minutes in a solution containing papain (0.9 mg/ml; Sigma, Cat. No. P4762), L-cysteine (0.2 mg/ml; Sigma, Cat. No. A8199), and EDTA (0.2 mg/ml; Sigma, Cat. No. E6758) diluted in HBSS (Invitrogen, Cat. No. 14175079). The resulting cell suspension was then filtered through a 40µm cell nylon strainer and transferreCD1d to poly-D-lysine (PDL, Sigma, Cat. No. P6407)-coated flasks in Dulbecco's modified Eagle medium (DMEM, Invitrogen, Cat. No. 11960-044) medium supplemented with 10% fetal bovine serum (FBS, Gibco, by Thermo Fisher Scientific, MD, USA, Cat. No. 10082-147) and 1% penicillin–streptomycin–neomycin (PSN, Invitrogen, Cat. No. 1564005). Cultures were incubated at 37°C in a 5% CO_2 environment, with media refreshed every 2-3 days. After 10-12 days and upon reaching confluence, cultures were shaken (on shaker, Thermo Fisher scientific-2314) for 2h at 250 rpm at 37ºC and the supernatant media containing microglia were collected. Then the cells were seeded in PDL coated dishes in complete DMEM

media with 10% FBS. For collection of OPCs, after the removal of microglia, the medium was refreshed, and the cultures were shaken overnight for 16-18 hours at 0.66 xg at 37ºC. The OPC-containing medium was filtered through a 40-µm cell nylon strainer (BD Biosciences, Cat. No. 21008-949), centrifuged at 168 xg for 10 min, and transferred to uncoated Petri dishes (Fisher Scientific, Cat. No. FB0875712) to eliminate astrocytes and the remaining microglia. After 1 hour, the media was collected again, centrifuged for 10 min at 168 xg, and the isolated OPCs were collected. These cells were then plated for use in various conditions as described below.

Animals were euthanized under deep anesthesia induced by an isoflurane and propylene glycol (60:40 ratio) mixture, followed by cervical dislocation. Adult NPCs were isolated from the subventricular zone (SVZ) of three 6-8 weeks old C57BL/6 mice.[125] Brains were transferred into ice-cold artificial cerebrospinal fluid (aCSF), and the SVZ was micro-dissected and enzymatically dissociated for 20 min at 37 °C using trypsin, hyaluronidase, and kynurenic acid (all Sigma). Digestion was stopped with trypsin inhibitor (Sigma), and cells were resuspended in serum-free medium (SFM) includes DMEM/F12 (Invitrogen, Cat. No. 21331020) supplemented with $NaHCO_3$ (Sigma Cat. No. S5761), glucose (Sigma Cat. No. G7021), HEPES (Sigma Cat. No. H3537), transferrin (Sigma Cat. No. T2252), insulin (Sigma Cat. No. I5500), putrescine (Sigma Cat. No. P7505), selenium selenite (Sigma Cat. No. S5261), progesterone (Sigma Cat. No. P6149), PSN, and L-glutamine (Invitrogen Cat. No. A2916801). Cultures were maintained in SFM containing fibroblast growth factor 2 (FGF2, Shenandoah, Cat. No. 200-12), EGF (Shenandoah Cat. No. 200-53), and Heparin (Sigma Cat. No. H3149) for analysis.

Inhibition of ErbB receptors

To investigate if the effects of Nrg-1 are through ErbB receptors, we combined microglia activation, Nrg-1, and myelin treatment with ErbB inhibitors. Two ErbB inhibitors were used:

Mubritinib or TAK-165 that is a potent and selective inhibitor of ErbB-2 (Selleckchem, Cat. No. S2216) and TX1-85-1 that potently inhibits ErbB-3 receptors, which can also bind to ErbB-2 with a lower affinity (Cayman, Cat. No. 19164). Multiple concentrations were used for each inhibitor based on previous studies to determine efficacy and toxicity of TAK 165 (100nM, 250nM, 500nM, 1 μM), and Tx1-85-1 (2, 5, 10 μM). Cultures were treated with ErbB-2 and ErbB-3 receptor inhibitors (alone or in combination) for 4 hours, followed by 1 hr of Nrg-1 treatment. Toxicity assessment was performed at 24 hours using a Live/Dead Viability/Cytotoxicity Kit. For assessment of efficacy, immunostaining was conducted for pErk1/2, a known downstream pathway of Nrg-1/ErbB signaling.

Microglia experiments

Microglia were seeded on PDL-coated 8-well multi-chamber glass slides (20,000 cells per well, LabTek, Invitrogen Cat. No. 12-565-5) for immunofluorescence assessments, and on 6-well plates (200,000 cells per well) in complete DMEM media. 24 hours after the initial seeding, the cells were switched to serum free Dulbecco's modified Eagle media supplemented with PSN and treated with vehicle (0.1% BSA), Nrg-1β1 (200ng/ml), lipopolysaccharide (LPS, Sigma, Cat. No. L4516) (100 ng/ml) + IFNγ (20 ng/ml, R&D Systems, Cat. No. 1240-1) or Nrg-1β1 + LPS + IFNγ with or without ErbB-2 and/or ErbB-3 inhibitors. Various assessments were conducted in these conditions as described below.

Phagocytosis experiments

EYFP+ myelin particles were added to each condition at 100μg/ml. Cells seeded on glass slides were fixed after 6 or 24 hours with 3% PFA and co-labeled with DAPI to assess myelin

phagocytosis by microglia (YFP signal intensity/DAPI). Purity and specificity of myelin particles were confirmed with Fluoromyelin (Thermo Fisher scientific, Cat. No. F34652).

Assessment of lipid and cholesterol accumulation and transport pathways

Microglia were stained with Filipin III or Oil-Red-O (ORO). Microglial expression of cholesterol biosynthesis and release pathways was conducted through qPCR on RNA lysates collected after 6 and 72 hours. The conditioned media was also collected from each condition after 72 hours for assessment of cholesterol content and for use in OPC maturation and myelination assays as described below. Cholesterol content of conditioned media was measured using the Amplex™ Red Cholesterol Assay Kit (Invitrogen, Cat. No. A12216) per manufacturer's instructions. To investigate if the effects of Nrg-1 are through cholesterol efflux machinery, we combined microglia activation, Nrg-1, and myelin treatment with pharmacological antagonists of the upstream pathways to cholesterol efflux transport pathways, namely LXR (GSK2033; Tocris, Cat. No. 5694) and PPARγ (GW9662; Santa-Cruz, Cat. No. sc-202641). Multiple doses were used for each inhibitor based on previous studies to determine their efficacy and toxicity (GSK2033: 0.5, 1, 5, 10 and 20 μM, GW9662: 1, 5, 10, 15 and 20 μM). Toxicity assessment was done using a Live/Dead Viability/Cytotoxicity Kit (Invitrogen, Cat. No. L3224). RNA lysates and conditioned media were collected from these conditions after 72 hours, for qPCR and assessment of cholesterol content, respectively.

Cholesterol measurement

To determine the concentration of cholesterol in the conditioned media of the microglia, the Amplex™ Red Cholesterol Assay Kit (Invitrogen, A12216) was used. In summary, microglia

conditioned media was diluted in the reaction buffer provided in the kit. A working solution of 300 μM Amplex® Red reagent containing 2 U/mL HRP, 2 U/mL cholesterol oxidase, and 0.2 U/mL cholesterol esterase in the reaction buffer was prepared and added to the conditioned media in each well. A no cholesterol condition (blank) as negative control and a gradient of known cholesterol concentrations (from 0 to 2 μg/ml) were used to create a standard curve. The reactions were incubated in 37° C protected from light for 30 minutes and the fluorescence signal was measured every 2 minutes in a fluorescence microplate reader using excitation in the range of 530–560 nm and emission detection at ~590 nm. The cholesterol concentrations were interpolated based on the standard curve, using the GraphPad Prism software after correcting for the initial dilution rate of the samples in the reaction buffer.

OPC proliferation and maturation assays

For assessment of OPC maturation in the presence of microglia conditioned media (MCM), OPCs were plated on PDL-coated 8-well multi-chamber glass slides at 20,000 cells per well in complete DMEM media. After 24 hours, the cells were divided into 10 different conditions: vehicle treated, Nrg-1β1 treated (200 ng/ml), and MCM treated from the 4 microglia conditions (vehicle, Nrg-1β1, LPS + IFNγ, Nrg-1β1 + LPS + IFNγ) without and with myelin exposure. The media was changed to OPC culture media (DMEM [Invitrogen], insulin [10 μg/ml], Apo-transferrin [100 μg/ml], sodium selenite [5.2 ng/ml], hydrocortisone [18 ng/ml, Sigma, Cat. No. H0135], putrescine [16 μg/ml], progesterone [6.3 ng/ml], biotin [10 ng/ml, Sigma, Cat. No. B4639], N-acetyl-L-cysteine [5 μg/ml], BSA (100 μg/ml), 1% B27, and PSN [Invitrogen]) along with the treatment specific to each condition. For MCM treated conditions, MCM was added to the OPC culture medium at a ratio of 1:1. The cultures were maintained at 37°C and 5% CO_2 and the media was refreshed every

other day. After 14 days, the cells were fixed with 3% PFA and used for immunostaining. For assessment of OPC proliferation, 10 μM EdU was added to the OPC culture medium, and the same experiments were repeated. After 72 hours, the cells were fixed with 3% PFA and used for immunostaining.

Myelination assay

To assess the myelination capacity of oligodendrocytes treated with MCM, OPCs were seeded on PDL-coated glass coverslips in 24-well plates in the presence of electrospun polycaprolactone (PCL) nanofibers at 20,000 cells per well in complete DMEM medium. After 24 hours, the media was switched to OPC culture media treated with and without Nrg-1 or treated with MCM from various experimental conditions including LPS + IFNγ + myelin treated, Nrg-1β1 + LPS + IFNγ+myelin treated microglia with or without ErbB receptor inhibitors. For MCM treated conditions, MCM was added to the OPC culture medium at a ratio of 1:1. The cultures were maintained at 37°C and 5% CO_2 and the media was refreshed every other day. After 28 days, the cells were fixed with 3% PFA and used for immunostaining.

Human brain MS specimens

Post-mortem frozen brain tissues from people with MS were obtained from The Multiple Sclerosis and Parkinson's Tissue Bank situated at Imperial College, London. Donors had provided informed consent during life of their willingness to donate to the bank. There was no financial compensation for their decision. All MS tissues were obtained and utilized with approval from the institutional ethics committee at the University of Calgary (Ethics No.: REB15-0444-REN11). Four brain tissue samples from individuals with chronic MS, each containing active lesions, were analyzed in this

study. The lesions met the morphologic criteria for active inflammatory demyelinating process characteristic of MS when stained with Hematoxylin/Eosin (H&E) and Luxol Fast Blue (LFB). Detailed information on individual MS samples is available in Supplementary Table 1. Human frozen tissue sections were fixed with 3.5% PFA and immunostained using similar procedures that we described above for mouse tissue.

Statistical analysis

For all analyses, we ensured unbiased evaluation by employing randomization and blinding to experimental conditions. All graphs were generated with GraphPad Prism versions 8 and 10. Data are presented as means ± standard error of the mean (SEM), and a p-value of ≤ 0.05 was considered statistically significant in all the analyses. When two groups were compared, two tailed unpaired Student's t-test was used. When comparing more than two groups, One-way ANOVA with Tukey's post-hoc correction was applied. For comparisons involving two variables across more than two groups, two-way ANOVA was used, with Tukey's or Fisher's post-hoc test applied to compare means at each time point. Details for each statistical analysis are described in the figure legends.

Data availability

All data presented in this study are included in the article and its accompanying Supplementary Information and Source Data Files. RNA sequencing data are deposited in Gene Expression Omnibus database (GEO) under accession code: GSE282653 [https://www.ncbi.nlm.nih.gov/geo/query/acc.cgi?acc=GSE282653].

References

1. Franklin RJ, Ffrench-Constant C. Remyelination in the CNS: from biology to therapy. *Nat Rev Neurosci*. Nov 2008;9(11):839-55. doi:10.1038/nrn2480
2. Neumann B, Segel M, Chalut KJ, Franklin RJ. Remyelination and ageing: Reversing the ravages of time. *Mult Scler*. Dec 2019;25(14):1835-1841. doi:10.1177/1352458519884006
3. Lubetzki C, Zalc B, Williams A, Stadelmann C, Stankoff B. Remyelination in multiple sclerosis: from basic science to clinical translation. *Lancet Neurol*. Aug 2020;19(8):678-688. doi:10.1016/S1474-4422(20)30140-X
4. Lopez-Otin C, Blasco MA, Partridge L, Serrano M, Kroemer G. The hallmarks of aging. *Cell*. Jun 6 2013;153(6):1194-217. doi:10.1016/j.cell.2013.05.039
5. Goldschmidt T, Antel J, Konig FB, Bruck W, Kuhlmann T. Remyelination capacity of the MS brain decreases with disease chronicity. *Neurology*. Jun 2 2009;72(22):1914-21. doi:10.1212/WNL.0b013e3181a8260a
6. Wolswijk G. Chronic stage multiple sclerosis lesions contain a relatively quiescent population of oligodendrocyte precursor cells. *J Neurosci*. Jan 15 1998;18(2):601-9. doi:10.1523/JNEUROSCI.18-02-00601.1998
7. Chang A, Nishiyama A, Peterson J, Prineas J, Trapp BD. NG2-positive oligodendrocyte progenitor cells in adult human brain and multiple sclerosis lesions. *J Neurosci*. Sep 1 2000;20(17):6404-12. doi:10.1523/JNEUROSCI.20-17-06404.2000
8. Chang A, Tourtellotte WW, Rudick R, Trapp BD. Premyelinating oligodendrocytes in chronic lesions of multiple sclerosis. *N Engl J Med*. Jan 17 2002;346(3):165-73. doi:10.1056/NEJMoa010994
9. Reynolds R, Dawson M, Papadopoulos D, *et al*. The response of NG2-expressing oligodendrocyte progenitors to demyelination in MOG-EAE and MS. *J Neurocytol*. Jul-Aug 2002;31(6-7):523-36. doi:10.1023/a:1025747832215
10. Wang S, Sdrulla AD, diSibio G, *et al*. Notch receptor activation inhibits oligodendrocyte differentiation. *Neuron*. Jul 1998;21(1):63-75. doi:10.1016/s0896-6273(00)80515-2
11. Jurynczyk M, Jurewicz A, Bielecki B, Raine CS, Selmaj K. Inhibition of Notch signaling enhances tissue repair in an animal model of multiple sclerosis. *J Neuroimmunol*. Dec 30 2005;170(1-2):3-10. doi:10.1016/j.jneuroim.2005.10.013
12. Back SA, Tuohy TM, Chen H, *et al*. Hyaluronan accumulates in demyelinated lesions and inhibits oligodendrocyte progenitor maturation. *Nat Med*. Sep 2005;11(9):966-72. doi:10.1038/nm1279
13. Kuhlmann T, Miron V, Cui Q, Wegner C, Antel J, Bruck W. Differentiation block of oligodendroglial progenitor cells as a cause for remyelination failure in chronic multiple sclerosis. *Brain*. Jul 2008;131(Pt 7):1749-58. doi:10.1093/brain/awn096
14. Masuda T, Sankowski R, Staszewski O, *et al*. Spatial and temporal heterogeneity of mouse and human microglia at single-cell resolution. *Nature*. Feb 2019;566(7744):388-392. doi:10.1038/s41586-019-0924-x
15. Prinz M, Masuda T, Wheeler MA, Quintana FJ. Microglia and Central Nervous System-Associated Macrophages-From Origin to Disease Modulation. *Annu Rev Immunol*. Apr 26 2021;39:251-277. doi:10.1146/annurev-immunol-093019-110159
16. Zia S, Hammond BP, Zirngibl M, *et al*. Single-cell microglial transcriptomics during demyelination defines a microglial state required for lytic carcass clearance. *Mol Neurodegener*. Dec 13 2022;17(1):82. doi:10.1186/s13024-022-00584-2

17. Colonna M, Butovsky O. Microglia Function in the Central Nervous System During Health and Neurodegeneration. *Annu Rev Immunol*. Apr 26 2017;35:441-468. doi:10.1146/annurev-immunol-051116-052358
18. Berghoff SA, Spieth L, Sun T, *et al*. Microglia facilitate repair of demyelinated lesions via post-squalene sterol synthesis. *Nat Neurosci*. Jan 2021;24(1):47-60. doi:10.1038/s41593-020-00757-6
19. Bogie JFJ, Grajchen E, Wouters E, *et al*. Stearoyl-CoA desaturase-1 impairs the reparative properties of macrophages and microglia in the brain. *J Exp Med*. May 4 2020;217(5)doi:10.1084/jem.20191660
20. Lloyd AF, Davies CL, Holloway RK, *et al*. Central nervous system regeneration is driven by microglia necroptosis and repopulation. *Nat Neurosci*. Jul 2019;22(7):1046-1052. doi:10.1038/s41593-019-0418-z
21. McNamara NB, Munro DAD, Bestard-Cuche N, *et al*. Microglia regulate central nervous system myelin growth and integrity. *Nature*. Jan 2023;613(7942):120-129. doi:10.1038/s41586-022-05534-y
22. Baaklini CS, Ho MFS, Lange T, *et al*. Microglia promote remyelination independent of their role in clearing myelin debris. *Cell Rep*. Dec 26 2023;42(12):113574. doi:10.1016/j.celrep.2023.113574
23. Berghoff SA, Spieth L, Saher G. Local cholesterol metabolism orchestrates remyelination. *Trends Neurosci*. Apr 2022;45(4):272-283. doi:10.1016/j.tins.2022.01.001
24. Marschallinger J, Iram T, Zardeneta M, *et al*. Lipid-droplet-accumulating microglia represent a dysfunctional and proinflammatory state in the aging brain. *Nat Neurosci*. Feb 2020;23(2):194-208. doi:10.1038/s41593-019-0566-1
25. Cantuti-Castelvetri L, Fitzner D, Bosch-Queralt M, *et al*. Defective cholesterol clearance limits remyelination in the aged central nervous system. *Science*. Feb 9 2018;359(6376):684-688. doi:10.1126/science.aan4183
26. Grajchen E, Hendriks JJA, Bogie JFJ. The physiology of foamy phagocytes in multiple sclerosis. *Acta Neuropathol Commun*. Nov 19 2018;6(1):124. doi:10.1186/s40478-018-0628-8
27. Chinetti G, Lestavel S, Bocher V, *et al*. PPAR-alpha and PPAR-gamma activators induce cholesterol removal from human macrophage foam cells through stimulation of the ABCA1 pathway. *Nat Med*. Jan 2001;7(1):53-8. doi:10.1038/83348
28. Wouters E, Grajchen E, Jorissen W, *et al*. Altered PPARgamma Expression Promotes Myelin-Induced Foam Cell Formation in Macrophages in Multiple Sclerosis. *Int J Mol Sci*. Dec 7 2020;21(23)doi:10.3390/ijms21239329
29. Safaiyan S, Kannaiyan N, Snaidero N, *et al*. Age-related myelin degradation burdens the clearance function of microglia during aging. *Nat Neurosci*. Aug 2016;19(8):995-8. doi:10.1038/nn.4325
30. Kuhlmann T, Ludwin S, Prat A, Antel J, Bruck W, Lassmann H. An updated histological classification system for multiple sclerosis lesions. *Acta Neuropathol*. Jan 2017;133(1):13-24. doi:10.1007/s00401-016-1653-y
31. Frischer JM, Bramow S, Dal-Bianco A, *et al*. The relation between inflammation and neurodegeneration in multiple sclerosis brains. *Brain*. May 2009;132(Pt 5):1175-89. doi:10.1093/brain/awp070

32. Faissner S, Plemel JR, Gold R, Yong VW. Progressive multiple sclerosis: from pathophysiology to therapeutic strategies. *Nat Rev Drug Discov*. Dec 2019;18(12):905-922. doi:10.1038/s41573-019-0035-2
33. Meyer D, Birchmeier C. Multiple essential functions of neuregulin in development. *Nature*. Nov 23 1995;378(6555):386-90. doi:10.1038/378386a0
34. Falls DL. Neuregulins: functions, forms, and signaling strategies. *Exp Cell Res*. Mar 10 2003;284(1):14-30. doi:10.1016/s0014-4827(02)00102-7
35. Kataria H, Alizadeh A, Karimi-Abdolrezaee S. Neuregulin-1/ErbB network: An emerging modulator of nervous system injury and repair. *Prog Neurobiol*. Sep 2019;180:101643. doi:10.1016/j.pneurobio.2019.101643
36. Kataria H, Hart CG, Alizadeh A, *et al*. Neuregulin-1 beta 1 is implicated in pathogenesis of multiple sclerosis. *Brain*. Feb 12 2021;144(1):162-185. doi:10.1093/brain/awaa385
37. Kataria H, Alizadeh A, Shahriary GM, *et al*. Neuregulin-1 promotes remyelination and fosters a pro-regenerative inflammatory response in focal demyelinating lesions of the spinal cord. *Glia*. Mar 2018;66(3):538-561. doi:10.1002/glia.23264
38. Zirngibl M, Assinck P, Sizov A, Caprariello AV, Plemel JR. Oligodendrocyte death and myelin loss in the cuprizone model: an updated overview of the intrinsic and extrinsic causes of cuprizone demyelination. *Mol Neurodegener*. May 7 2022;17(1):34. doi:10.1186/s13024-022-00538-8
39. Schmued L, Bowyer J, Cozart M, Heard D, Binienda Z, Paule M. Introducing Black-Gold II, a highly soluble gold phosphate complex with several unique advantages for the histochemical localization of myelin. *Brain Res*. Sep 10 2008;1229:210-7. doi:10.1016/j.brainres.2008.06.129
40. Gauthier MK, Kosciuczyk K, Tapley L, Karimi-Abdolrezaee S. Dysregulation of the neuregulin-1-ErbB network modulates endogenous oligodendrocyte differentiation and preservation after spinal cord injury. *Eur J Neurosci*. Sep 2013;38(5):2693-715. doi:10.1111/ejn.12268
41. Miron VE, Boyd A, Zhao JW, *et al*. M2 microglia and macrophages drive oligodendrocyte differentiation during CNS remyelination. *Nat Neurosci*. Sep 2013;16(9):1211-1218. doi:10.1038/nn.3469
42. Sariol A, Mackin S, Allred MG, *et al*. Microglia depletion exacerbates demyelination and impairs remyelination in a neurotropic coronavirus infection. *Proc Natl Acad Sci U S A*. Sep 29 2020;117(39):24464-24474. doi:10.1073/pnas.2007814117
43. Plemel JR, Stratton JA, Michaels NJ, *et al*. Microglia response following acute demyelination is heterogeneous and limits infiltrating macrophage dispersion. *Sci Adv*. Jan 2020;6(3):eaay6324. doi:10.1126/sciadv.aay6324
44. Kent SA, Miron VE. Microglia regulation of central nervous system myelin health and regeneration. *Nat Rev Immunol*. Jan 2024;24(1):49-63. doi:10.1038/s41577-023-00907-4
45. Peterson AR, Garcia TA, Ford BD, Binder DK. Regulation of NRG-1-ErbB4 signaling and neuroprotection by exogenous neuregulin-1 in a mouse model of epilepsy. *Neurobiol Dis*. Dec 2021;161:105545. doi:10.1016/j.nbd.2021.105545
46. Li Y, Lein PJ, Ford GD, *et al*. Neuregulin-1 inhibits neuroinflammatory responses in a rat model of organophosphate-nerve agent-induced delayed neuronal injury. *J Neuroinflammation*. Apr 2 2015;12:64. doi:10.1186/s12974-015-0283-y

47. Spangenberg E, Severson PL, Hohsfield LA, *et al*. Sustained microglial depletion with CSF1R inhibitor impairs parenchymal plaque development in an Alzheimer's disease model. *Nat Commun*. Aug 21 2019;10(1):3758. doi:10.1038/s41467-019-11674-z
48. Westerterp M, Fotakis P, Ouimet M, *et al*. Cholesterol Efflux Pathways Suppress Inflammasome Activation, NETosis, and Atherogenesis. *Circulation*. Aug 28 2018;138(9):898-912. doi:10.1161/CIRCULATIONAHA.117.032636
49. Ponath G, Ramanan S, Mubarak M, *et al*. Myelin phagocytosis by astrocytes after myelin damage promotes lesion pathology. *Brain*. Feb 2017;140(2):399-413. doi:10.1093/brain/aww298
50. Li L, Cleary S, Mandarano MA, Long W, Birchmeier C, Jones FE. The breast proto-oncogene, HRGalpha regulates epithelial proliferation and lobuloalveolar development in the mouse mammary gland. *Oncogene*. Jul 25 2002;21(32):4900-7. doi:10.1038/sj.onc.1205634
51. Mei L, Nave KA. Neuregulin-ERBB signaling in the nervous system and neuropsychiatric diseases. *Neuron*. Jul 2 2014;83(1):27-49. doi:10.1016/j.neuron.2014.06.007
52. Kidani Y, Bensinger SJ. Liver X receptor and peroxisome proliferator-activated receptor as integrators of lipid homeostasis and immunity. *Immunol Rev*. Sep 2012;249(1):72-83. doi:10.1111/j.1600-065X.2012.01153.x
53. Castrillo A, Tontonoz P. Nuclear receptors in macrophage biology: at the crossroads of lipid metabolism and inflammation. *Annu Rev Cell Dev Biol*. 2004;20:455-80. doi:10.1146/annurev.cellbio.20.012103.134432
54. Camargo N, Goudriaan A, van Deijk AF, *et al*. Oligodendroglial myelination requires astrocyte-derived lipids. *PLoS Biol*. May 2017;15(5):e1002605. doi:10.1371/journal.pbio.1002605
55. Wang H, Eckel RH. What are lipoproteins doing in the brain? *Trends Endocrinol Metab*. Jan 2014;25(1):8-14. doi:10.1016/j.tem.2013.10.003
56. Berghoff SA, Spieth L, Sun T, *et al*. Neuronal cholesterol synthesis is essential for repair of chronically demyelinated lesions in mice. *Cell Rep*. Oct 26 2021;37(4):109889. doi:10.1016/j.celrep.2021.109889
57. Prinz M, Jung S, Priller J. Microglia Biology: One Century of Evolving Concepts. *Cell*. Oct 3 2019;179(2):292-311. doi:10.1016/j.cell.2019.08.053
58. Stratoulias V, Venero JL, Tremblay ME, Joseph B. Microglial subtypes: diversity within the microglial community. *EMBO J*. Sep 2 2019;38(17):e101997. doi:10.15252/embj.2019101997
59. Haase S, Linker RA. Inflammation in multiple sclerosis. *Ther Adv Neurol Disord*. 2021;14:17562864211007687. doi:10.1177/17562864211007687
60. Haider L, Fischer MT, Frischer JM, *et al*. Oxidative damage in multiple sclerosis lesions. *Brain*. Jul 2011;134(Pt 7):1914-24. doi:10.1093/brain/awr128
61. Lassmann H, Raine CS, Antel J, Prineas JW. Immunopathology of multiple sclerosis: report on an international meeting held at the Institute of Neurology of the University of Vienna. *J Neuroimmunol*. Jun 15 1998;86(2):213-7. doi:10.1016/s0165-5728(98)00031-9
62. Henderson AP, Barnett MH, Parratt JD, Prineas JW. Multiple sclerosis: distribution of inflammatory cells in newly forming lesions. *Ann Neurol*. Dec 2009;66(6):739-53. doi:10.1002/ana.21800

63. Trapp BD, Peterson J, Ransohoff RM, Rudick R, Mork S, Bo L. Axonal transection in the lesions of multiple sclerosis. *N Engl J Med*. Jan 29 1998;338(5):278-85. doi:10.1056/NEJM199801293380502
64. Bitsch A, Schuchardt J, Bunkowski S, Kuhlmann T, Bruck W. Acute axonal injury in multiple sclerosis. Correlation with demyelination and inflammation. *Brain*. Jun 2000;123 (Pt 6):1174-83. doi:10.1093/brain/123.6.1174
65. Fischer MT, Sharma R, Lim JL, *et al*. NADPH oxidase expression in active multiple sclerosis lesions in relation to oxidative tissue damage and mitochondrial injury. *Brain*. Mar 2012;135(Pt 3):886-99. doi:10.1093/brain/aws012
66. Lampron A, Larochelle A, Laflamme N, *et al*. Inefficient clearance of myelin debris by microglia impairs remyelinating processes. *J Exp Med*. Apr 6 2015;212(4):481-95. doi:10.1084/jem.20141656
67. Wlodarczyk A, Holtman IR, Krueger M, *et al*. A novel microglial subset plays a key role in myelinogenesis in developing brain. *EMBO J*. Nov 15 2017;36(22):3292-3308. doi:10.15252/embj.201696056
68. Natrajan MS, de la Fuente AG, Crawford AH, *et al*. Retinoid X receptor activation reverses age-related deficiencies in myelin debris phagocytosis and remyelination. *Brain*. Dec 2015;138(Pt 12):3581-97. doi:10.1093/brain/awv289
69. Arnett HA, Mason J, Marino M, Suzuki K, Matsushima GK, Ting JP. TNF alpha promotes proliferation of oligodendrocyte progenitors and remyelination. *Nat Neurosci*. Nov 2001;4(11):1116-22. doi:10.1038/nn738
70. Mason JL, Suzuki K, Chaplin DD, Matsushima GK. Interleukin-1beta promotes repair of the CNS. *J Neurosci*. Sep 15 2001;21(18):7046-52. doi:10.1523/JNEUROSCI.21-18-07046.2001
71. Duncan GJ, Ingram SD, Emberley K, *et al*. Remyelination protects neurons from DLK-mediated neurodegeneration. *Nat Commun*. Oct 23 2024;15(1):9148. doi:10.1038/s41467-024-53429-5
72. Huang JK, Jarjour AA, Nait Oumesmar B, *et al*. Retinoid X receptor gamma signaling accelerates CNS remyelination. *Nat Neurosci*. Jan 2011;14(1):45-53. doi:10.1038/nn.2702
73. Repa JJ, Turley SD, Lobaccaro JA, *et al*. Regulation of absorption and ABC1-mediated efflux of cholesterol by RXR heterodimers. *Science*. Sep 1 2000;289(5484):1524-9. doi:10.1126/science.289.5484.1524
74. Schulman IG. Liver X receptors link lipid metabolism and inflammation. *FEBS Lett*. Oct 2017;591(19):2978-2991. doi:10.1002/1873-3468.12702
75. Repa JJ, Berge KE, Pomajzl C, Richardson JA, Hobbs H, Mangelsdorf DJ. Regulation of ATP-binding cassette sterol transporters ABCG5 and ABCG8 by the liver X receptors alpha and beta. *J Biol Chem*. May 24 2002;277(21):18793-800. doi:10.1074/jbc.M109927200
76. Meffre D, Shackleford G, Hichor M, *et al*. Liver X receptors alpha and beta promote myelination and remyelination in the cerebellum. *Proc Natl Acad Sci U S A*. Jun 16 2015;112(24):7587-92. doi:10.1073/pnas.1424951112
77. Vanherle S, Jorissen W, Dierckx T, *et al*. The ApoA-I mimetic peptide 5A enhances remyelination by promoting clearance and degradation of myelin debris. *Cell Rep*. Nov 8 2022;41(6):111591. doi:10.1016/j.celrep.2022.111591
78. Xu G, Watanabe T, Iso Y, *et al*. Preventive effects of heregulin-beta1 on macrophage foam cell formation and atherosclerosis. *Circ Res*. Aug 28 2009;105(5):500-10. doi:10.1161/CIRCRESAHA.109.193870

79. Joseph SB, Castrillo A, Laffitte BA, Mangelsdorf DJ, Tontonoz P. Reciprocal regulation of inflammation and lipid metabolism by liver X receptors. *Nat Med*. Feb 2003;9(2):213-9. doi:10.1038/nm820
80. Ghisletti S, Huang W, Ogawa S, *et al*. Parallel SUMOylation-dependent pathways mediate gene- and signal-specific transrepression by LXRs and PPARgamma. *Mol Cell*. Jan 12 2007;25(1):57-70. doi:10.1016/j.molcel.2006.11.022
81. Ito A, Hong C, Rong X, *et al*. LXRs link metabolism to inflammation through Abca1-dependent regulation of membrane composition and TLR signaling. *Elife*. Jul 14 2015;4:e08009. doi:10.7554/eLife.08009
82. Alizadeh A, Santhosh KT, Kataria H, Gounni AS, Karimi-Abdolrezaee S. Neuregulin-1 elicits a regulatory immune response following traumatic spinal cord injury. *J Neuroinflammation*. Feb 21 2018;15(1):53. doi:10.1186/s12974-018-1093-9
83. Kim M, Wende H, Walcher J, *et al*. Maf links Neuregulin1 signaling to cholesterol synthesis in myelinating Schwann cells. *Genes Dev*. May 1 2018;32(9-10):645-657. doi:10.1101/gad.310490.117
84. Wang JQ, Gao MY, Gao R, Zhao KH, Zhang Y, Li X. Oligodendrocyte lineage cells: Advances in development, disease, and heterogeneity. *J Neurochem*. Feb 2023;164(4):468-480. doi:10.1111/jnc.15728
85. Elbaz B, Popko B. Molecular Control of Oligodendrocyte Development. *Trends Neurosci*. Apr 2019;42(4):263-277. doi:10.1016/j.tins.2019.01.002
86. Molina-Gonzalez I, Holloway RK, Jiwaji Z, *et al*. Astrocyte-oligodendrocyte interaction regulates central nervous system regeneration. *Nat Commun*. Jun 8 2023;14(1):3372. doi:10.1038/s41467-023-39046-8
87. Alizadeh A, Dyck SM, Kataria H, *et al*. Neuregulin-1 positively modulates glial response and improves neurological recovery following traumatic spinal cord injury. *Glia*. Jul 2017;65(7):1152-1175. doi:10.1002/glia.23150
88. Lau LW, Keough MB, Haylock-Jacobs S, *et al*. Chondroitin sulfate proteoglycans in demyelinated lesions impair remyelination. *Ann Neurol*. Sep 2012;72(3):419-32. doi:10.1002/ana.23599
89. Keough MB, Rogers JA, Zhang P, *et al*. An inhibitor of chondroitin sulfate proteoglycan synthesis promotes central nervous system remyelination. *Nat Commun*. Apr 26 2016;7:11312. doi:10.1038/ncomms11312
90. Lei F, Cui N, Zhou C, Chodosh J, Vavvas DG, Paschalis EI. CSF1R inhibition by a small-molecule inhibitor is not microglia specific; affecting hematopoiesis and the function of macrophages. *Proc Natl Acad Sci U S A*. Sep 22 2020;117(38):23336-23338. doi:10.1073/pnas.1922788117
91. Montilla A, Zabala A, Er-Lukowiak M, *et al*. Microglia and meningeal macrophages depletion delays the onset of experimental autoimmune encephalomyelitis. *Cell Death Dis*. Jan 12 2023;14(1):16. doi:10.1038/s41419-023-05551-3
92. Ye K, Chen Z, Xu Y. The double-edged functions of necroptosis. *Cell Death Dis*. Feb 27 2023;14(2):163. doi:10.1038/s41419-023-05691-6
93. Mifflin L, Hu Z, Dufort C, *et al*. A RIPK1-regulated inflammatory microglial state in amyotrophic lateral sclerosis. *Proc Natl Acad Sci U S A*. Mar 30 2021;118(13)doi:10.1073/pnas.2025102118

94. Ma XR, Yang SY, Zheng SS, *et al*. Inhibition of RIPK1 by ZJU-37 promotes oligodendrocyte progenitor proliferation and remyelination via NF-kappaB pathway. *Cell Death Discov*. Apr 1 2022;8(1):147. doi:10.1038/s41420-022-00929-2
95. Zhu X, Yu G, Lv Y, *et al*. Neuregulin-1, a member of the epidermal growth factor family, mitigates STING-mediated pyroptosis and necroptosis in ischaemic flaps. *Burns Trauma*. 2024;12:tkae035. doi:10.1093/burnst/tkae035
96. Decout A, Katz JD, Venkatraman S, Ablasser A. The cGAS-STING pathway as a therapeutic target in inflammatory diseases. *Nat Rev Immunol*. Sep 2021;21(9):548-569. doi:10.1038/s41577-021-00524-z
97. Modol-Caballero G, Santos D, Navarro X, Herrando-Grabulosa M. Neuregulin 1 Reduces Motoneuron Cell Death and Promotes Neurite Growth in an in Vitro Model of Motoneuron Degeneration. *Front Cell Neurosci*. 2017;11:431. doi:10.3389/fncel.2017.00431
98. Yoo JY, Kim HB, Baik TK, Lee JH, Woo RS. Neuregulin 1/ErbB4/Akt signaling attenuates cytotoxicity mediated by the APP-CT31 fragment of amyloid precursor protein. *Exp Mol Pathol*. Jun 2021;120:104622. doi:10.1016/j.yexmp.2021.104622
99. Michailov GV, Sereda MW, Brinkmann BG, *et al*. Axonal neuregulin-1 regulates myelin sheath thickness. *Science*. Apr 30 2004;304(5671):700-3. doi:10.1126/science.1095862
100. Hu X, Hicks CW, He W, *et al*. Bace1 modulates myelination in the central and peripheral nervous system. *Nat Neurosci*. Dec 2006;9(12):1520-5. doi:10.1038/nn1797
101. Willem M, Garratt AN, Novak B, *et al*. Control of peripheral nerve myelination by the beta-secretase BACE1. *Science*. Oct 27 2006;314(5799):664-6. doi:10.1126/science.1132341
102. Taveggia C, Thaker P, Petrylak A, *et al*. Type III neuregulin-1 promotes oligodendrocyte myelination. *Glia*. Feb 2008;56(3):284-93. doi:10.1002/glia.20612
103. Newbern J, Birchmeier C. Nrg1/ErbB signaling networks in Schwann cell development and myelination. *Semin Cell Dev Biol*. Dec 2010;21(9):922-8. doi:10.1016/j.semcdb.2010.08.008
104. Park SK, Miller R, Krane I, Vartanian T. The erbB2 gene is required for the development of terminally differentiated spinal cord oligodendrocytes. *J Cell Biol*. Sep 17 2001;154(6):1245-58. doi:10.1083/jcb.200104025
105. Vartanian T, Fischbach G, Miller R. Failure of spinal cord oligodendrocyte development in mice lacking neuregulin. *Proc Natl Acad Sci U S A*. Jan 19 1999;96(2):731-5. doi:10.1073/pnas.96.2.731
106. Brinkmann BG, Agarwal A, Sereda MW, *et al*. Neuregulin-1/ErbB signaling serves distinct functions in myelination of the peripheral and central nervous system. *Neuron*. Aug 28 2008;59(4):581-95. doi:10.1016/j.neuron.2008.06.028
107. Jakel S, Agirre E, Mendanha Falcao A, *et al*. Altered human oligodendrocyte heterogeneity in multiple sclerosis. *Nature*. Feb 2019;566(7745):543-547. doi:10.1038/s41586-019-0903-2
108. Schirmer L, Velmeshev D, Holmqvist S, *et al*. Neuronal vulnerability and multilineage diversity in multiple sclerosis. *Nature*. Sep 2019;573(7772):75-82. doi:10.1038/s41586-019-1404-z
109. Falcao AM, van Bruggen D, Marques S, *et al*. Disease-specific oligodendrocyte lineage cells arise in multiple sclerosis. *Nat Med*. Dec 2018;24(12):1837-1844. doi:10.1038/s41591-018-0236-y
110. Filippi M, Bar-Or A, Piehl F, *et al*. Multiple sclerosis. *Nat Rev Dis Primers*. Nov 8 2018;4(1):43. doi:10.1038/s41572-018-0041-4

111. Thomson PA, Christoforou A, Morris SW, *et al*. Association of Neuregulin 1 with schizophrenia and bipolar disorder in a second cohort from the Scottish population. *Mol Psychiatry*. Jan 2007;12(1):94-104. doi:10.1038/sj.mp.4001889
112. Georgieva L, Dimitrova A, Ivanov D, *et al*. Support for neuregulin 1 as a susceptibility gene for bipolar disorder and schizophrenia. *Biol Psychiatry*. Sep 1 2008;64(5):419-27. doi:10.1016/j.biopsych.2008.03.025
113. Prata DP, Breen G, Osborne S, Munro J, St Clair D, Collier DA. An association study of the neuregulin 1 gene, bipolar affective disorder and psychosis. *Psychiatr Genet*. Jun 2009;19(3):113-6. doi:10.1097/YPG.0b013e32832a4f69
114. Stefansson H, Sigurdsson E, Steinthorsdottir V, *et al*. Neuregulin 1 and susceptibility to schizophrenia. *Am J Hum Genet*. Oct 2002;71(4):877-92. doi:10.1086/342734
115. Law AJ, Lipska BK, Weickert CS, *et al*. Neuregulin 1 transcripts are differentially expressed in schizophrenia and regulated by 5' SNPs associated with the disease. *Proc Natl Acad Sci U S A*. Apr 25 2006;103(17):6747-52. doi:10.1073/pnas.0602002103
116. Corfas G, Roy K, Buxbaum JD. Neuregulin 1-erbB signaling and the molecular/cellular basis of schizophrenia. *Nat Neurosci*. Jun 2004;7(6):575-80. doi:10.1038/nn1258
117. Kastin AJ, Akerstrom V, Pan W. Neuregulin-1-beta1 enters brain and spinal cord by receptor-mediated transport. *J Neurochem*. Feb 2004;88(4):965-70. doi:10.1046/j.1471-4159.2003.02224.x
118. Kang SH, Fukaya M, Yang JK, Rothstein JD, Bergles DE. NG2+ CNS glial progenitors remain committed to the oligodendrocyte lineage in postnatal life and following neurodegeneration. *Neuron*. Nov 18 2010;68(4):668-81. doi:10.1016/j.neuron.2010.09.009
119. Fricker FR, Antunes-Martins A, Galino J, *et al*. Axonal neuregulin 1 is a rate limiting but not essential factor for nerve remyelination. *Brain*. Jul 2013;136(Pt 7):2279-97. doi:10.1093/brain/awt148
120. Kramer R, Bucay N, Kane DJ, Martin LE, Tarpley JE, Theill LE. Neuregulins with an Ig-like domain are essential for mouse myocardial and neuronal development. *Proc Natl Acad Sci U S A*. May 14 1996;93(10):4833-8. doi:10.1073/pnas.93.10.4833
121. Hart CG, Dyck SM, Kataria H, *et al*. Acute upregulation of bone morphogenetic protein-4 regulates endogenous cell response and promotes cell death in spinal cord injury. *Exp Neurol*. Mar 2020;325:113163. doi:10.1016/j.expneurol.2019.113163
122. Buck SB, Bradford J, Gee KR, Agnew BJ, Clarke ST, Salic A. Detection of S-phase cell cycle progression using 5-ethynyl-2'-deoxyuridine incorporation with click chemistry, an alternative to using 5-bromo-2'-deoxyuridine antibodies. *Biotechniques*. Jun 2008;44(7):927-9. doi:10.2144/000112812
123. Spangenberg EE, Lee RJ, Najafi AR, *et al*. Eliminating microglia in Alzheimer's mice prevents neuronal loss without modulating amyloid-beta pathology. *Brain*. Apr 2016;139(Pt 4):1265-81. doi:10.1093/brain/aww016
124. Ge SX, Son EW, Yao R. iDEP: an integrated web application for differential expression and pathway analysis of RNA-Seq data. *BMC Bioinformatics*. Dec 19 2018;19(1):534. doi:10.1186/s12859-018-2486-6
125. Shahriary GM, Kataria H, Karimi-Abdolrezaee S. Neuregulin-1 Fosters Supportive Interactions between Microglia and Neural Stem/Progenitor Cells. *Stem Cells Int*. 2019;2019:8397158. doi:10.1155/2019/8397158

Acknowledgements: This project was funded by operating grants held by S. K-A from the Multiple Sclerosis Canada Discovery Grant (EGID3742 and 1241879), and the Canadian Institute of Health Research (PJT-191850). S.M.Z was supported by a studentship from Multiple Sclerosis Canada and the University of Manitoba Graduate Fellowship and the Hillary Kaufman Memorial Funds in Multiple Sclerosis from the University of Manitoba. E.J. was supported by a Fellowship from the Canadian Stem Cell Network and Multiple Sclerosis Canada. S.M.H. was supported by a Doctoral Studentship Grant from the Wings for Life Foundation and the Hillary Kaufman Memorial Funds in Multiple Sclerosis from the University of Manitoba. G.M. was supported by the BSc Med Program at the Rady Faculty of Health Sciences, the University of Manitoba.

The authors would like to acknowledge Ms. Maria Astrid Bravo Jimenez for her assistance with animal care and some cell culture. Electron microscopy was performed by Histology Service Lab in the Department of Human Anatomy and Cell Science, University of Manitoba. Service provider for library preparation and RNA sequencing was Genome Quebec, Montreal, QC, Canada. Schematic figures were prepared with the help of items from BioRender.com online tool.

Authors contributions: S.K-A and H.K. conceived and designed the study. S.M.Z performed several cuprizone and Nrg-1 mutant animal experiments, majority of in vitro studies, microglia, and myelin analysis of cuprizone mice, performed data interpretation and preparation for RNA sequencing, prepared the initial figures and the first draft of original manuscript. S.N. conducted cuprizone live animal experiments and performed immunohistochemistry, imaging, and tissue analysis of cuprizone and EAE mice as well as data preparation for RNA sequencing, tissue culture and PCR experiments. H.K. conducted live EAE mice experiment, analysis of oligodendrocytes in cuprizone mice, designed in vitro experiments and in vivo cuprizone and Nrg-1 knockout mice studies. E.J. and S.M.H have contributed equally to this work. E.J. conducted live cuprizone animal experiments and performed several tissue processing and immunohistochemical staining, imaging and analysis in cuprizone and EAE. S.M.H performed MACS, RNA extraction, data interpretation and bioinformatics for RNA sequencing. P.G. and A.T. designed and prepared nanofibers. G.M. performed myelination analyses in EAE. V.W.Y. contributed to MS brain samples and editing. S. K-A. supervised the study, designed experiments, analyzed data and interpreted the results, provided operational support, wrote, prepared, edited and finalized the original and revised manuscript and figures. All authors reviewed and approved the manuscript.

Competing interest: 1) S.K-A and H.K. are inventors on a patent entitled "USE OF NRG-1β1 FOR DETECTION AND/OR TREATMENT OF MULTIPLE SCLEROSIS" that is filed through three applications: A) Published PCT Application WO2022/056619 (completed), B) Published US Patent Application US2024/0009274, published January 11, 2024 (pending), C) Canadian Patent Application 3,191,086, date of national phase entry – February 27, 2023 (pending) - US Patent App. 18/043,199, 2024). This patent is related to the potential use of Nrg-1β1 as a treatment for multiple sclerosis. 2) S.K-A is also an inventor on a provisional patent application titled "the NRG-1 CONDITIONAL KNOCKOUT MOUSE", US Provisional Patent Application Serial Number 63/802,795, filed May 9, 2025 (pending). This provisional patent application is related to the Nrg-1 conditional knockout mouse model that is used in this article. The relevant interests regarding these two patent applications are managed by the University of Manitoba. All other authors declare no competing interests related to this work.

Figure legends

Figure 1: Impaired remyelination in chronic demyelinated lesions is associated with persistent dysregulation of Nrg-1. a) Schematic of experimental design for induction of short-term and chronic long-term cuprizone (CPZ) demyelination in tamoxifen inducible PDGFRα-Cre^{ERTM}:Rosa26mGFP(mT/mG) reporter mice (PDGFRα-Cre) for tracking OPCs and oligodendrocytes by GFP expression (green). b, c) Corpus callosum was assessed for demyelination and remyelination. Black Gold II (BGII) staining (purple) of the corpus callosum shows short-term demyelination is followed with significant remyelination after 2 weeks of recovery. In contrast, remyelination is impaired after chronic demyelination, despite the presence of GFP+ OPC progeny (green). One Way ANOVA- Tukey's multiple comparisons test (two-sided); short-term study: N=5 PDGFRα-Cre mice /group; chronic study: N=3 mice for control and CPZ 10wk, N=4 PDGFRα-Cre mice/group. Each mouse is a biological replicate. Black dashed lines in 'b' demarcate CC. d-g) Immunostaining for Nrg-1 (red) the cortex and corpus callosum after short-term and chronic demyelination/recovery. White dashed lines in 'e' demarcate CC. h-i) Nrg-1 protein is downregulated significantly after short-term demyelination the cortex and corpus callosum but was restored significantly during the recovery period. h and i: One Way ANOVA- Tukey's multiple comparisons test (two-sided); N=5 PDGFRα-Cre mice (biological replicates)/group. j-k) After chronic demyelination, Nrg-1 expression was significantly downregulated in the cortex and corpus callosum that persisted during the 4 weeks recovery. One Way ANOVA- Tukey's multiple comparisons test (two-sided); j: N=3 mice for control, N=4 PDGFRα-Cre mice for CPZ 10wk and CPZ 10+4wk; k: N=3 PDGFRα-Cre mice for control and CPZ 10wk, N=4 PDGFRα-Cre mice for CPZ 10+4wk. Each mouse is a biological replicate. Source data are provided as a Source Data file.

Figure 2: Lipid laden microglia are abundant in human progressive MS lesions and in chronic CPZ demyelinated lesions. a) Representative images from chronic active demyelinating lesions from specimens acquired from individuals with secondary progressive MS. Immunostaining for CD11b (red) as a marker of microglia and macrophages and TMEM119 (grey) as a specific marker of microglia showed abundance of CD11b+TMEM119+ microglia in these lesions. ORO staining (purple) of the same tissue sections showed intracellular accumulation of cholesterol in CD11b+TMEM119+ microglia at the rim and to some level, within the lesion, while cholesterol accumulations was not detected within the normal appearing white matter (NAWM). Black and white dashed boxes identify the magnified fields illustrated in each panel. b) Iba-1 (green) and DAPI (blue) immunostaining and ORO staining (purple) of the chronically demyelinated CPZ lesions of corpus callosum show the abundance of phagocytes with myelin-derived lipid accumulation. c) Immunostaining of microglia with CD11b (green), TMEM119 (red) and DAPI (blue). d) After 2- and 4 weeks of recovery after CPZ (10+2wk CPZ and 10+4wk CPZ mice), analysis of CD11b+TMEM119+ cells showed that microglia are the predominant cells in the chronic demyelinated lesions of CPZ as compared to CD11b+TMEM119- cells (macrophages). No healthy control group was included in this experiment as the aim was to analyze the abundance of microglia verses macrophages within CPZ demyelinated lesions. Two Way ANOVA- Tukey's multiple comparisons test (two-sided); N=4 PDGFRα-Cre mice (biological replicates)/group. Source data are provided as a Source Data file.

Figure 3: Nrg-1 promotes remyelination in chronic cuprizone lesions in a microglia dependent manner. a) Animal study design. b) Iba-1 immunostaining (green) confirms successful microglia depletion in PLX5622. One Way ANOVA- Tukey's multiple comparisons test (two-

sided), PDGFRα-Cre mice (N=3 control, N=5 10WCPZ, N=4 10WCPZ+PLX5622, 10+4wk and 10+4wk-PLX5622. Each mouse is a biological replicate. c) BGII staining (purple), dMBP (red) and GFP (green). d-e) BGII and dMBP intensity shows extensive demyelination after 10WCPZ. Poor remyelination after 2- and 4 weeks recovery. Nrg-1β1 significantly increased remyelination and decreased dMBP. PLX5622 treatment abolished Nrg-1β1 effects. White and black dashed lines in 'c' demarcate CC. One Way ANOVA- Tukey's multiple comparisons test (two-sided); d (BGII): PDGFRα-Cre mice for CPZ10wk+2wkN/D, (N=3 control, 10wkCPZ, PLX5622+Vehicle, PLX5622+Nrg-1, N=5 vehicle, N=4 Nrg-1); for CPZ10wk+4wk N/D: (N=3 control and 10wkCPZ, N=4 vehicle, Nrg-1, PLX5622+Vehicle, PLX5622+Nrg-1). e (dMBP): PDGFRα-Cre mice for CPZ10wk+2wk N/D (N=4 control, 10wkCPZ, PLX5622+Vehicle, N=5 vehicle and Nrg-1, N=3 PLX5622+Nrg-1); CPZ10wk+4wkN/D: N=4 PDGFRα-Cre mice/group. Each mouse is a biological replicate. f) Electron-micrographs. g) 10WCPZ mice showed significant demyelination (higher g-ratio) compared to control. Post-CPZ recovery led to low degree of remyelination in vehicle mice. Nrg-1β1 increased myelin thickness which was reversed in PLX5622 mice. One Way ANOVA- Tukey's multiple comparisons test (two-sided); PDGFRα-Cre mice (N=3 control, 10wkCPZ, PLX5622+Vehicle, N=4 vehicle, Nrg-1 and PLX5622+Nrg-1). h-i) The g-ratio patterns were consistent across different axon diameters, with Nrg-1 mice having fewer thinly myelinated axons and more heavily myelinated axons compared to vehicle mice. In PLX5622 mice, the effect of Nrg-1β1 was not significant. Two Way ANOVA-Tukey's multiple comparisons test (two-sided); PDGFRα-Cre mice (N=3 control, 10wkCPZ, PLX5622+Vehicle, N=4 vehicle, Nrg-1 and PLX5622+Nrg-1. Each mouse is a biological replicate. k-l) Density of myelinated axons significantly decreased after 10WCPZ compared to control. No significant improvement in vehicle mice. Nrg-1β1 significantly increased myelinated axons compared to 10WCPZ mice. No

difference between Nrg-1β1 and vehicle. Nrg-1β1 effect was not observed in PLX5622 mice. One Way ANOVA- Tukey's multiple comparisons test (two-sided); PDGFRα-Cre mice (N=3 control and 10wkCPZ; N=4 vehicle, Nrg-1, PLX5622+Vehicle and PLX5622+Nrg-1). Each mouse is a biological replicate. Source data are provided as a Source Data file.

Figure 4: Nrg-1β1 treatment promotes oligodendrogenesis and oligodendrocyte maturation in chronic CPZ lesions partially through microglia. a) Schematic of study design. b) Images from the chronic CPZ lesions of corpus callosum at 12-week and 14-week time points from PDGFRα-Cre mice show new oligodendrocytes marked as GFP+ (green), Olig2 (red) and EdU (grey). c) Quantification of Olig2+/GFP+ cells shows a significant decrease in oligodendrocytes after 10WCPZ compared to control. Dotted line delineates the total count of Olig2-expressing cells in control mice, while the control column signifies the baseline of new oligogenesis characterized by Olig2+/GFP+ cells. Nrg-1β1 significantly promoted Olig2+/GFP+ cells at 2 weeks post-CPZ compared to the vehicle counterpart irrespective of microglia depletion. The same pattern was observed at 4 weeks after CPZ withdrawal, but the effects of Nrg-1β1 treatment were not statistically significant. One Way ANOVA- Tukey's multiple comparisons test (two-sided); PDGFRα-Cre mice (N=3 control, 10wkCPZ, 10+2wk PLX5622+Vehicle; N=5 10+2wk+Vehicle; N=4 10+2wk Nrg-1, 10+2wk PLX5622+Nrg-1, 10+4wk Vehicle, 10+4wk Nrg-1, 10+4wk PLX5622+Vehicle, 10+4wk PLX5622+Nrg-1). d) OPC proliferation was assessed by EdU injection during the first week of recovery. Nrg-1β1 promotes OPC proliferation and oligodendrogenesis (Olig2+GFP+EdU+) in a microglia independent manner. One Way ANOVA-Tukey's multiple comparisons test (two-sided); PDGFRα-Cre mice (N=5 10+2wk+Vehicle; N=4 10+2wk Nrg-1, 10+2wk PLX5622+Nrg-1; 10+4wk+Vehicle; 10+4wk Nrg-1; 10+4wk

PLX5622+Vehicle; 10+4wk PLX5622+Nrg-1; N=3 10+2wk PLX5622+Vehicle). e) Images show newly mature oligodendrocytes marked by APC (red), EdU (grey) and GFP (green). f) Quantification of APC+GFP+ cells confirms loss of oligodendrocytes after 10WCPZ. Nrg-1β1 significantly enhanced repopulation of mature oligodendrocytes after 2 and 4 weeks of recovery in a microglia-dependent manner. One Way ANOVA- Tukey's multiple comparisons test (two-sided); PDGFRα-Cre mice (N=3 control, 10wkCPZ, 10+2wk PLX5622+Vehicle; N=5 10+2wk+Vehicle; N=4 10+2wk Nrg-1, 10+2wk PLX5622+Nrg-1; 10+4wk+Vehicle; 10+4wk Nrg-1; 10+4wk PLX5622+Vehicle; 10+4wk PLX5622+Nrg-1). g) Nrg-1β1 promoted the maturation of new oligodendrocytes (APC+GFP+EdU+) during 2- and 4 weeks recovery that was independent of microglia. One Way ANOVA- Tukey's multiple comparisons test (two-sided); PDGFRα-Cre mice (N=4 10+2wk+Vehicle; 10+2wk Nrg-1, 10+2wk PLX5622+Nrg-1; 10+4wk+Vehicle; 10+4wk Nrg-1; 10+4wk PLX5622+Vehicle; 10+4wk PLX5622+Nrg-1; N=3 10+2wk PLX5622+Vehicle). Each mouse is a biological replicate. Source data are provided as a Source Data file.

Figure 5: Nrg-1β1 treatment increases microglia number within chronically demyelinated lesions by attenuating microglial cell death and enhancing microglia proliferation. a) Co-immunostaining of CD11b (green), P2Y12 (red), a specific marker of microglia, and DAPI (blue) in 10+2wk and 10+4wk CPZ mice. b) Nrg-1β1 treatment promoted the number of CD11b+/P2Y12+ microglia compared to vehicle. No control group was included as the aim was to analyze the abundance of microglia verses macrophages during the recovery phase after CPZ demyelination. Two Way ANOVA- Tukey's multiple comparisons test (two-sided). PDGFR-Cre mice: N=4 biological replicates for 10+2wk Vehicle and 10+4wk Vehicle groups and N=4

biological replicates for 10+2wk Nrg-1 and 10+4wk Nrg-1 groups. c-d) Analysis of EdU+ (grey)/CD11b+ (green) cells in 10WCPZ lesions showed a significant increase in proliferating microglia compared to healthy controls. Analysis of EdU+/CD11b+ cells (red arrowheads) during the 2 weeks recovery post-CPZ showed a significant decrease in proliferating microglia compared to 10WCPZ mice. Nrg-1β1 treatment significantly enhanced microglia proliferation compared to vehicle treatment in 10+2wk mice. Microglia proliferation over 4 weeks recovery period remained unchanged in vehicle treated mice compared to their proliferative status after 2 weeks of recovery. Nrg-1 treated mice showed a significant rise in the number of EdU+/CD11b+ cells that was comparable to the number of proliferating microglia in 10WCPZ mice and significantly higher than the 10+4wk Vehicle mice. One Way ANOVA-Tukey's multiple comparisons test (two-sided), PDGFR-Cre mice: N=4 biological replicates/group e-f) Assessment of microglia necroptosis within CPZ lesion using co-immunolabeling of RIP3 (red), CD11b (green) and DAPI (blue) (white arrowhead) revealed a significant increase in necroptotic microglia at 10+2wk and 10+4wk time points, which was attenuated by Nrg-1β1 treatment. One Way ANOVA-Tukey's multiple comparisons test. PDGFR-Cre mice: N=4 biological replicates for 10+2wk Vehicle, 10+4wk Vehicle and 10+2wk Nrg-1 groups and N=3 biological replicates for 10+2wk Nrg-1group. Source data are provided as a Source Data file.

Figure 6: Nrg-1β1 treatment attenuates microglia lipid load in chronic CPZ lesions and preserves myelin during active demyelination.

a) ORO (purple) was analyzed for esterified lipid in the CC of control and chronic CPZ mice. b) ORO significantly increased in 10WCPZ mice. Following CPZ withdrawal, ORO decreases in vehicle and Nrg-1β1 treated mice. PLX5622 partially reverses Nrg-1 effects. One Way ANOVA-

Tukey's multiple comparisons test (two-sided); PDGFR-Cre mice, N=4 mice for Control, 10WCPZ, 10+2wk Vehicle, 10+2wk Nrg-1, 10+2wk PLX5622+Vehicle, 10+2wk PLX5622+Nrg-1, 10+4wk Nrg-1, 10+4wk PLX5622+Vehicle, N=3 for 10+4wk Vehicle. Each mouse is a biological replicate. c-d**)** ORO (purple, black arrowhead) Analysis in Iba-1+ microglia (green, white arrowhead) showed a significant decrease by Nrg-1β1 compared to vehicle. One Way ANOVA-Tukey's multiple comparisons test (two-sided); PDGFR-Cre mice; N=5 mice for 10+2wk Vehicle; N=4 mice for 10+2wk Nrg-1 and 10+4wk Nrg-1; N=3 mice for 10+4wk Vehicle. Each mouse is a biological replicate. e-f) Number of microglia was comparable between the PLX5622-Vehicle and PLX5622-Nrg-1 mice. Iba-1+ microglia (green, white arrowhead) contained ORO (purple, black arrowhead) and Nrg-1 had no effect on microglia ORO content. Unpaired Student-t-test (two-sided), PDGFR-Cre mice, N=4 mice/group. g-h) In PLX5622 mice, ORO (purple, black arrowhead) was observed in GFAP+ astrocytes (red) which was significantly reduced by Nrg-1β1. Unpaired Student-t-test (two-sided), PDGFR-Cre mice, N=4 mice/group. Each mouse is a biological replicate. In c, e, and g, no control group was included as this analysis assessed microglia and astrocytes lipid load in demyelinating lesions. i-j) ABCA-1 (red) increased in CD11b+ cells (green) with Nrg-1β1 at 10+2wk compared to vehicle. One Way ANOVA-Tukey's multiple comparisons test (two-sided); PDGFR-Cre mice, N=4 mice/group. Each mouse is a biological replicate. k-l) BGII (purple) analysis showed 10WCPZ results in significant demyelination and Nrg-1β1 treatment during active demyelination preserves myelin compared to vehicle. m-n) dMBP (red) was reduced by Nrg-1β1 compared to vehicle. o-p) Significant reduction in ORO (purple) under Nrg-1β1. White dashed lines in ‘m’ demarcate CC. For l, n, p: One Way ANOVA-Tukey's multiple comparisons test (two-sided); PDGFR-Cre mice, N=4 mice/group. Each mouse is a biological replicate. Source data are provided as a Source Data file.

Figure 7: **Nrg-1β1 treatment promotes remyelination in EAE lesions**. a) Images of new oligodendrocytes [Olig2 (red) and EdU (white)] in EAE lesions. b**)** Olig2+ oligodendrocytes were significantly higher under Nrg-1β1 compared to vehicle. c) Olig2+/EdU+ new oligodendrocytes significantly increased with Nrg-1 treatment. Unpaired t-test (two-sided), C57/BL6 mice, N= 4 biological replicates/group. No control group as the aim was to analyze oligodendrocytes in EAE. d-e) Myelin g-ratio on electron-micrograph of spinal cord EAE lesions exhibited a significant reduction in myelin thickness compared to control. Nrg-1β1 significantly increased the thickness of myelin in EAE lesions compared to vehicle, reaching the baseline levels. One Way ANOVA-Tukey's multiple comparisons test (two-sided), C57/BL6 mice, N= 4 biological replicates/group. f) Pooling of the g-ratio values per axon diameter showed a decrease with Nrg-1β1 across all axon diameters. g) Frequency distribution of g-ratio showed an increase in heavily myelinated axons and a decrease in thinly myelinated fibers with Nrg-1β1. Two Way ANOVA-Tukey's multiple comparisons test (two-sided), C57/BL6 mice, N= 4 biological replicates/group. h) Nrg-1β1 did not change number of (CD11b+ (white)/TMEM119+ (red) /DAPI+ (blue) microglia in EAE lesions. Number of CD11b+ (white)/TMEM119- (red)/ DAPI (blue) macrophages also showed no changes under Nrg-1β1. One Way ANOVA- Tukey's multiple comparisons test (two-sided), C57/BL6 mice, N= 5 biological replicates/group. i) Nrg-1β1 significantly reduced ORO in EAE lesions compared to vehicle. Unpaired t-test (two-sided), C57/BL6 mice, N= 5 biological replicates/group. No control group was included as the aim was to analyze the ORO in EAE demyelinated lesions. j) Analysis of daily clinical scoring of EAE mice for 42 days post-EAE induction showed that Nrg-1β1 treatment at the peak of disease reduces EAE disease burden compared to vehicle treated mice that was significantly different at several timepoints. However, the overall area under the curve did not reach the statistical significance point. Two Way ANOVA-Tukey's multiple comparisons

test (two-sided) for daily clinical score and Mann Whitney test- two-sided for area under the curve. C57/BL6 mice, N=7/vehicle, N=8/ Nrg-1β1. No control group as neurological recovery was compared in EAE mice under treatments. Source data are provided as a Source Data file.

Figure 8: Ablation of endogenous Nrg-1 results in spontaneous demyelination and suppresses remyelination in chronic CPZ lesions. a) Study design. b-c) Knockout of Nrg-1 EGF domain (red) was confirmed in the brain of Nrg-1 cKO mice. Unpaired t-test (two-sided), Nrg-1 cKO mice and WT littermate, N=3 biological replicates/group. d-e) BGII staining (purple) revealed significant demyelination in Nrg-1 cKO mice at 16wk post-tamoxifen as compared to WT controls. After 4wk recovery, Nrg-1 cKO mice showed less remyelination compared to WT. Nrg-1β1 treatment promoted remyelination in Nrg-1 cKO mice. One Way ANOVA-Tukey's multiple comparisons (two-sided), Nrg-1 cKO mice and WT littermate, N=4 biological replicates/group. f-g) dMBP (red) was detected in Nrg-1 cKO mice. Nrg-1 cKO mice on 10WCPZ diet showed higher dMBP compared to counterparts on normal diet. Exogenous Nrg-1β1 reduced dMBP in WT and Nrg-1 cKO mice compared to vehicle counterparts. One Way ANOVA-Tukey's multiple comparisons (two-sided), Nrg-1 cKO mice and WT littermate, N=4 biological replicates/group. h-i) ORO was significantly increased in WT and Nrg-1 cKO mice after 10WCPZ compared to counterparts on normal diet. One Way ANOVA-Tukey's multiple comparisons (two-sided), Nrg-1 cKO mice and WT littermate, N=4 biological replicates/group. j-k) Myelin g-ratio on electron-micrographs showed a significant decrease in myelin thickness in Nrg-1 cKO compared to WT on normal diet and was significantly lower in WT and Nrg-1 cKO at 4wk post-CPZ compared to counterparts on normal diet. Nrg-1β1 treatment promoted remyelination and g-ratio in Nrg-1 cKO mice compared to vehicle counterparts. One Way ANOVA-Tukey's multiple comparisons (two-

sided), Nrg-1 cKO mice and WT littermate, N=5 biological replicates except for 10+4wk WT (N=4). l) These changes were similar across axon diameters. M) The frequency distribution of g-ratio showed a lower percentage of thickly myelinated fibers in Nrg-1 cKO mice compared to WT. m) In CPZ mice and 4wk post-CPZ, thinly myelinated axons were frequent in vehicle treated WT and Nrg-1 cKO mice. Thickly myelinated axons were more frequent in Nrg-1β1-treated cKO mice. One Way ANOVA-Tukey's multiple comparisons (two-sided), Nrg-1 cKO mice and WT littermate, N=5 biological replicates except for 10+4wk WT (N=4). Source data are provided as a Source Data file.

Figure 9: Nrg-1/ErbB signaling promotes microglial myelin phagocytosis and cholesterol recycling and release through PPARγ and LXR pathways. a) Microglia isolated from CD1 mice are cultured in 4 different conditions: 1) control), 2) control+Nrg-1β1, 3) LPS+IFN-γ, 4) LPS+IFN-γ+Nrg-1β1. Images of microglia exposed to myelin (green) isolated from YFP mice with insets showing magnified cells. b**)** Z-stack of magnified field confirms myelin phagocytosis (YFP+myelin: green) by microglia [Iba-1+ (red)/ DAPI+ (blue)]. c**)** After 24 hours, Nrg-1β1 significantly enhanced myelin phagocytosis **(**YFP signal) by activated microglia. One Way ANOVA-Tukey's multiple comparisons (two-sided), N=4 independent culture (biological replicates). d) Nrg-1β1 significantly reduced mRNA expression of *IL-1β, IL6 and TNF-α* in activated microglia. One Way ANOVA-Tukey's multiple comparisons (two-sided), N=5 independent culture (biological replicates). e-f) Filipin III (blue) and ORO (purple) that stain free cholesterol and esterified lipids, respectively were enhanced by Nrg-1β1 in microglia that were exposed to myelin. One Way ANOVA-Tukey's multiple comparisons (two-sided), N=4 for Filipin III and N=3 for ORO independent culture (biological replicates). g) *Abcg-1* and *Abca-1* expression

were reduced in activated myelin-exposed microglia and remained unaffected by Nrg-1β1. One Way ANOVA-Tukey's multiple comparisons (two-sided), N=4 independent culture (biological replicates). h**)** Cholesterol levels in MCM were significantly elevated after myelin exposure. Activation of myelin-exposed microglia led to a decrease in cholesterol release that was enhanced with Nrg-1β1. One Way ANOVA-Tukey's multiple comparisons (two-sided), N=4 independent culture (biological replicates). i) Inhibition of ErbB3 receptor alone or in combination with ErbB2 receptor reversed Nrg-1 effects on enhanced cholesterol release by activated microglia. One Way ANOVA-Tukey's multiple comparisons (two-sided) One Way ANOVA- Tukey's multiple comparisons (two-sided), N=4 for control+Nrg-1, TX 2μM+Nrg-1, TX 2μM+TAK 250nM+Nrg-1, and N=3 for control, TX 2μM, TX 2μM+TAK 250nM independent culture (biological replicates). j) PPARγ antagonist GW9662 and LXR antagonist GSK2033 were added to microglia cultures to functionally block these pathways. Nrg-1β1 effects on cholesterol release was diminished by PPARγ and LXR blockade. One Way ANOVA-Tukey's multiple comparisons (two-sided), N=4 independent culture (biological replicates). No non-activated control microglia condition was included as this experiment assessed myelin phagocytosis and processing in activated microglia. Source data are provided as a Source Data file.

Figure 10: Nrg-1, through ErbB receptors, promotes the capacity of activated microglia in facilitating OPC maturation and myelination. a**)** a**)** OPCs from CD1 mice were cultured in the presence of MCM from various microglia condition for 14 days to assess their maturation using co-immunolabeling for O4 (red), MBP (white) and DAPI (blue). Control conditions with only OPC media and direct Nrg-1β1 treatment (200ng/ml) were included. b**)** Direct addition of Nrg-1β1 to OPCs cultures resulted in a significant increase in O4 expression level in oligodendrocytes.

OPCs cultured in the presence of MCM from activated microglia exposed to myelin and treated with Nrg-1β1 displayed markedly higher O4 expression compared to control or other MCM treated conditions, although the number of O4+ cells remained unchanged. One Way ANOVA- Tukey's multiple comparisons test (two-sided), N=4 CD1 mice independent culture (biological replicates). c**)** Nrg-1β1 treated OPCs showed enhanced maturation, as evidenced by both an increase in the number of MBP+ cells and the expression of MBP. OPCs treated with MCM from activated and myelin-exposed Nrg-1β1-treated microglia showed a higher MBP signal intensity compared to other MCM conditions. One Way ANOVA- Tukey's multiple comparisons test (two-sided), N=4 CD1 mice independent culture (biological replicates). d-e) OPCs were cultured on electro-spun nanofibrous scaffolds for 4 weeks. Myelination was assessed by MBP immunostaining. The quantity and length of myelin sheath per each wrapping oligodendrocyte exhibited a significant increase in oligodendrocyte cultures treated directly with Nrg-1β1 or with MCM from activated and myelin-exposed microglia treated with Nrg-1β1, as compared to MCM from non-Nrg-1 treated microglia. Inhibition of microglial ErbB receptors abolished the positive effects of Nrg-1 treated MCM on myelination. One Way ANOVA- Tukey's multiple comparisons test (two-sided), N=4 CD1 mice independent culture (biological replicates). Source data are provided as a Source Data file.

Editorial Summary:
Dysfunction of microglia in lipid processing after myelin phagocytosis contributes to the impaired remyelination in progressive multiple sclerosis. Here, the authors link depletion of neuregulin-1 in chronic demyelinated lesions to microglia foaminess that can be reversed therapeutically to promote remyelination in mice.

Peer review information: *Nature Communications* thanks Jerome Hendriks and the other anonymous reviewer(s) for their contribution to the peer review of this work. A peer review file is available.

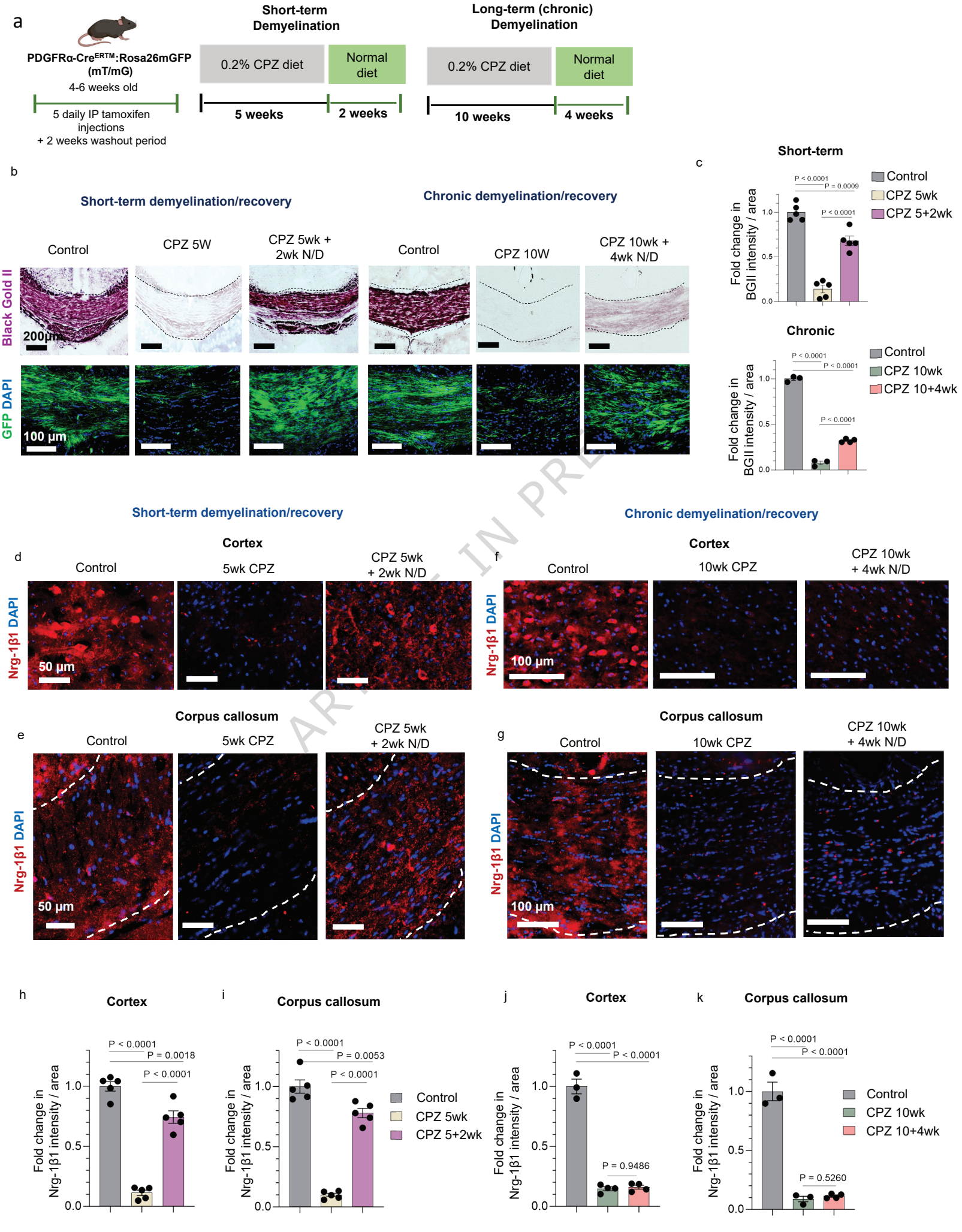
a
PDGFRα-CreERTM:Rosa26mGFP (mT/mG)
4-6 weeks old
5 daily IP tamoxifen injections
+ 2 weeks washout period
Short-term Demyelination
0.2% CPZ diet
Normal diet
5 weeks
2 weeks
Long-term (chronic) Demyelination
0.2% CPZ diet
Normal diet
10 weeks
4 weeks
b
Short-term demyelination/recovery
Chronic demyelination/recovery
Control
CPZ 5W
CPZ 5wk + 2wk N/D
Control
CPZ 10W
CPZ 10wk + 4wk N/D
Black Gold II
200μm
GFP DAPI
100 μm
c
Short-term
Fold change in BGII intensity / area
P < 0.0001
P = 0.0009
P < 0.0001
Control
CPZ 5wk
CPZ 5+2wk
Chronic
Fold change in BGII intensity / area
P < 0.0001
P < 0.0001
P < 0.0001
Control
CPZ 10wk
CPZ 10+4wk
Short-term demyelination/recovery
Chronic demyelination/recovery
d
Cortex
Control
5wk CPZ
CPZ 5wk + 2wk N/D
Nrg-1β1 DAPI
50 μm
f
Cortex
Control
10wk CPZ
CPZ 10wk + 4wk N/D
Nrg-1β1 DAPI
100 μm
e
Corpus callosum
Control
5wk CPZ
CPZ 5wk + 2wk N/D
Nrg-1β1 DAPI
50 μm
g
Corpus callosum
Control
10wk CPZ
CPZ 10wk + 4wk N/D
Nrg-1β1 DAPI
100 μm
h
Cortex
Fold change in Nrg-1β1 intensity / area
P < 0.0001
P = 0.0018
P < 0.0001
i
Corpus callosum
Fold change in Nrg-1β1 intensity / area
P < 0.0001
P = 0.0053
P < 0.0001
Control
CPZ 5wk
CPZ 5+2wk
j
Cortex
Fold change in Nrg-1β1 intensity / area
P < 0.0001
P < 0.0001
P = 0.9486
k
Corpus callosum
Fold change in Nrg-1β1 intensity / area
P < 0.0001
P < 0.0001
P = 0.5260
Control
CPZ 10wk
CPZ 10+4wk

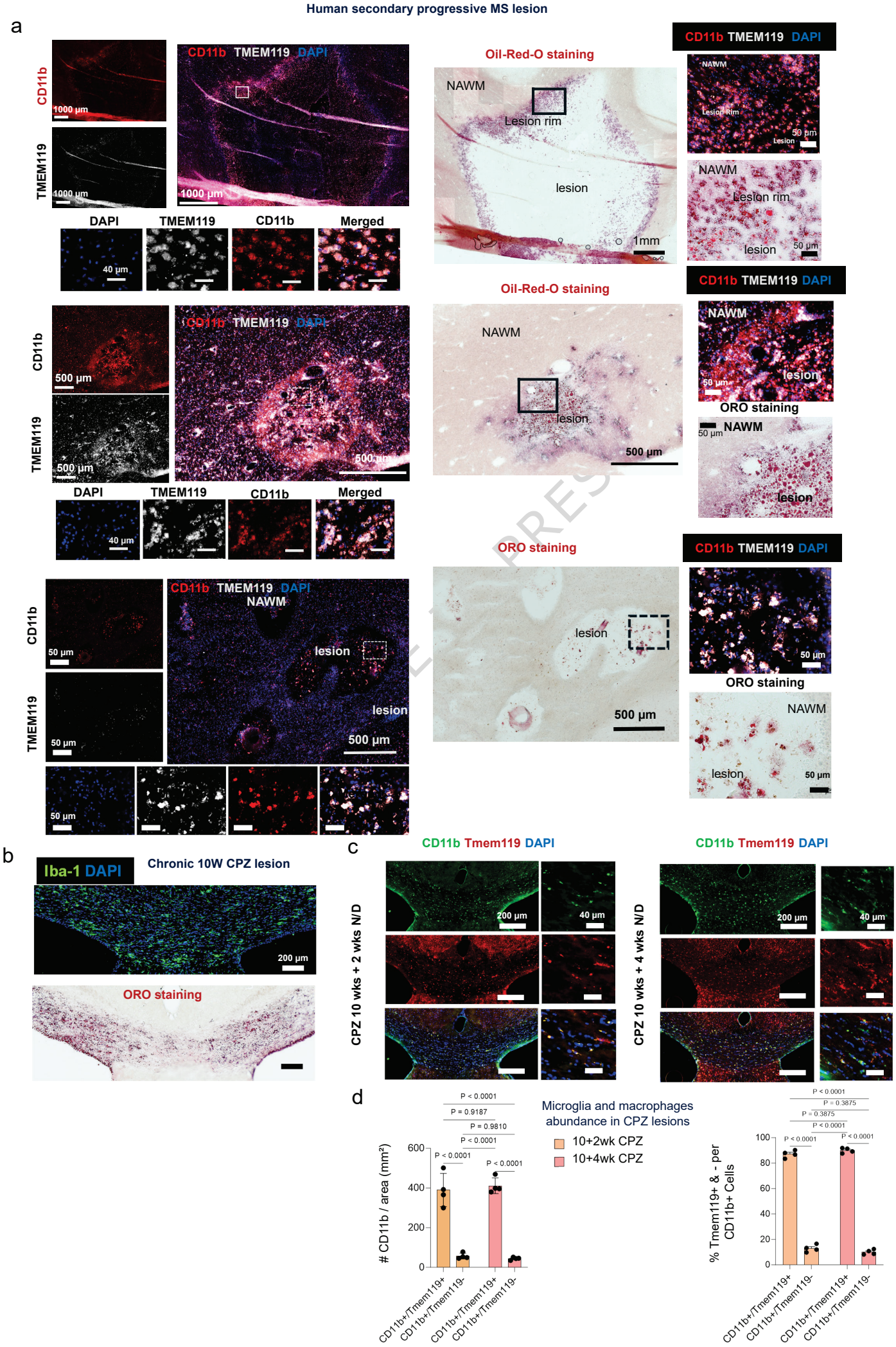
Human secondary progressive MS lesion
a
CD11b
TMEM119
CD11b TMEM119 DAPI
1000 µm
DAPI
TMEM119
CD11b
Merged
40 µm
Oil-Red-O staining
NAWM
Lesion rim
lesion
1mm
500 µm
ORO staining
50 µm
Lesion
b
Iba-1 DAPI
Chronic 10W CPZ lesion
200 µm
ORO staining
c
CD11b Tmem119 DAPI
CPZ 10 wks + 2 wks N/D
CPZ 10 wks + 4 wks N/D
200 µm
40 µm
d
Microglia and macrophages abundance in CPZ lesions
10+2wk CPZ
10+4wk CPZ
CD11b / area (mm²)
% Tmem119+ & - per CD11b+ Cells
P < 0.0001
P = 0.9187
P = 0.9810
P = 0.3875
CD11b+/Tmem119+
CD11b+/Tmem119-

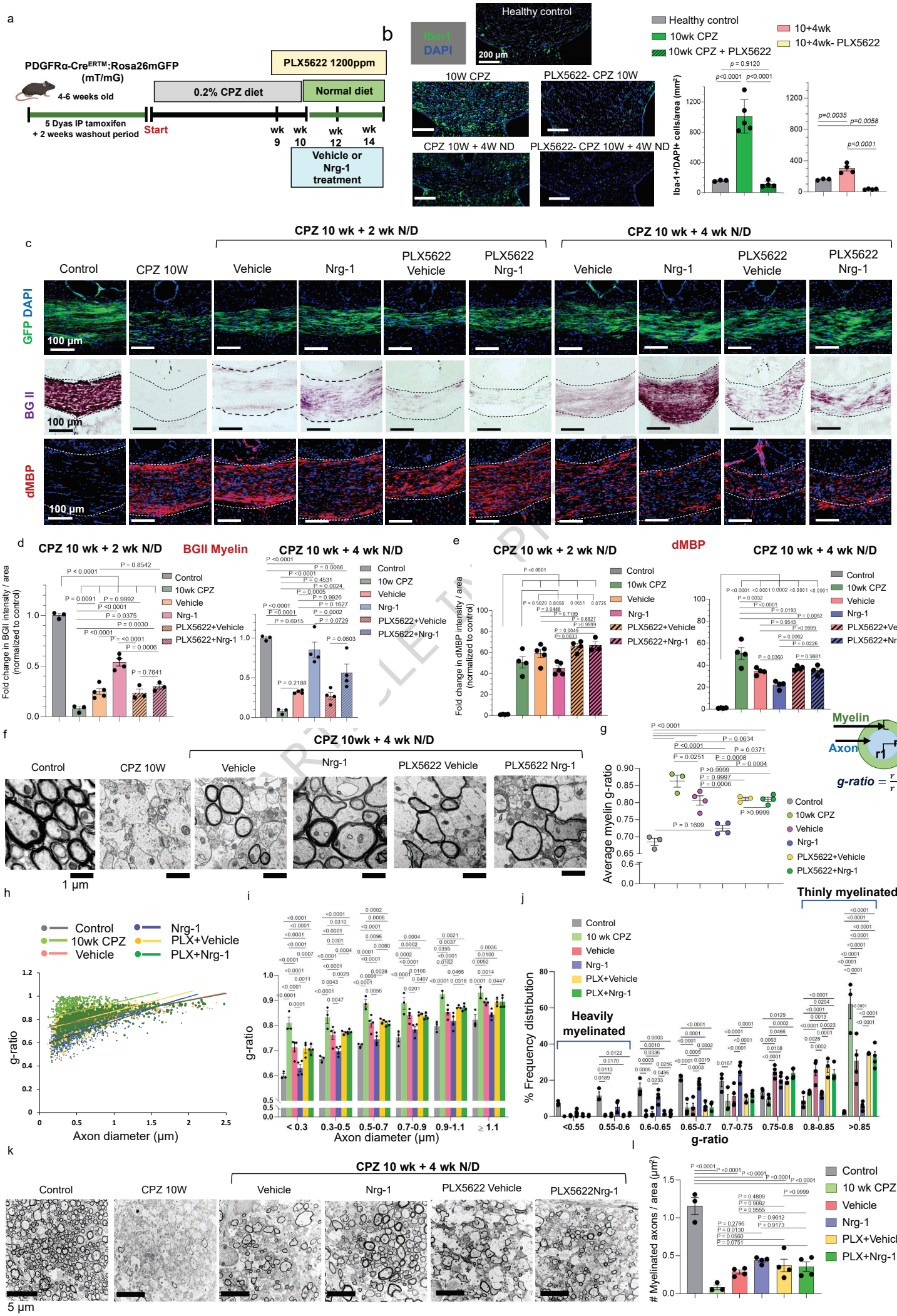
a
PDGFRα-CreERTM:Rosa26mGFP
(mT/mG)
4-6 weeks old
5 Dyas IP tamoxifen
+ 2 weeks washout period
Start
0.2% CPZ diet
PLX5622 1200ppm
Normal diet
wk 9
wk 10
wk 12
wk 14
Vehicle or Nrg-1 treatment
b
Iba-1
DAPI
Healthy control
200 µm
10W CPZ
PLX5622- CPZ 10W
CPZ 10W + 4W ND
PLX5622- CPZ 10W + 4W ND
Healthy control
10wk CPZ
10wk CPZ + PLX5622
10+4wk
10+4wk- PLX5622
Iba-1+/DAPI+ cells/area (mm²)
c
CPZ 10 wk + 2 wk N/D
CPZ 10 wk + 4 wk N/D
Control
CPZ 10W
Vehicle
Nrg-1
PLX5622 Vehicle
PLX5622 Nrg-1
GFP DAPI
BG II
dMBP
100 µm
d
CPZ 10 wk + 2 wk N/D
BGII Myelin
CPZ 10 wk + 4 wk N/D
Fold change in BGII intensity / area (normalized to control)
Control
10wk CPZ
Vehicle
Nrg-1
PLX5622+Vehicle
PLX5622+Nrg-1
10w CPZ
e
CPZ 10 wk + 2 wk N/D
dMBP
CPZ 10 wk + 4 wk N/D
Fold change in dMBP intensity / area (normalized to control)
f
CPZ 10wk + 4 wk N/D
Control
CPZ 10W
Vehicle
Nrg-1
PLX5622 Vehicle
PLX5622 Nrg-1
1 µm
g
Myelin
Axon
r1
r2
g-ratio = r1/r2
Average myelin g-ratio
h
Control
10wk CPZ
Vehicle
Nrg-1
PLX+Vehicle
PLX+Nrg-1
g-ratio
Axon diameter (µm)
i
g-ratio
< 0.3
0.3-0.5
0.5-0.7
0.7-0.9
0.9-1.1
≥ 1.1
Axon diameter (µm)
j
Thinly myelinated
Heavily myelinated
Control
10 wk CPZ
Vehicle
Nrg-1
PLX+Vehicle
PLX+Nrg-1
% Frequency distribution
<0.55
0.55-0.6
0.6-0.65
0.65-0.7
0.7-0.75
0.75-0.8
0.8-0.85
>0.85
g-ratio
k
CPZ 10 wk + 4 wk N/D
Control
CPZ 10W
Vehicle
Nrg-1
PLX5622 Vehicle
PLX5622Nrg-1
5 µm
l
Myelinated axons / area (µm²)
Control
10 wk CPZ
Vehicle
Nrg-1
PLX+Vehicle
PLX+Nrg-1

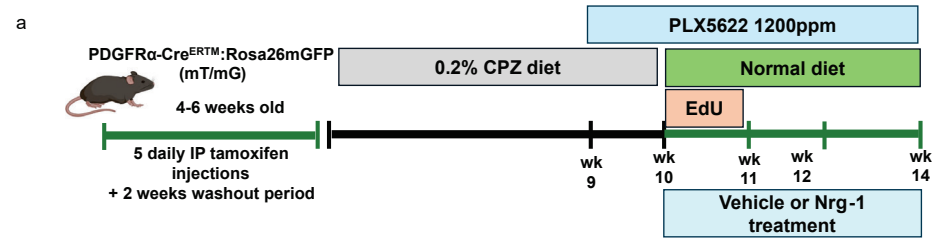
a
PLX5622 1200ppm
PDGFRα-CreERTM:Rosa26mGFP
(mT/mG)
0.2% CPZ diet
Normal diet
4-6 weeks old
EdU
5 daily IP tamoxifen
injections
+ 2 weeks washout period
wk 9
wk 10
wk 11
wk 12
wk 14
Vehicle or Nrg-1
treatment

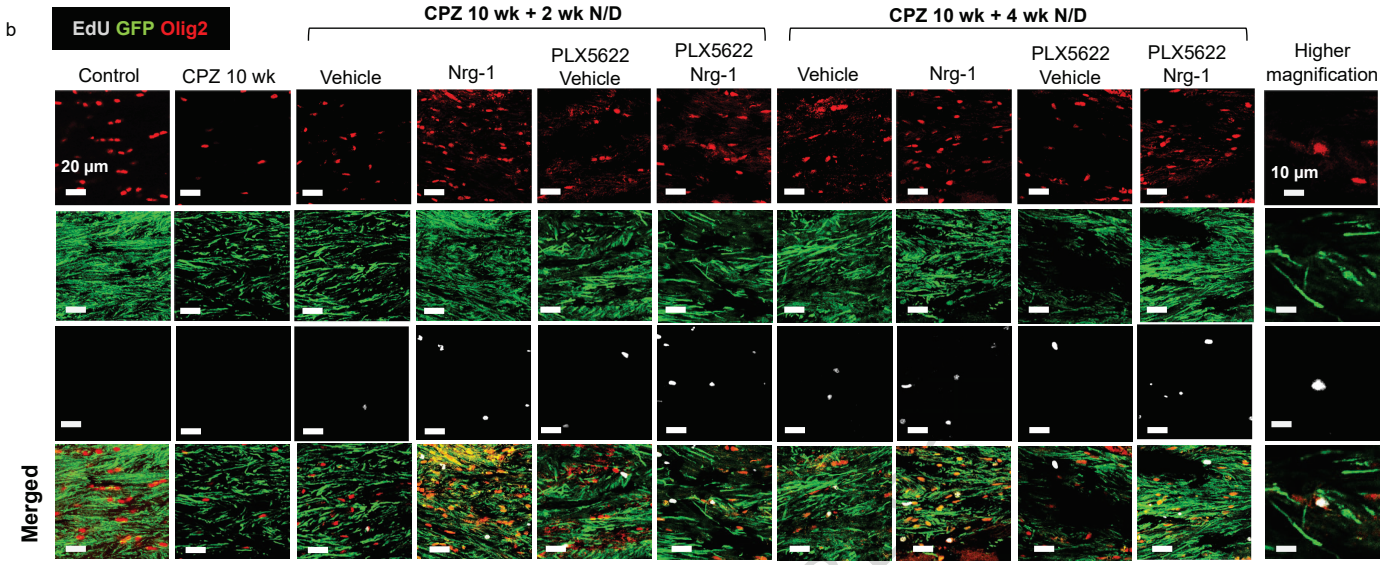
b
EdU GFP Olig2
CPZ 10 wk + 2 wk N/D
CPZ 10 wk + 4 wk N/D
Control
CPZ 10 wk
Vehicle
Nrg-1
PLX5622 Vehicle
PLX5622 Nrg-1
Higher magnification
20 µm
10 µm
Merged

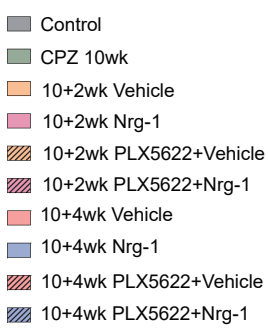
Control
CPZ 10wk
10+2wk Vehicle
10+2wk Nrg-1
10+2wk PLX5622+Vehicle
10+2wk PLX5622+Nrg-1
10+4wk Vehicle
10+4wk Nrg-1
10+4wk PLX5622+Vehicle
10+4wk PLX5622+Nrg-1

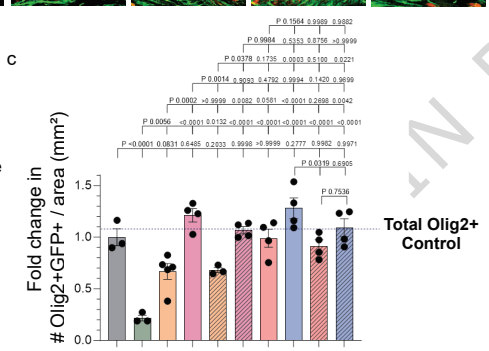
c
Fold change in
Olig2+GFP+ / area (mm²)
Total Olig2+
Control

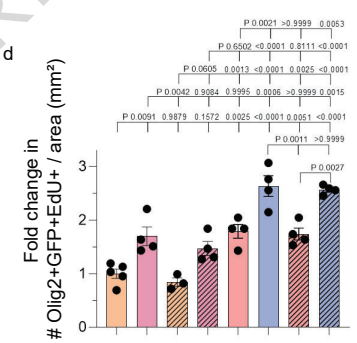
d
Fold change in
Olig2+GFP+EdU+ / area (mm²)

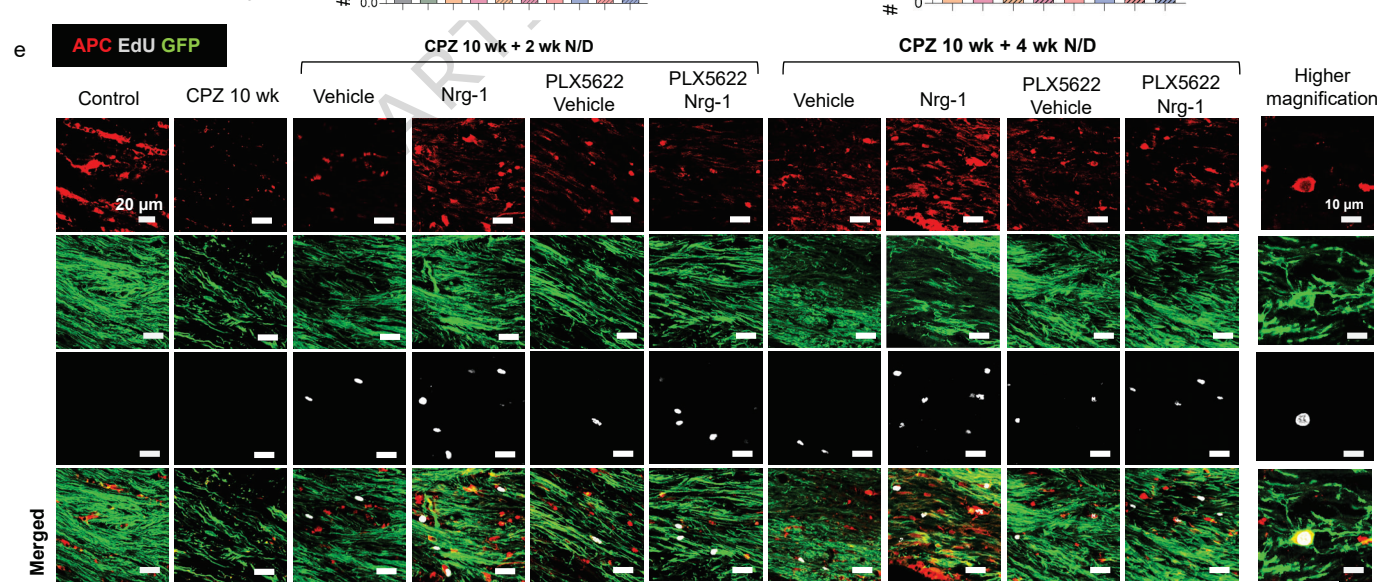
e
APC EdU GFP
CPZ 10 wk + 2 wk N/D
CPZ 10 wk + 4 wk N/D
Control
CPZ 10 wk
Vehicle
Nrg-1
PLX5622 Vehicle
PLX5622 Nrg-1
Higher magnification
20 µm
10 µm
Merged

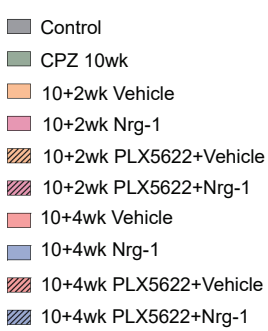
Control
CPZ 10wk
10+2wk Vehicle
10+2wk Nrg-1
10+2wk PLX5622+Vehicle
10+2wk PLX5622+Nrg-1
10+4wk Vehicle
10+4wk Nrg-1
10+4wk PLX5622+Vehicle
10+4wk PLX5622+Nrg-1

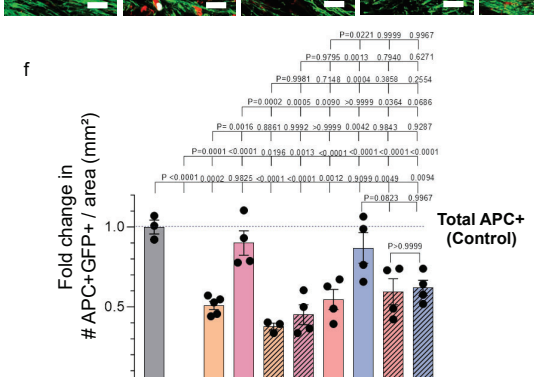
f
Fold change in
APC+GFP+ / area (mm²)
Total APC+
(Control)

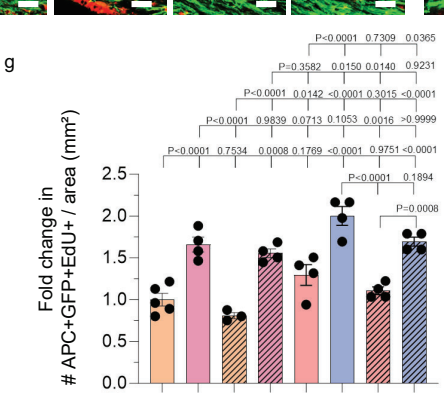
g
Fold change in
APC+GFP+EdU+ / area (mm²)

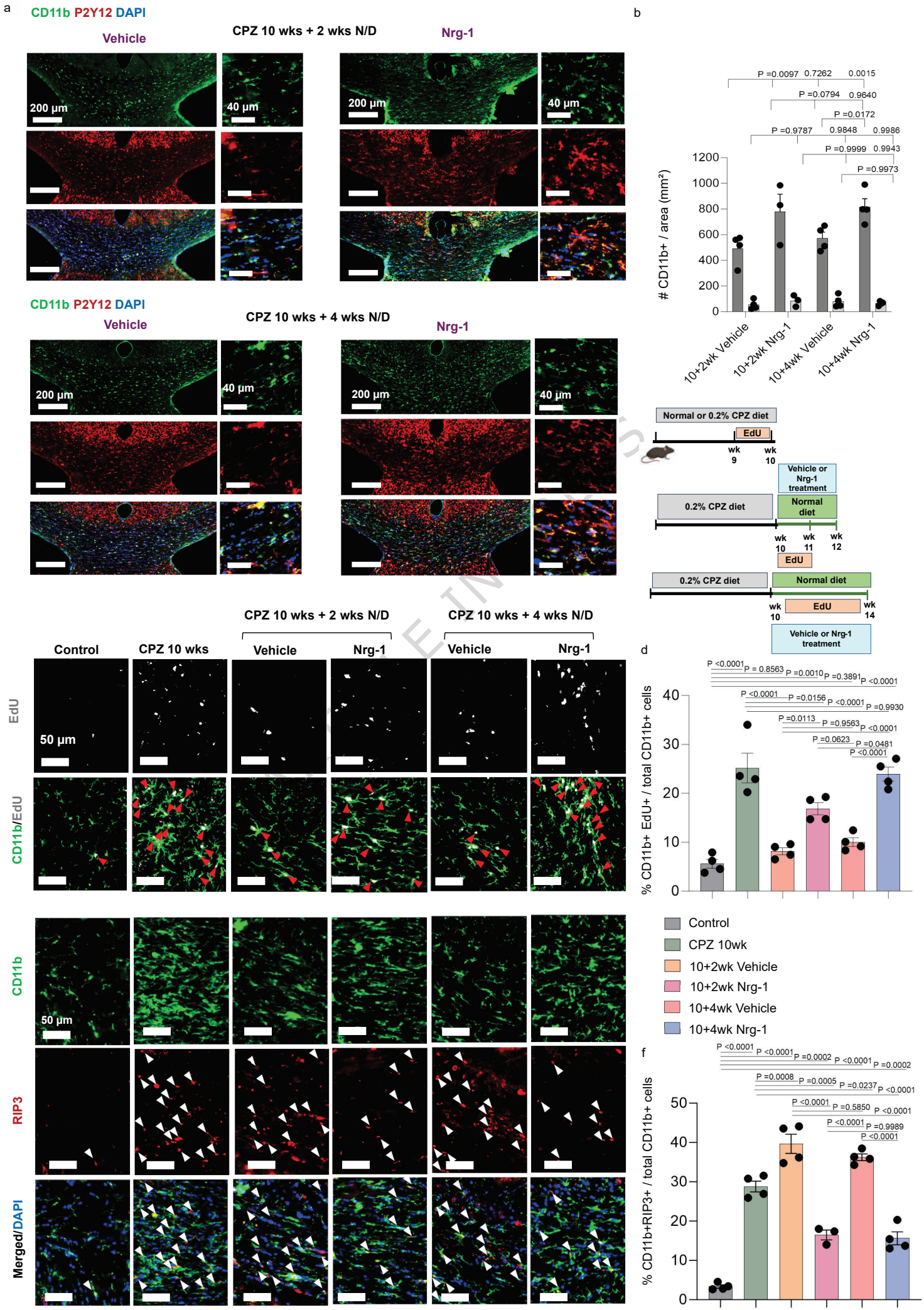
a
CD11b P2Y12 DAPI
Vehicle
CPZ 10 wks + 2 wks N/D
Nrg-1
200 µm
40 µm
CD11b P2Y12 DAPI
Vehicle
CPZ 10 wks + 4 wks N/D
Nrg-1
b
P =0.0097 0.7262 0.0015
P =0.0794 0.9640
P =0.0172
P =0.9787 0.9848 0.9986
P =0.9999 0.9943
P =0.9973
# CD11b+ / area (mm²)
10+2wk Vehicle
10+2wk Nrg-1
10+4wk Vehicle
10+4wk Nrg-1
Normal or 0.2% CPZ diet
EdU
wk 9
wk 10
Vehicle or Nrg-1 treatment
0.2% CPZ diet
Normal diet
wk 10
wk 11
wk 12
EdU
0.2% CPZ diet
Normal diet
wk 10
EdU
wk 14
Vehicle or Nrg-1 treatment
c
CPZ 10 wks + 2 wks N/D
CPZ 10 wks + 4 wks N/D
Control
CPZ 10 wks
Vehicle
Nrg-1
Vehicle
Nrg-1
EdU
CD11b/EdU
50 µm
d
% CD11b+ EdU+ / total CD11b+ cells
P <0.0001 P = 0.8563 P =0.0010 P =0.3891 P <0.0001
P <0.0001 P =0.0156 P <0.0001 P =0.9930
P =0.0113 P =0.9563 P <0.0001
P =0.0623 P =0.0481
P <0.0001
e
CD11b
RIP3
Merged/DAPI
50 µm
Control
CPZ 10wk
10+2wk Vehicle
10+2wk Nrg-1
10+4wk Vehicle
10+4wk Nrg-1
f
% CD11b+RIP3+ / total CD11b+ cells
P <0.0001 P <0.0001 P =0.0002 P <0.0001 P =0.0002
P =0.0008 P =0.0005 P =0.0237 P <0.0001
P <0.0001 P =0.5850 P <0.0001
P <0.0001 P =0.9989
P <0.0001

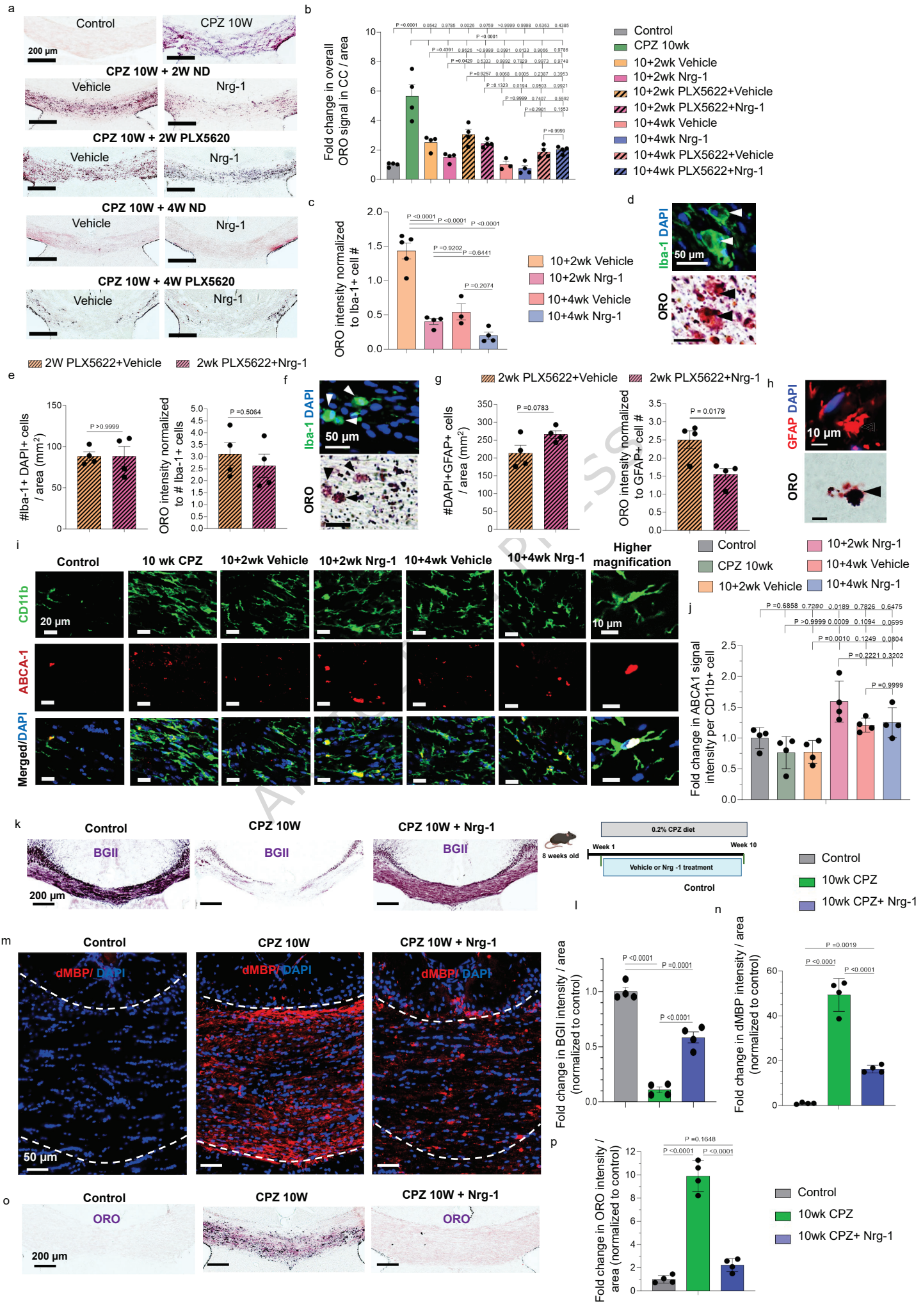
a
Control
CPZ 10W
200 µm
CPZ 10W + 2W ND
Vehicle
Nrg-1
CPZ 10W + 2W PLX5620
CPZ 10W + 4W ND
CPZ 10W + 4W PLX5620
2W PLX5622+Vehicle
2wk PLX5622+Nrg-1
b
Fold change in overall ORO signal in CC / area
Control
CPZ 10wk
10+2wk Vehicle
10+2wk Nrg-1
10+2wk PLX5622+Vehicle
10+2wk PLX5622+Nrg-1
10+4wk Vehicle
10+4wk Nrg-1
10+4wk PLX5622+Vehicle
10+4wk PLX5622+Nrg-1
c
ORO intensity normalized to Iba-1+ cell #
d
Iba-1 DAPI
ORO
50 µm
e
#Iba-1+ DAPI+ cells / area (mm2)
ORO intensity normalized to # Iba-1+ cells
f
g
#DAPI+GFAP+ cells / area (mm2)
ORO intensity normalized to GFAP+ cell #
h
GFAP DAPI
10 µm
i
Control
10 wk CPZ
10+2wk Vehicle
10+2wk Nrg-1
10+4wk Vehicle
10+4wk Nrg-1
Higher magnification
CD11b
ABCA-1
Merged/DAPI
20 µm
j
Fold change in ABCA1 signal intensity per CD11b+ cell
k
Control
CPZ 10W
CPZ 10W + Nrg-1
BGII
200 µm
8 weeks old
0.2% CPZ diet
Week 1
Week 10
Vehicle or Nrg -1 treatment
Control
l
Fold change in BGII intensity / area (normalized to control)
m
dMBP/ DAPI
50 µm
n
Fold change in dMBP intensity / area (normalized to control)
o
ORO
p
Fold change in ORO intensity / area (normalized to control)

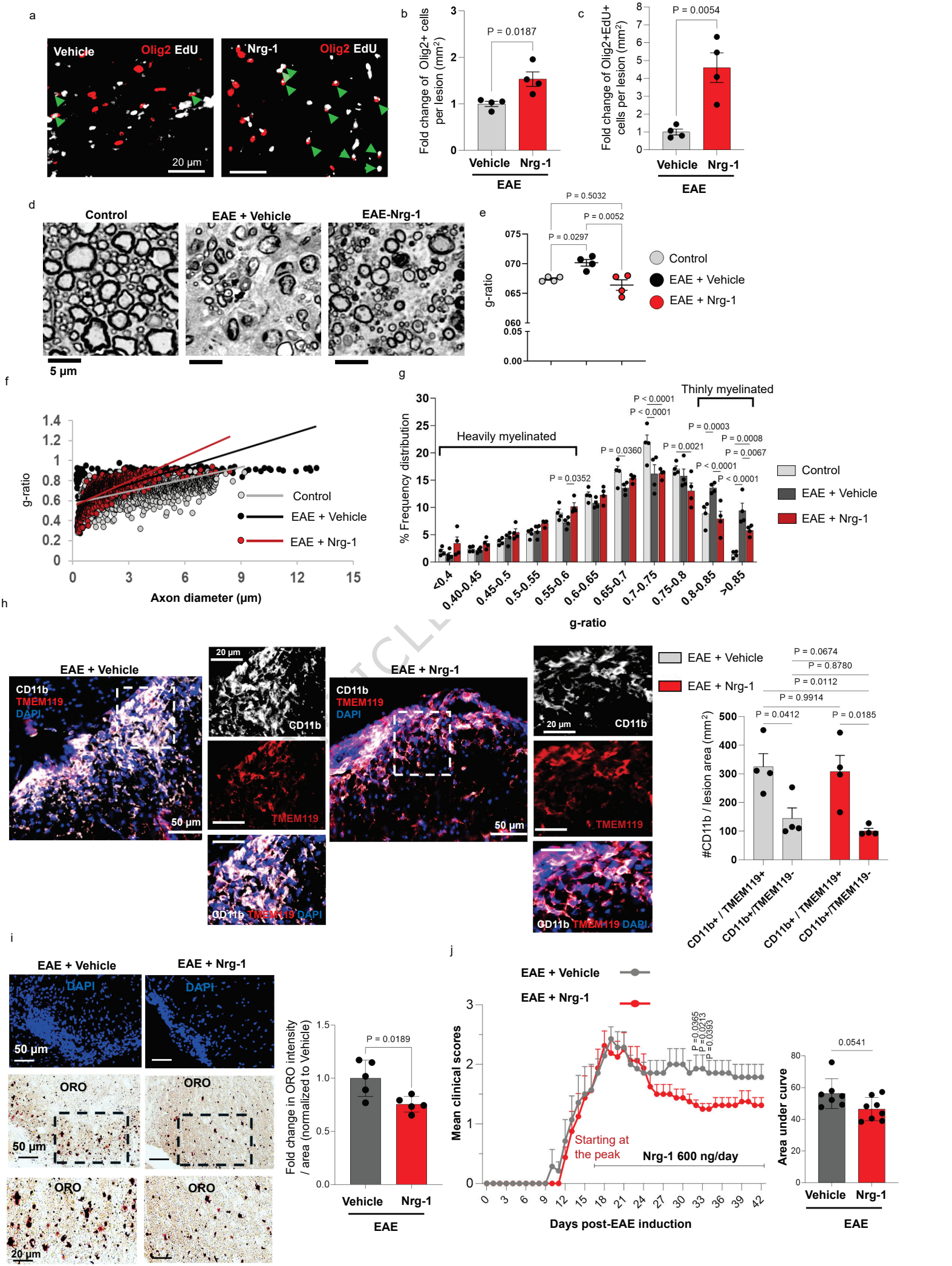
a
Vehicle
Olig2 EdU
Nrg-1
Olig2 EdU
20 µm
b
Fold change of Olig2+ cells per lesion (mm²)
P = 0.0187
Vehicle
Nrg-1
EAE
c
Fold change of Olig2+EdU+ cells per lesion (mm²)
P = 0.0054
Vehicle
Nrg-1
EAE
d
Control
EAE + Vehicle
EAE-Nrg-1
5 µm
e
P = 0.5032
P = 0.0052
P = 0.0297
g-ratio
Control
EAE + Vehicle
EAE + Nrg-1
f
g-ratio
Control
EAE + Vehicle
EAE + Nrg-1
Axon diameter (µm)
g
Thinly myelinated
Heavily myelinated
% Frequency distribution
P < 0.0001
P < 0.0001
P = 0.0003
P = 0.0008
P = 0.0067
P = 0.0360
P = 0.0021
P < 0.0001
P = 0.0352
P < 0.0001
Control
EAE + Vehicle
EAE + Nrg-1
<0.4
0.40-0.45
0.45-0.5
0.5-0.55
0.55-0.6
0.6-0.65
0.65-0.7
0.7-0.75
0.75-0.8
0.8-0.85
>0.85
g-ratio
h
EAE + Vehicle
CD11b
TMEM119
DAPI
50 µm
20 µm
CD11b
TMEM119
CD11b TMEM119 DAPI
EAE + Nrg-1
CD11b
TMEM119
DAPI
50 µm
20 µm
CD11b
TMEM119
CD11b TMEM119 DAPI
EAE + Vehicle
EAE + Nrg-1
P = 0.0674
P = 0.8780
P = 0.0112
P = 0.9914
P = 0.0412
P = 0.0185
#CD11b / lesion area (mm²)
CD11b+ / TMEM119+
CD11b+/TMEM119-
CD11b+ / TMEM119+
CD11b+/TMEM119-
i
EAE + Vehicle
EAE + Nrg-1
DAPI
DAPI
50 µm
ORO
ORO
50 µm
ORO
ORO
20 µm
Fold change in ORO intensity / area (normalized to Vehicle)
P = 0.0189
Vehicle
Nrg-1
EAE
j
EAE + Vehicle
EAE + Nrg-1
Mean clinical scores
P = 0.0365
P = 0.0213
P = 0.0393
Starting at the peak
Nrg-1 600 ng/day
Days post-EAE induction
Area under curve
0.0541
Vehicle
Nrg-1
EAE

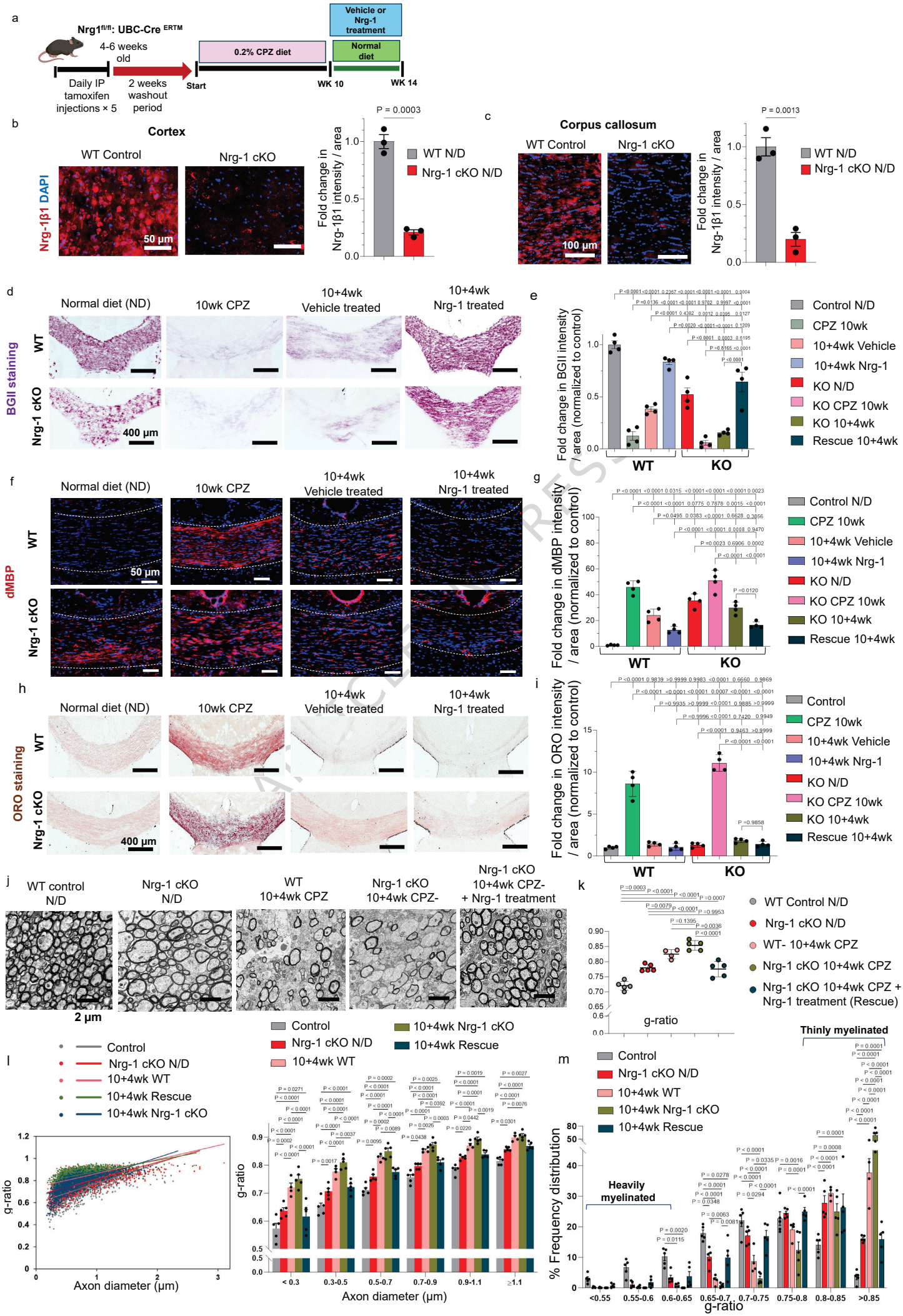

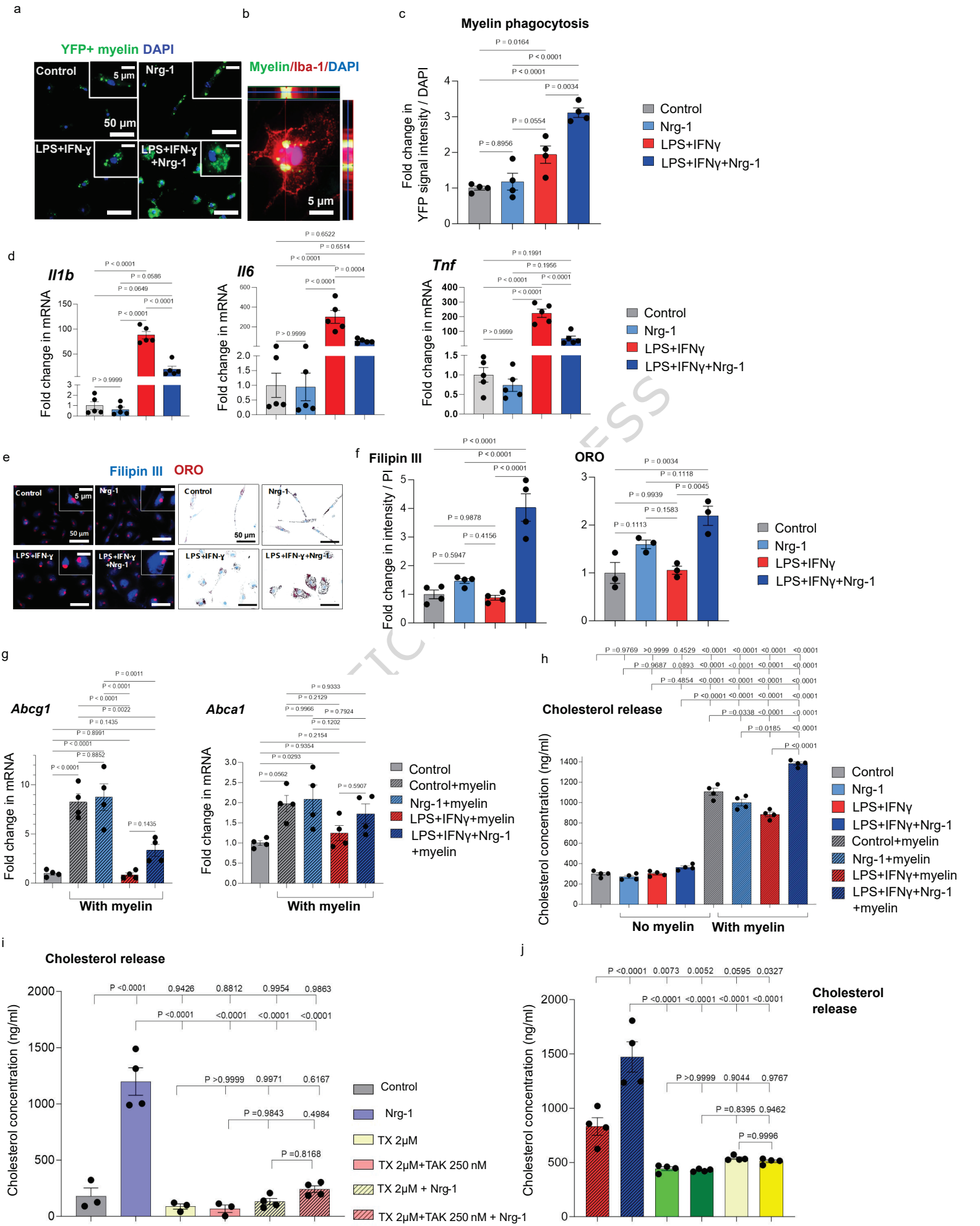
a
YFP+ myelin DAPI
Control
Nrg-1
LPS+IFN-γ
LPS+IFN-γ +Nrg-1
5 μm
50 μm
b
Myelin/Iba-1/DAPI
5 μm
c
Myelin phagocytosis
Fold change in YFP signal intensity / DAPI
P = 0.0164
P < 0.0001
P < 0.0001
P = 0.0034
P = 0.0554
P = 0.8956
Control
Nrg-1
LPS+IFNγ
LPS+IFNγ+Nrg-1
d
Il1b
Il6
Tnf
Fold change in mRNA
P < 0.0001
P = 0.0586
P = 0.0649
P < 0.0001
P < 0.0001
P > 0.9999
P = 0.6522
P = 0.6514
P < 0.0001
P = 0.0004
P < 0.0001
P > 0.9999
P = 0.1991
P = 0.1956
P < 0.0001
P < 0.0001
P < 0.0001
P > 0.9999
Control
Nrg-1
LPS+IFNγ
LPS+IFNγ+Nrg-1
e
Filipin III ORO
Control
Nrg-1
LPS+IFN-γ
LPS+IFN-γ +Nrg-1
5 μm
50 μm
f
Filipin III
Fold change in intensity / PI
P < 0.0001
P < 0.0001
P < 0.0001
P = 0.9878
P = 0.4156
P = 0.5947
ORO
P = 0.0034
P = 0.1118
P = 0.0045
P = 0.9939
P = 0.1583
P = 0.1113
Control
Nrg-1
LPS+IFNγ
LPS+IFNγ+Nrg-1
g
Abcg1
Abca1
Fold change in mRNA
P = 0.0011
P < 0.0001
P < 0.0001
P = 0.0022
P = 0.1435
P = 0.8991
P < 0.0001
P = 0.8852
P < 0.0001
P = 0.1435
P = 0.9333
P = 0.2129
P = 0.9966
P = 0.7924
P = 0.1202
P = 0.2154
P = 0.9354
P = 0.0293
P = 0.0562
P = 0.5907
With myelin
With myelin
Control
Control+myelin
Nrg-1+myelin
LPS+IFNγ+myelin
LPS+IFNγ+Nrg-1 +myelin
h
Cholesterol release
Cholesterol concentration (ng/ml)
P =0.9769 >0.9999 0.4529 <0.0001 <0.0001 <0.0001 <0.0001
P =0.9687 0.0893 <0.0001 <0.0001 <0.0001 <0.0001
P =0.4854 <0.0001 <0.0001 <0.0001 <0.0001
P <0.0001 <0.0001 <0.0001 <0.0001
P =0.0338 <0.0001 <0.0001
P =0.0185 <0.0001
P <0.0001
No myelin
With myelin
Control
Nrg-1
LPS+IFNγ
LPS+IFNγ+Nrg-1
Control+myelin
Nrg-1+myelin
LPS+IFNγ+myelin
LPS+IFNγ+Nrg-1 +myelin
i
Cholesterol release
Cholesterol concentration (ng/ml)
P <0.0001 0.9426 0.8812 0.9954 0.9863
P <0.0001 <0.0001 <0.0001 <0.0001
P >0.9999 0.9971 0.6167
P =0.9843 0.4984
P =0.8168
Control
Nrg-1
TX 2μM
TX 2μM+TAK 250 nM
TX 2μM + Nrg-1
TX 2μM+TAK 250 nM + Nrg-1
j
Cholesterol release
Cholesterol concentration (ng/ml)
P <0.0001 0.0073 0.0052 0.0595 0.0327
P <0.0001 <0.0001 <0.0001 <0.0001
P >0.9999 0.9044 0.9767
P =0.8395 0.9462
P =0.9996

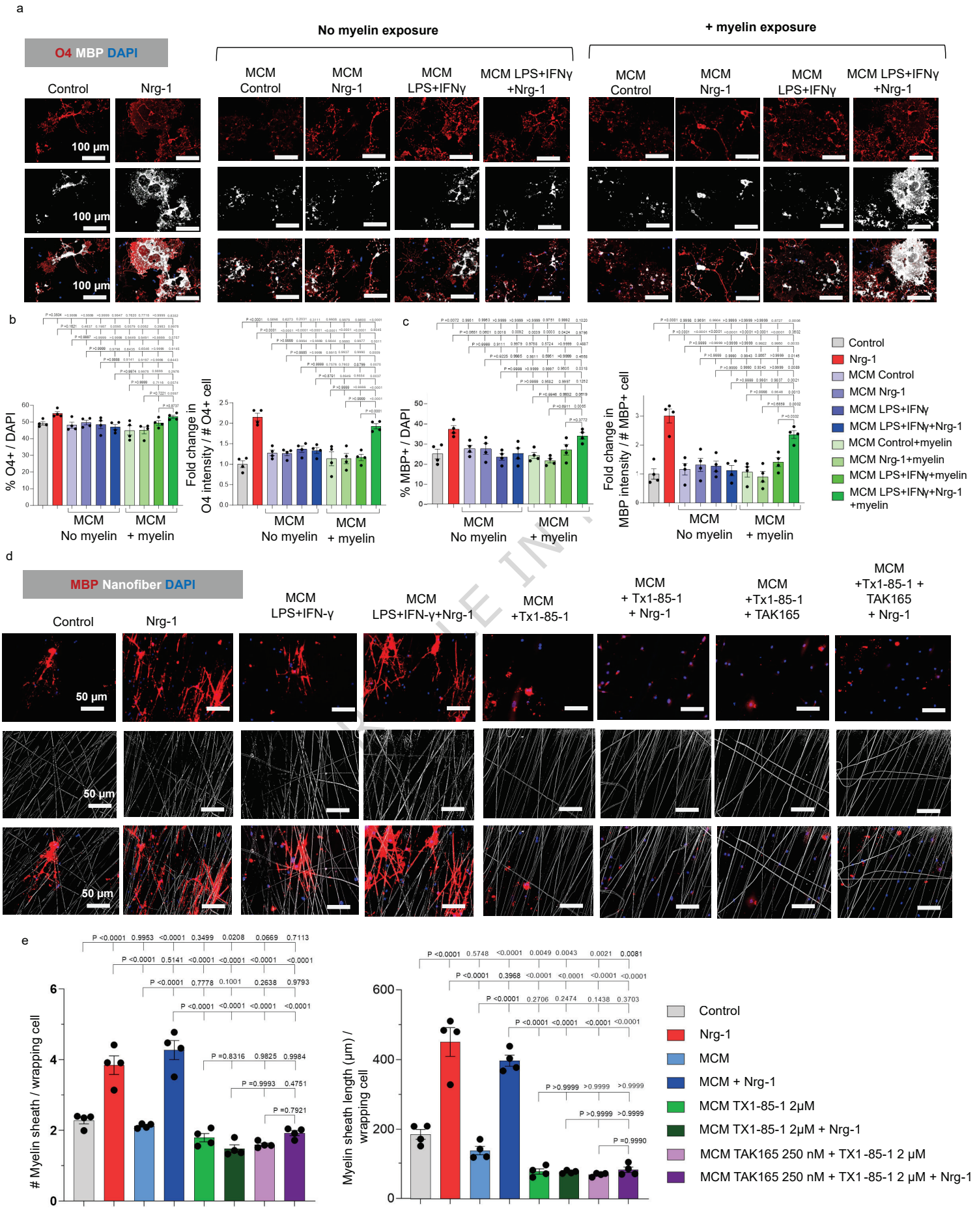
a
O4 MBP DAPI
No myelin exposure
+ myelin exposure
Control
Nrg-1
MCM Control
MCM Nrg-1
MCM LPS+IFNγ
MCM LPS+IFNγ +Nrg-1
100 µm
b
% O4+ / DAPI
Fold change in O4 intensity / # O4+ cell
MCM No myelin
MCM + myelin
c
% MBP+ / DAPI
Fold change in MBP intensity / # MBP+ cell
Control
Nrg-1
MCM Control
MCM Nrg-1
MCM LPS+IFNγ
MCM LPS+IFNγ+Nrg-1
MCM Control+myelin
MCM Nrg-1+myelin
MCM LPS+IFNγ+myelin
MCM LPS+IFNγ+Nrg-1 +myelin
d
MBP Nanofiber DAPI
MCM LPS+IFN-γ
MCM LPS+IFN-γ+Nrg-1
MCM +Tx1-85-1
MCM + Tx1-85-1 + Nrg-1
MCM +Tx1-85-1 + TAK165
MCM +Tx1-85-1 + TAK165 + Nrg-1
50 µm
e
Myelin sheath / wrapping cell
Myelin sheath length (µm) / wrapping cell
Control
Nrg-1
MCM
MCM + Nrg-1
MCM TX1-85-1 2µM
MCM TX1-85-1 2µM + Nrg-1
MCM TAK165 250 nM + TX1-85-1 2 µM
MCM TAK165 250 nM + TX1-85-1 2 µM + Nrg-1